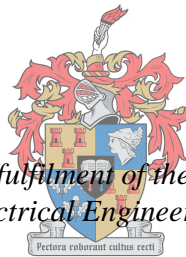


Development and application of intelligent histogram logger for load profiling applications

By

Wynand Dreyer Terblanche



*Thesis presented in partial fulfilment of the requirements for the degree
Master of Engineering in Electrical Engineering at Stellenbosch University*

UNIVERSITEIT
iYUNIVESITHI
STELLENBOSCH
UNIVERSITY

100
1918 · 2018

Supervisor: Prof. H.J. Vermeulen
Department of Electrical and Electronic Engineering

March 2018

Declaration

1. Plagiarism is the use of ideas, material and other intellectual property of another's work and to present it as my own.
2. I agree that plagiarism is a punishable offence because it constitutes theft.
3. I also understand that direct translations are plagiarism.
4. Accordingly, all quotations and contributions from any source whatsoever (including the internet) have been cited fully. I understand that the reproduction of text without quotation marks (even when the source is cited) is plagiarism.
5. I declare that the work contained in this assignment, except where otherwise stated, is my original work and that I have not previously (in its entirety or in part) submitted it for grading in this module/assignment or another module/assignment.

W.D. Terblanche

March 2018

Copyright © 2018 Stellenbosch University

All rights reserved

Acknowledgements

I would like to thank the following individuals for their valuable contribution to this project:

- My study leader, Prof H.J. Vermeulen, for his guidance, inspiration and commitment throughout my last two years at Stellenbosch University and his contribution to improve the presentation of the work done for the project.
- My mother, Joana Terblanche, father, Gerhard Terblanche, brother, Niel Terblanche, sister, Lindi Terblanche, and all my family members who provided unwavering support and love throughout the completion of the project.
- Matthew Groch, Edwin Mangwende and Chantelle Janse van Vuuren and other friends who supported me and made my time unforgettable in room E222.
- Riatha van Zyl for being an incredible friend who supported me throughout my project with love, patience and sacrifices.
- Johan Arendse at Stellenbosch University who assisted in the manufacturing process of the logger devices developed for the project.
- The property management officers at Robben Island, Wayne Bessick and Linda Penicela, for their assistance and support during the collection of data from the site and making the necessary arrangements for site visits.
- Sola Future, for providing information on the energy system installed at Robben Island and Andrew Galbraith from WSP for assisting in the arrangements made to conduct the study at the site.

Abstract

Over the past few years, rising electricity cost has increasingly put focus on energy management and energy efficient interventions with the aim at consuming electrical energy sustainably and decrease dependency on fossil fuels. Energy management and energy conservation exercises, however, require accurate and reliable load-specific energy consumption data and statistics. To date, high costs of logging instrumentation and data communication remains the restrictive aspect for acquiring statistically significant distributed load modelling data. Conventional long-term measuring instrumentation is, furthermore, highly intrusive which motivates research in non-intrusive load modelling and emphasizes the limiting factor towards energy management exercises.

This project provides a solution for modern large-scale load monitoring studies by proposing a low-cost event-based histogram logger. Several studies in the literature were investigated to develop a cost-effective alternative logging device with the aim at design objectives such as low-cost hardware, power efficiency, small physical footprint and non-intrusive current sensing. The proposed system is thoroughly discussed in terms of the system topology, firmware design and the implementation of application software. Numerous methods of data acquisition are investigated to find the optimal recording technique that satisfies the requirements of energy management exercises. Histogram data logging is studied and introduced as an attempt to reduce non-volatile memory requirements in modern data loggers. The application software, which offers a user-friendly interface to assist in setting up the logger, as well as retrieving and presenting data, is presented. Performance results are also presented for the power consumption characteristics of the design.

Energy management interventions give rise to the implementation of renewable energy sources and micro-grid energy systems. The proposed system has been studied in the case study using an islanded micro-grid energy system. Historical data is provided for the photovoltaic power plant, battery storage system and diesel generator energy system, while the proposed loggers were installed at certain targeted residential appliances to gather usage data. Simulation software is presented, together with mathematical formulations, to determine various energy profiles and possible energy saving opportunities.

The results of the case study prove the concept of histogram event recording and feasibility of implementing the proposed system for energy management exercises.

Opsomming

Oor die afgelope paar jaar het stygende elektrisiteitskoste toenemende fokus op energie bestuur en energie-effektiewe ontwikkelinge geplaas. Die doel daarvan is om elektriese energie meer effektief te gebruik en ons afhanklikheid van fossielbrandstowwe te verminder. Energie bestuur en energie-effektiewe ontwikkelinge vereis egter akkurate en betroubare energie verbruikers data. Tot op hede, bly die hoë koste van data versameling toestelle en datakommunikasie die beperkende aspek vir die verkryging van verspreide toestel modellerings data. Konvensionele langtermyn meet instrumente is hoogs indringend wat navorsing in nie-indringende verbruikers data modellering motiveer en die beperkende faktor tot energie besparing oefeninge beklemtoon.

Hierdie projek bied 'n oplossing vir moderne, grootskaalse gebruikers monitering studies deur 'n lae koste gebeurtenis gebaseerde histogram data versamelaar voor te stel. Verskeie studies in die literatuur is ondersoek om 'n koste-effektiewe alternatief te ontwikkel met die doel om die ontwerp doelwitte te bereik. Dit sluit in, 'n relatiewe goedkoop hardware ontwerp, energie doeltreffendheid, optimale toestel grootte en 'n nie-indringende stroom sensor. Die voorgestelde stelsel word deeglik bespreek in terme van die stelsel topologie, sagteware-ontwerp en die implementering van 'n rekenaar program. Verskeie metodes van data versameling word ondersoek om die optimale data versamelings tegniek te vind wat aan die vereistes van energie besparings oefeninge voldoen. Histogram data versameling word bestudeer as 'n poging om geheue vereistes in moderne data versameling toestelle te verminder. Die rekenaar program, wat 'n gebruikersvriendelike koppelvlak bied om te help met die opstel van die data versamelaar toestel, sowel as die herwinning en aanbieding van data, word aangebied. Drywing resultate van die ontwerp word ook aangebied.

Energie besparings projekte gee aanleiding tot die implementering van hernubare energie bronne en mikro-netwerke. Die voorgestelde stelsel is in die gevallestudie bestudeer deur gebruik te maak van 'n mikro-netwerk energie stelsel. Historiese data word verskaf vir die son plaas, battery energie storing stelsel en die diesel generator energie sisteem, terwyl die voorgestelde toestel by sekere huishoudelike toestelle geïnstalleer is om gebruikers data te versamel. Simulasie sagteware word saam met wiskundige formulerings aangebied om verskeie energie profiele en moontlike energie besparings geleenthede te bepaal.

Die resultate van die gevallestudie bewys die konsep van histogram data versameling en die haalbaarheid van die voorgestelde toestel vir energie bestuur oefeninge.

Table of Contents

Declaration	i
Acknowledgements	ii
Abstract	iii
Opsomming	iv
Table of Contents	v
List of Figures	ix
List of Tables.....	xiv
List of Appendix Figures.....	xvi
List of Appendix Tables.....	xvii
List of Abbreviations.....	xix
1 Project Overview	1
1.1 Introduction	1
1.2 Project Motivation	2
1.3 Project Description	4
1.3.1 Research Objectives	4
1.3.2 Key Questions	5
1.3.3 Research Tasks	6
1.4 Thesis Structure	7
2 Literature Review.....	9
2.1 Overview	9
2.2 Residential Load Modelling	10
2.2.1 Appliance Load Monitoring	10
2.2.2 Non-intrusive Load Monitoring Technology	11
2.2.3 Load Profile Forecasting	12
2.3 Residential Hot Water Systems	13
2.3.1 Overview	13
2.3.2 Traditional Hot Water Cylinders.....	13
2.3.3 Heat-pump Technology.....	15
2.4 Micro-grid Systems	16
2.4.1 Introduction	16
2.4.2 Diesel Generators and Fuel Consumption.....	18
2.4.3 Battery Storage Systems.....	19
2.5 Software Development Platforms and Applications	23

2.5.1	Overview	23
2.5.2	Atmel Studio	23
2.5.3	Eclipse	23
2.5.4	Qt Creator	24
2.5.5	Altium Designer	24
2.5.6	Matlab.....	24
2.5.7	Python.....	24
3	System Design	25
3.1	Overview	25
3.2	System Topology	25
3.3	Logic Core Design.....	26
3.4	Current Sensor Design.....	28
3.5	Power Supply and Power Management.....	30
3.6	Cost Analysis.....	35
4	Embedded Software Implementation.....	37
4.1	Overview	37
4.2	Top Level Program.....	39
4.2.1	Start-up and Initialization.....	39
4.2.2	Main Program.....	40
4.3	USB Communication.....	44
4.3.1	Overview	44
4.3.2	Configuration	44
4.4	System Frequency and Clock	45
4.4.1	Overview	45
4.4.2	System Clock Frequency.....	45
4.4.3	Real Time Clock.....	46
4.5	Analogue to Digital Conversion	48
4.6	System Memory.....	48
4.7	Data Recording Use Cases	49
4.7.1	Overview	49
4.7.2	Raw Event Recording.....	50
4.7.3	Raw Analogue Recording	52
4.7.4	Event Histogram Recording	55
4.7.5	Analogue Histogram Recording.....	58
4.7.6	Expert Recording.....	60
5	Application Software	63

5.1	Introduction	63
5.2	High-level Application Software	63
5.2.1	Overview	63
5.2.2	Device Information	65
5.2.3	Memory Information	66
5.2.4	Real Time Clock Information	66
5.2.5	Interval Recording Setup.....	67
5.2.6	Recording and Data Acquisition Modes	68
6	Data Simulation Software	70
6.1	Introduction	70
6.2	Software structure design to import measured and historical data	71
6.3	Software structure design to generate energy profiles.....	73
6.4	Software structure design to average and forecast energy profiles	75
6.5	Software structure design to calculate energy savings and payback period.....	77
7	Case Study and Results	79
7.1	Introduction	79
7.2	Site Description	80
7.2.1	Overview	80
7.2.2	Building Infrastructure	80
7.2.3	Electrical Infrastructure.....	80
7.3	Demand Profile Data Acquisition.....	85
7.3.1	Overview	85
7.3.2	Installation Procedure.....	86
7.3.3	Logger Configuration	88
7.4	Demand, Diesel Generation, PV Generation and Battery Storage Power Profiles ...	88
7.4.1	Overview	88
7.4.2	Demand Profile	89
7.4.3	Diesel Generation Profile	91
7.4.4	Solar Generation Profile.....	94
7.4.5	Battery Storage Profile	98
7.5	Measured Usage Data and Results for the geysers and stoves	102
7.5.1	Overview	102
7.5.2	Load Profile Formulation	103
7.5.3	Desalination Water Plant Demand Profile	105
7.5.4	Sanitary Hot Water Demand Profile	107
7.5.5	Cooking Demand Profile.....	111

7.5.6	Histogram Recordings	114
7.6	Energy System Topology	117
7.6.1	Overview	117
7.6.2	Micro-grid Energy Model	118
7.6.3	Power Flow Constraints	119
7.7	Financial Analysis	120
7.7.1	Overview	120
7.7.2	Potential Energy Savings	121
7.7.3	Payback Period of Heat Pump Systems	125
8	Conclusions and Recommendations	137
8.1	Overview	137
8.2	Conclusions	137
8.2.1	Design and Development	137
8.2.2	Case Study and Analysis	139
8.3	Recommendations	141
8.3.1	Future Work	141
	References	143
	Appendix A : Case study energy profile data	149
	Appendix B : Energy saving calculations for a non-ideal solar day	170
	Appendix C : Heat pump systems cost breakdown.....	174
	Appendix D : Data logger manufacturing costs	176

List of Figures

Figure 1.1	Development, analysis and reporting tasks covered in thesis	7
Figure 2.1	Appliance classification categories [11]	10
Figure 2.2	Appliance monitoring example over a period of two hours [10]	11
Figure 2.3	Different focus levels of top-down and bottom-up load modelling approaches [20] 12	
Figure 2.4	Forecasted energy demand compared with rising population numbers [29]	14
Figure 2.5	Power consumption of a traditional geyser compared to solar heating and a heat pump system [35]	16
Figure 2.6	Typical micro-grid energy system [40]	17
Figure 2.7	Technological maturity of energy types [56]	20
Figure 2.8	Lithium-ion battery price decrease over the past six years [61]	21
Figure 2.9	Discharging results of a lead acid battery at different loads [67]	22
Figure 2.10	Charging phases of a lead acid battery [67]	23
Figure 3.1	Functional block diagram describing the system topology	26
Figure 3.2	PCB designed for logic core unit	28
Figure 3.3	Event sensing circuit topology	28
Figure 3.4	Analog sensing circuit topology	29
Figure 3.5	DC output error vs input frequency of LTC1966 RMS/DC converter [75]	30
Figure 3.6	PCB designed for current sensor unit	30
Figure 3.7	Power supply connection overview	31
Figure 3.8	Microprocessor power consumption at different clock frequencies [76]	32
Figure 3.9	Capacitor charge circuit implemented for high frequency current measurements [76] 33	
Figure 3.10	Measured logic core unit sleep mode supply current [76]	34
Figure 3.11	Measured supply current of the logic core unit during an event log [76]	35
Figure 3.12	Projected battery lifetime of the logger for several event logs [76]	35

Figure 4.1	Embedded software top level program overview.....	37
Figure 4.2	Top level software flow diagram	43
Figure 4.3	System initialization software flow diagram.....	44
Figure 4.4	Real time clock flow diagram [77].....	47
Figure 4.5	Internal storage memory allocation [78]	49
Figure 4.6	Event data compressing format used.....	51
Figure 4.7	Raw event recording software flow diagram	52
Figure 4.8	Analogue data compressing format used	53
Figure 4.9	Repeated analogue recording wake-up time software flow diagram	54
Figure 4.10	Raw analogue software flow diagram	55
Figure 4.11	Event histogram memory mapping on internal memory	56
Figure 4.12	Memory map used for histogram recording modes [76]	57
Figure 4.13	Histogram event recording software flow diagram	58
Figure 4.14	Analogue histogram memory mapping on internal memory.....	59
Figure 4.15	Histogram analogue recording software flow diagram	60
Figure 4.16	Combined raw event and analogue (expert) recording software flow diagram 62	
Figure 5.1	High-level application software overview	63
Figure 5.2	Device settings accessible from the computer application.....	64
Figure 5.3	Device information available to the user via the computer application.....	65
Figure 5.4	Memory information of the logger displayed in the computer application.....	66
Figure 5.5	Real-time clock interaction options via the computer application.....	67
Figure 5.6	Interval recording setup within the computer application.....	67
Figure 5.7	Sensor trigger and data acquisition mode setup interface	68
Figure 6.1	Simulation software execution process	70
Figure 6.2	Input and output parameter overview for the software function generateMFile	72
Figure 6.3	Input and output parameter overview for the generateProfile software function 73	

Figure 6.4	Timeline example of an event and the conversion to a usage profile	75
Figure 6.5	Input and output parameters required for profile prediction simulations.....	76
Figure 6.6	Input and output parameters for profileAverage software function.....	76
Figure 6.7	Input and output parameter overview of the software function energySavings.	77
Figure 7.1	Total demand profile with the desalination plant in operation for the whole day 89	
Figure 7.2	Total demand profile with the desalination plant operating for half the day	90
Figure 7.3	Overall average daily demand profile for the period of study	90
Figure 7.4	Diesel generation profile for a sunny day with no cloud cover	91
Figure 7.5	Diesel generation profile for a cloudy and rainy day	92
Figure 7.6	Overall average daily diesel generation profiles for weekdays, Saturdays and Sundays for the study period.....	93
Figure 7.7	Overall average daily diesel generation profile for the study period	94
Figure 7.8	Solar profile on an ideal solar day.....	95
Figure 7.9	Solar generation profile for a cloudy and rainy day.....	96
Figure 7.10	Overall average daily solar generation profile for weekdays, Saturdays and Sundays for the study period.....	97
Figure 7.11	Overall average daily solar generation profile for the study period	98
Figure 7.12	Battery storage profile for an ideal sunny day with high demand.....	98
Figure 7.13	Battery storage profile for an ideal sunny day with low demand.....	99
Figure 7.14	Battery storage profile for a cloudy and rainy day	100
Figure 7.15	Overall average daily battery storage profile for weekdays, Saturdays and Sundays for the study period.....	101
Figure 7.16	Overall average daily battery storage profile for the study period	102
Figure 7.17	Formulation overview of energy profile.....	103
Figure 7.18	Desalination water plant daily demand profile for Friday the 25 th of August 2017	106

Figure 7.19	Desalination water plant daily demand profile for Saturday the 2 nd of September 2017.....	106
Figure 7.20	Desalination water plant daily demand profile for Tuesday the 5 th of September 2017	107
Figure 7.21	Geyser daily demand profile for a residence with seven people – Friday 08/09/2017	107
Figure 7.22	Geyser daily demand profile for a residence with seven people – Saturday 09/09/2017	108
Figure 7.23	Geyser daily demand profile for a residence with seven people – Sunday 10/09/2017	108
Figure 7.24	Average daily geysers demand profile for weekdays, Sundays and Saturdays for the study period.....	110
Figure 7.25	Overall average daily geysers demand profile for the study period.....	111
Figure 7.26	Average daily demand profile comparison between the geysers load, stove load and other loads at the site for the study period.....	112
Figure 7.27	Stove demand profile for Wednesday the 20 th of September 2017 for one individual stove	113
Figure 7.28	Stove power consumption profile clustering example	114
Figure 7.29	Geysers usage profile constructed using duration histogram data.....	115
Figure 7.30	Histogram of geysers usage durations for the geysers targeted in the field recordings	116
Figure 7.31	Histogram of the geysers usage durations for the geysers targeted in the field recordings, grouped according to the half-hourly daily start-time bins	117
Figure 7.32	Topology of the Robben Island micro-grid energy system	118
Figure 7.33	Total forecasted daily energy savings profile for the 6 th of September 2017	126
Figure 7.34	Diesel generator energy savings profile for the 6 th of September 2017	127
Figure 7.35	Additional battery energy gained and energy reduction profile for the 6 th of September 2017.....	127
Figure 7.36	Battery storage charge status for the 6 th of September 2017	128

Figure 7.37	Illustration of the impact on the battery storage system for the 6 th of September 2017	129
Figure 7.38	Total daily diesel generator energy savings for the 6 th of September 2017 .	129
Figure 7.39	Daily diesel generation profile with energy savings for the 6 th of September 2017	130
Figure 7.40	Heat pump system installation cost comparison.....	132
Figure 7.41	Typical diesel generator power profile as retrieved from [78].....	134
Figure 7.42	Forecasted diesel cost savings over a period of two years	135
Figure 7.43	Remaining cost after a number of days for two profile averaging methods.	136

List of Tables

Table 2.1	Cost comparison of four residential water heating systems.....	14
Table 2.2	Industry diesel generator fuel consumption approximations [54].....	19
Table 3.1	Total manufacturing costs for one complete logger device	36
Table 4.1	Command message structure.....	41
Table 4.2	Recording capabilities offered by the implemented software	50
Table 4.3	Bits allocated for each variable contained in a single raw event data packet	50
Table 4.4	Bits allocated for each variable contained in a single raw analogue data packet	53
Table 5.1	Maximum number of bins for different trigger modes available in histogram recording	69
Table 6.1	Software functions implemented for simulation purposes.....	71
Table 6.2	Description of the input parameters for generateMFile function.....	72
Table 6.3	Description of the output parameters for generateMFile function.....	72
Table 6.4	Descriptions of energy profile types available to generate through simulation .	73
Table 6.5	Description of the input parameters for profilePrediction	76
Table 6.6	Output parameters for profileAverage software function	76
Table 6.7	Description of the input parameters required by energySavings software function	77
Table 7.1	Transformer ratings at various mini-sub installations at Robben Island [79]....	81
Table 7.2	Summary of power sources at Robben Island [79]	82
Table 7.3	Residential load inventory results from the survey conducted in August 2017.	83
Table 7.4	Residential properties used at Robben Island for the study	86
Table 7.5	Summary of data recording types and durations for the study.....	88
Table 7.6	Energy contribution and operating timelines of diesel generation for a sunny and cloudy day	92
Table 7.7	Summary of total energy supplied on both ideal solar and cloudy days.....	95
Table 7.8	Typical energy consumed and supplied by the battery storage system.....	99

Table 7.9	Number of appliances in use at Robben Island	104
Table 7.10	Total average daily energy consumption of the targeted loads	112
Table 7.11	Stove power consumption for a period of a week	112
Table 7.12	Power flow and energy profile constraints applicable to the energy system at the site	119
Table 7.13	Maximum and minimum constraint values of the Robben Island energy system	120
Table 7.14	Summary of energy exchange scenarios	121
Table 7.15	Predicted diesel generator energy savings over a period of ten days	130
Table 7.16	Per day average diesel generator energy savings for the period of the study ..	131
Table 7.17	Total heat pump installation costs of two different suppliers	132
Table 7.18	Approximate diesel fuel consumption standards for a 400 kW generator [54]	134
Table 7.19	Predicted payback period for two types of energy saving results	136

List of Appendix Figures

Appendix Figure B.1	Total forecasted energy saving profile for a cloudy and rainy day ..	170
Appendix Figure B.2	Additional battery energy gained and energy reduction profile for a cloudy and rainy day	171
Appendix Figure B.3	Battery system charge status for a cloudy and rainy day.....	171
Appendix Figure B.4	Illustration of the impact on the battery storage system for a cloudy and rainy day	172
Appendix Figure B.5	Total diesel generator energy savings for a cloudy and rainy day ...	172
Appendix Figure B.6	Diesel generator profile with energy savings for a cloudy and rainy day	173

List of Appendix Tables

Appendix Table A.1 (Sunny day)	Energy supplied by the diesel generators on the 1 st of September 2017	149
Appendix Table A.2 (Cloudy day)	Energy supplied by the diesel generators on the 5 th of September 2017	150
Appendix Table A.3	Averaged energy supplied by the diesel generators for the period of the study	151
Appendix Table A.4	Energy delivered by the PV plant on the 1 st of September 2017 (Sunny day)	152
Appendix Table A.5	Energy delivered by the PV plant on the 5 th of September 2017 (Cloudy day)	153
Appendix Table A.6	Averaged energy delivered by the PV plant for the period of the study	154
Appendix Table A.7	Energy supplied/used by the battery storage system on the 1 st of September 2017 (Sunny day)	155
Appendix Table A.8	Energy supplied/used by the battery storage system on the 5 th of September 2017 (Cloudy day).....	156
Appendix Table A.9	Average energy supplied/used by the battery storage system for the period of the study	157
Appendix Table A.10	Energy demand on the 5 th of September 2017	158
Appendix Table A.11	Energy demand on the 10 th of September 2017	159
Appendix Table A.12	Average energy demand for the period of the study	160
Appendix Table A.13	Total daily energy consumed by the desalination water plant.....	161
Appendix Table A.14	Average geyser energy consumption for the period of the study	163
Appendix Table A.15	Memory map of the average geyser usage data over a period of two weeks	164
Appendix Table C.1	Heat pump system installation cost breakdown quoted by ITS Heat Pumps	174

Appendix Table C.2	Heat pump system installation cost breakdown quoted by Deacon's Solar and Plumbing	175
Appendix Table D.1	Cost of components required for one logic core unit.....	176
Appendix Table D.2	Cost of components required for one current sensor unit.....	177

List of Abbreviations

PCB	Printed Circuit Board
RTC	Real Time Clock
EEPROM	Electrically Erasable Programmable Memory
I ² C	Inter-Integrated Circuit
USB	Universal Serial Bus
SPI	Serial Peripheral Interface Bus
UART	Universal Asynchronous Receiver/Transmitter
GPIO	General-Purpose Input/output
RMS	Root Mean Squared
DC	Direct Current
ADC	Analog to Digital Converter
AC	Alternating Current
TWI	Two Wire Interface
ESD	Electrostatic Discharge
DAC	Digital to Analog Converter
PDI	Program and Debug Interface
IDE	Integrated Development Environment
GUI	Graphic User Interface
HTML	Hypertext Markup Language
AVR	Alf and Vegard's RISC
EM	Energy Management
EE	Energy Efficiency
EC	Energy Conservation
PoS	Point of Supply
NILM	Non-Intrusive Load Monitoring
CoP	Coefficient of Performance

SoC	State of Charge
DoD	Depth of Discharge
GPU	Graphics Processing Unit
ESD	Electrostatic Discharge
LED	Light-Emitting Diode
CDC	Communication Device Class
RIWHS	Robben Island World Heritage Site
RE	Renewable Energy
EMVS	Energy Management and Validation Services
UNESCO	United Nations Educational, Scientific and Cultural Organization
LV	Low Voltage
MV	Medium Voltage
PV	Photo Voltaic
CFL	Compact Fluorescent Lamp
PF	Power Factor

1 Project Overview

1.1 Introduction

Rising electricity costs and the urgent need to pursue environmentally sustainable usage of electrical energy have given rise to increasing emphasis on Energy Management (EM) and Energy Efficiency (EE) in recent years. The Measurement and Verification (M&V) scoping studies, baseline characterisation and performance assessment exercises associated with EM and Energy Conservation (EC) interventions require detailed load modelling [1].

Load modelling has historically focussed predominantly on applications related to power system planning and operations, including reticulation, distribution and transmission system design, load forecasting for optimal dispatch, etc., using aggregated load data measured at a Point of Supply (PoS). Conventional aggregated load data are, however, of limited use for EM applications, which typically target specific load technologies or load classes. De-aggregating PoS load profiles to extract models for individual loads or load classes is highly complex, requiring the application of advanced machine learning techniques [2].

Conventional instrumentation for load profile recording typically logs the energy consumption of one or more loads using a predetermined logging interval. For long-term monitoring, such instrumentation requires extensive volatile storage capacity, which increases manufacturing costs, system complexity, power consumption and data retrieval costs. Power measurement requires both voltage and current signals. This increases installation costs and results in intrusive load connections that represent potential safety risks in environments associated with the residential and commercial sectors.

The energy consumption profiles associated with most loads, especially in the commercial and residential sectors, exhibit pronounced daily, weekly and seasonal cycles. From a load modelling perspective, this implies that load data must ideally be acquired continuously over an extensive period, e.g. one year, in order to model the cyclic behaviour adequately. Distributed loads with usage patterns determined by human behaviour, such as appliances in residences, further require that load data are acquired for a statistically significant sample of individual loads. As a result of these factors, together with the high capital costs, installation costs and data retrieval costs associated with conventional load profile logging instrumentation, load surveys targeting individual load classes are expensive and time consuming [3].

This project aims at easing load surveys by the development of an intelligent histogram event logger for de-aggregated load modelling applications. Strong focus is placed in this project on logger functionalities such as non-intrusiveness, low-cost and power consumption characteristics. The system is implemented in an independent micro-grid energy system, answering questions related to various energy subsystems and highlighting energy saving possibilities. Historic aggregated data measured at the PoS of the micro-grid system is retrieved, analysed and averaged to forecast the payback period of replacing the resistive element of conventional geysers with heat pump technology.

1.2 Project Motivation

Despite advances in recent years, load characterisation in the context of EM and for implementing bottom-up load-modelling approaches [4] [5] remains constrained by the high cost of acquiring de-aggregated load data. While modern technology makes it possible to reduce the manufacturing cost of conventional load monitoring devices, the overall cost of deploying these devices on a statistically significant scale remains high due to the costs associated with the installation, data retrieval and data processing [3]. As a result, studies aimed at modelling loads classes in the residential sector, for instance, often rely on statistically insignificant sample sizes [3] [4]. Addressing these issues requires innovative approaches in the functional design of load monitoring devices.

It is important to identify key factors required within the functional design of modern load monitoring devices based on the statistical representations required by EE and EM interventions. The usage event data of individual appliances within the residential environment remains the problem for most bottom-up load-modelling studies. Energy consumption models are easily accumulated when the usage event data are known [6]. Usage event data consist of on/off states and requires only the name plate power rating value for load profile construction. This eliminates the requirement of power measuring circuitry within load monitoring devices. Recording the on/off states introduces the following additional advantages within these devices:

- Storage requirements are reduced, as events rather than a continuous sequence of data values are recorded. This reduces the use of non-volatile storage, which reduces power consumption.
- The system can make full use of the power management capabilities of modern microprocessors. The on-board microprocessor typically operates in sleep mode and only

wakes when an event is registered through an interrupt signal. This makes it possible to design a battery-powered device that can operate for an extended period.

- Low-cost, non-intrusive current sensors, i.e. without galvanic connections, can be used. This also reduces installation costs and mitigates the safety risks associated with the installation.
- Power consumption is reduced by eliminating the Analogue to Digital Conversion (ADC) process.

Histogram logging is introduced to further reduce components required for individual load class monitoring devices. A histogram is essentially an estimate of the probability distribution of a continuous variable [7] [8]. The data range is divided into a number of regions or bins and the data samples are allocated to the various bins, yielding a frequency of occurrence value for each bin. The bins are adjacent and non-overlapping, but need not be of equal size. Various methodologies have been proposed for selecting the number of bins and bin sizes, including Freedman-Diaconis and Scott techniques [7] [8] [9].

By recording a histogram of usage events, rather than a sequence of events, the recorded data are presented in a format that is compatible with these statistical modelling approaches. Depending on the number of bins, histogram recording reduces the on-board storage requirements of the logging device and the associated data retrieval overheads dramatically. A foremost contribution to the projects motivation is that commercially available load monitoring devices do not at present offer the advantages of histogram recording. Incorporating the concept of histogram recording into the design of an event-based load-monitoring logger requires careful consideration of a number of factors, including the following:

- The optimal number of histogram bins and individual bin sizes are determined by the nature of the data. The bin number and bin sizes must therefore be software programmable in order to customise the logging device for specific load categories. This implies that the embedded control program must have the capability to configure the data storage memory map depending on the desired bin number and bin size parameters.
- In the most basic form, an event is defined by two parameters, namely a start timestamp and an end timestamp. These can be translated by the embedded control program to alternative representations for storage, such as a start timestamp and an event duration, which is more suitable for modelling load behaviour.

The proposed individual load data acquiring techniques give rise to key motivations behind this project. The first motivation is to develop an intelligent low-cost histogram load monitoring device with low power consumption characteristics. The second motivation is to test the proposed system on a micro energy system to find the influence of various appliances on the energy system. These motivations are meant to provide realistic load forecasting capabilities and a better understanding of the usage profiles of certain residential appliances.

The core set of goals for this project include:

- Provide a new basis for load monitoring devices which is more affordable for individual load modelling applications.
- Proof the concept and efficiency of histogram event data logging.
- Develop analysis tools to predict energy savings and payback period of replacing targeted residential appliances with more efficient alternatives.

This project aims to demonstrate and motivate the efficacy of the proposed system on an independent energy system in need of EM and EE interventions.

1.3 Project Description

1.3.1 Research Objectives

In view of the project motivations, the primary research objectives are listed below:

- To perform a literature study to provide a background of relevant load modelling topics, including non-intrusive load monitoring technologies, load profile forecasting and histogram load profile representations.
- To research alternative residential appliances used in the case study. The focus was placed on heat pump systems as a replacement for traditional geysers. This topic also includes research done on the coefficient of performance of heat pump systems.
- To analyse and understand the mathematical formulation of micro energy systems.
- To research the efficiency and fuel consumption of diesel generators implemented in a micro-grid topology.
- Investigate historical data required for energy saving simulation software.

The project requires research and development of embedded software for the proposed hardware. Additional development is required to retrieve and analyse the data accumulated. The achievement of these objectives will demonstrate the effectiveness of histogram load monitoring technology. This will lead to more affordable EE and EM intervention studies, as well as more reliable de-aggregated load models. The results will be applied to gain knowledge of different subsystems within in micro-grid system. This will highlight possible EE interventions and will also provide insight into the installation of heat pump systems and the payback period of such systems.

1.3.2 Key Questions

The project aims to answer the follow set of key questions:

- Is the design and development of the proposed system viable with the view to histogram event recording?
- What hardware design factors are important to minimize the cost for de-aggregated load monitoring?
- How does energy consumption profiles generated by histogram event recording compare to profiles generated by raw event recording?
- What factors influences the battery power consumption of modern load monitoring devices, and how can battery lifetime be expanded by histogram event logging?
- How do different residential loads within a micro-grid system influence the system when replaced with more energy efficient alternatives? What is the contribution of geyser and cooking loads towards the total demand in a micro-grid system?
- How does energy savings affect solar and battery storage systems within a micro-grid system?
- What are the financial advantages associated with energy savings in a micro-grid energy system depended on diesel generators as energy supplies? What will the payback period be for the replacement of resistive elements of conventional geysers with heat pump systems?

1.3.3 Research Tasks

The research objectives and key questions are answered and achieved by executing the following primary tasks:

- Develop logger hardware with the following primary characteristics: a small physical footprint; low manufacturing costs and low battery power consumption.
- Design and implement sensor hardware to be used for event triggering and analogue measurements.
- Construct embedded software for logger hardware, consisting of various event recording and low power consumption operating modes.
- Develop a software application, implemented as a GUI on a host computer, for system configuration and data retrieval.
- Formulate a set of energy saving scenarios applicable to a micro-grid energy system with multiple subsystems.
- Develop simulation software, able to predict energy savings within a micro-grid energy system using historical energy consumption data.
- Research the cost of generating electricity using diesel generators in an isolated energy system and forecast the payback period when replacing traditional geysers with modern heat pump systems.
- Investigate additional EE and EM interventions applicable to the case study.
- Analyse the results delivered by the case study. This include comparisons between raw event recording data and histogram event recording data.
- Derive a conclusion on the viability of histogram event recording and the effects caused by averaging energy consumption profiles.

The main development, analysis and reporting tasks are listed in Figure 1.1. The design and development phase cover all hardware designs, embedded software development, computer application design and the simulation software application. All results obtained are listed in the case study. The final report layout is described in section 1.4 below.

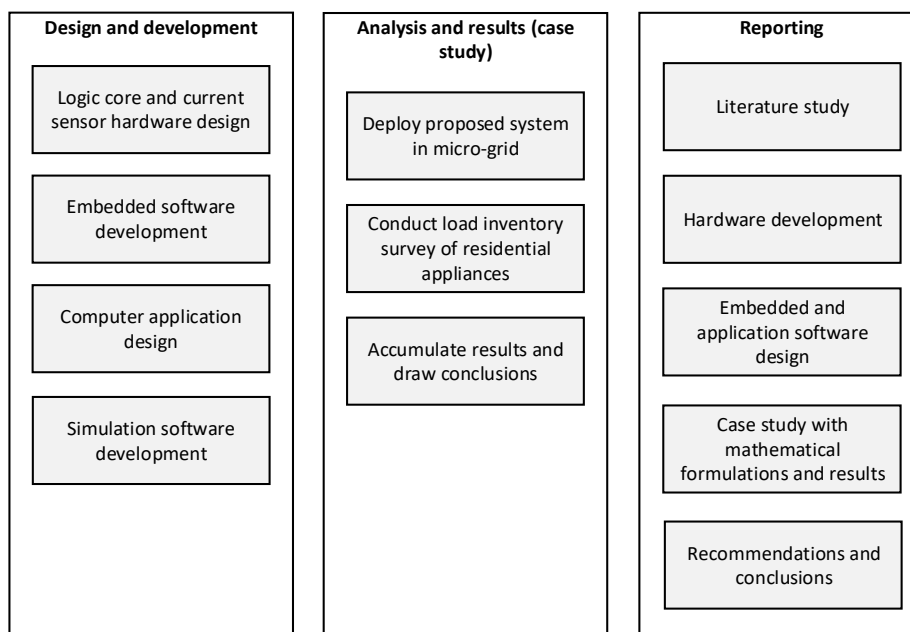


Figure 1.1 Development, analysis and reporting tasks covered in thesis

1.4 Thesis Structure

The remainder of this document is structured as follows:

- *Chapter 2: Literature Review*

The relevant literature topics are reviewed here. This topic includes residential load modelling, residential hot water systems, energy systems and software development platforms.

- *Chapter 3: System Design*

The logic core and current sensor hardware designed and developed for the proposed system are specified in this chapter. It elaborates on the printed circuit board (PCB) layouts for both the hardware modules. A short cost analysis and a thorough power consumption audit is provided.

- *Chapter 4: Embedded Software Implementation*

The embedded software implementation is presented here, setting out the various communication interfaces, real time clock interface, system non-volatile memory, sensor inputs and various data acquisition modes.

- *Chapter 5: Application Software*

This chapter comprises the development of application software required to retrieve data and set up various interfaces. Each interface is explained in terms of its functionality towards the proposed hardware. The application forms the link between hardware and simulation software.

- *Chapter 6: Data Simulation Software*

Simulation software is thoroughly defined and specified in this chapter. This includes software structures required to analyse and model data retrieved as historical and real time measured data.

- *Chapter 7: Case Study and Results*

This chapter aims to provide the results and answers to key questions. Details of the site used in the case study is given in the form of a load inventory audit. The case study defines the energy system with various subsystems of an independent micro-grid. A set of scenarios is formulated to find the possible energy savings of each subsystem. These are used in simulation software to analyse and deliver final results as set out by the key questions above.

- *Chapter 8: Conclusions and Recommendations*

The conclusions drawn from the development of the proposed system and case study are presented in this final chapter. Recommendations are made for further enhancements on the designed system.

2 Literature Review

2.1 Overview

The literature review presents research done on different fields applicable to this project. It explores related work done by referring to various literature sources and elaborates on factors required for the development of the proposed system. Technical options are described to meet the project objectives as well as software development tools required to simulate and answer the key questions. The remainder of this chapter elaborates on the following fields:

- Residential Load Modelling

This section elaborates on research done on appliance load monitoring in the residential sector. It discusses non-intrusive load monitoring technology and motivates the reason behind it. Research is also presented on the prediction of load profiles, emphasizing top-down and bottom up load modelling approaches.

- Residential Hot Water Systems

This section presents information found on residential geysers. It focusses on the replacement of the traditional hot water system with new heat pump technology. It includes a price comparison of geysers currently available and presents parameters required to calculate the efficiency of heat pump systems.

- Micro-grid Systems

Research around micro-grids, diesel generators and battery storage systems are presented in this section. An islanded micro-grid is researched with the view of grid independence. Smart grids are also reviewed here. Information of diesel generators are provided as a baseload energy source within micro-grid energy systems. Battery storage systems typically used in micro-grid systems are included, as well as technical parameters required for the modelling of battery systems.

- Software Development Platforms and Applications

Short descriptions of the development platforms used for this project are presented in this section. It includes embedded software platforms, hardware development environments and simulation platforms. Only the main platforms used are listed.

2.2 Residential Load Modelling

2.2.1 Appliance Load Monitoring

Appliance load monitoring is a process of analysing the voltage and current consumed by one or more appliances. Usually load monitoring technology generates load curves from multiple appliances as modern load monitoring technologies are simply too expensive to monitor individual appliances. Identifying individual loads from one load curve is challenging, as it depends predominantly on the load signatures, which are further characterized by the appliance category.

Work in this field was started by George Hart [10] in 1992, where his focus was to classify individual appliances based on their operational state. He originally proposed three different categories:

- *On/Off*: Loads with two states, but operating at fixed power when on (Figure 2.1 (a)).
- *Finite State Machine*: Loads with repeatable switching power levels (Figure 2.1 (b)).
- *Continuously Variable*: Loads with no fixed pattern of states (Figure 2.1 (c)).

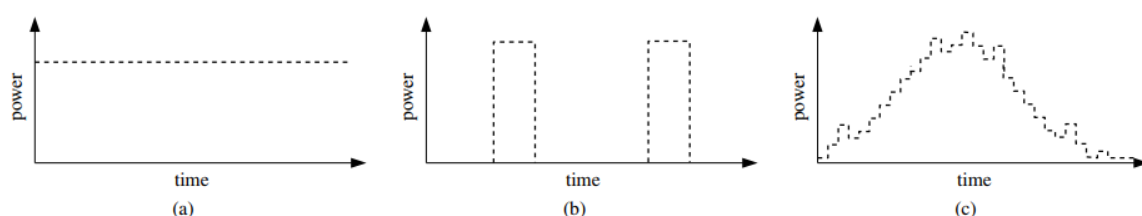


Figure 2.1 Appliance classification categories [11]

Hart developed and patented a non-intrusive appliance monitoring device to retrieve the power consumption vs. time profile and to demonstrate his classification techniques. Figure 2.2 shows a typical example for a single-family home over a two-hour period [10].

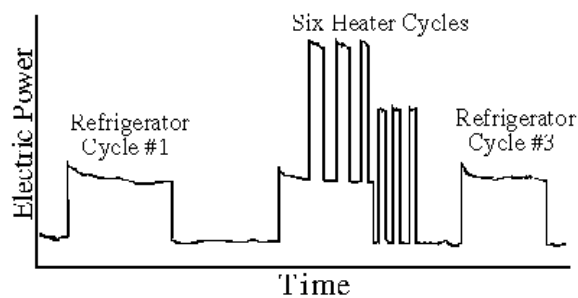


Figure 2.2 *Appliance monitoring example over a period of two hours [10]*

Since then, research has built upon Hart's work, improving classifications to suit the load profile of modern appliances. Recent research also added a fourth category known as Permanent Consumer Devices which is described as loads that are constantly active for a long period [12] [13]. Advanced load monitoring techniques, like steady-state, transient and harmonic analysis [14] are all used to improve modern load monitoring technologies. One example of research in this field is the evolving smart metering systems, offering many operational advantages for energy utilities, including [15]:

- enabling automated collection of fine-grained consumption data, eliminating premise visits for manual readings. This technology forms part of the Internet of Things (IoT) network and research as mentioned in [16].
- producing pricing schemes depending on the time-of-day, reducing electricity demands during peak times.

2.2.2 Non-intrusive Load Monitoring Technology

Since Hart's prototype, Non-Intrusive Load Monitoring (NILM) has become the more practical option for most researchers [13] [17] [18]. The main reason for this metering approach is that the meter does not cross the customer-utility boundary, and therefore never poses a safety threat.

Existing modern NILM devices typically consist of multiple memory storage devices which make them very expensive for de-aggregated load monitoring. To combat the high cost of these devices, researchers have turned their focus to low-cost and easy maintenance NILM devices [19]. Low-cost NILM devices have the ability to service rural and low-income consumers where expensive home automation systems cannot be implemented.

2.2.3 Load Profile Forecasting

Load profile forecasting generally requires information processing and knowledge ordering to use what is known about the past to predict what will happen in the future. A number of load profile forecasting strategies exist and can be categorised into top-down and bottom-up modelling approaches. The two approaches have been designed for different purposes and have a different theoretical background. In spite of the completely different properties and results, researchers have argued that top-down and bottom-up approaches can be integrated or linked [20] [21]. Further combinations of approaches or integrated models, have recently been developed to assist with environmental impact issues such as greenhouse gas emissions [20].

Literature [20] [21] [22] [23] provides good explanations of the two modelling approaches from a load profile forecasting perspective as well as an energy economic focus. Top-down modelling generally considers all important economic interactions, and is based on macroeconomic modelling and other important factors such as climate and population. These models typically focus on the energy consumption and the effects caused by long term residential changes and to forecast supply requirements [20] [22] [23]. Bottom-up is based on individual house hold energy consumption or load profiles to determine and extrapolate the results to represent a district or nation [20] [22] [23]. Jacobsen [20] demonstrates the two methods and how their focus differs by the illustration shown in Figure 2.3.

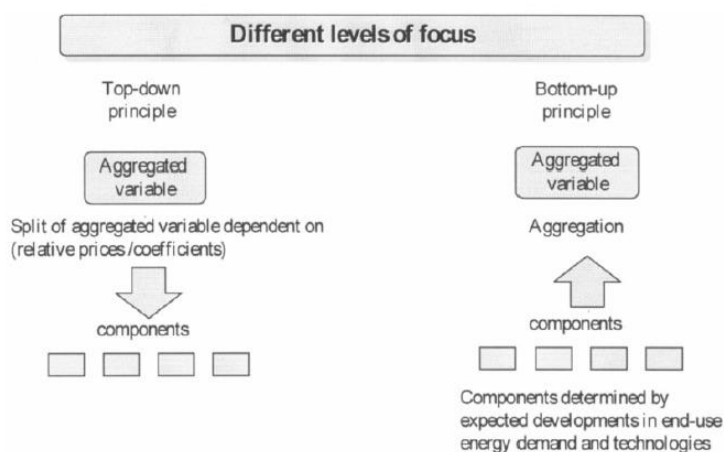


Figure 2.3 Different focus levels of top-down and bottom-up load modelling approaches [20]

Bottom-up models are typically limited by the extensive requirements of data about the different consumer appliances and consumers themselves. The de-aggregated data required is usually not available and differs according to the specific research or end goal. For example, the bottom-up model constructed in [4] requires the number of occupants per household or

property while other references [6] [24] require knowledge of each individual's appliances, name plate power ratings, time-of-use profiles and location of properties. Other studies, like reference [25], has made compromises in the accuracy of their results by building their bottom-up model with incomplete data sets. Recent studies have managed to completely bypass the need for detailed data by using representative data samples and statistical averages [26]. This results in a realistic electricity consumption profile forecast that can be constructed by only using generally available appliance information and time-of-use profiles. The less accurate results are compensated by reducing the data requirements for the model.

2.3 Residential Hot Water Systems

2.3.1 Overview

Water heating is a thermodynamic process that typically happens at least once or twice a day in most residential dwellings. Typical domestic uses of hot water include cleaning, cooking and space heating supplied by various modern electrical appliances to heat or boil water such as electric kettles and traditional hot water cylinders. Most appliances make use of high power resistance elements to supply the necessary energy to heat the water to a desired temperature.

Energy management and energy efficiency research are focussing on new hot water system technologies to replace the existing hot water cylinders with solar energy, heat pumps, hot water heat recycling and geothermal heating systems. This chapter focusses on research done to replace existing traditional hot water cylinders with heat pump technology. It further elaborates on the costs and benefits of both systems used in the case study.

2.3.2 Traditional Hot Water Cylinders

The traditional distributed hot water cylinder can be considered one of the most energy-intensive residential loads, followed by appliances such as electric stoves, swimming pool pumps, heaters, kettles and toasters.

Although the current global population growth rate is decreasing since the 1960's, the population is still growing at a rate of approximately 1.11% per year [27]. This continued increase in the human population is projected to reach 8.6 billion by 2030 and to further increase to 9.8 billion in 2050 [27]. With these rapidly evolving population patterns and figures, the demand for residential electric energy are growing exponentially [28]. An older reference [29] forecasted the energy-demand compared with the growing global population figures as shown in Figure 2.4. For South Africa alone, the total electricity energy demand grew approximately

50% from 1994 to 2007 [30]. South Africa's power utility, Eskom, had to resort to load shedding during peak demand hours as the company was simply not prepared for the population growth and the increase in energy demand.

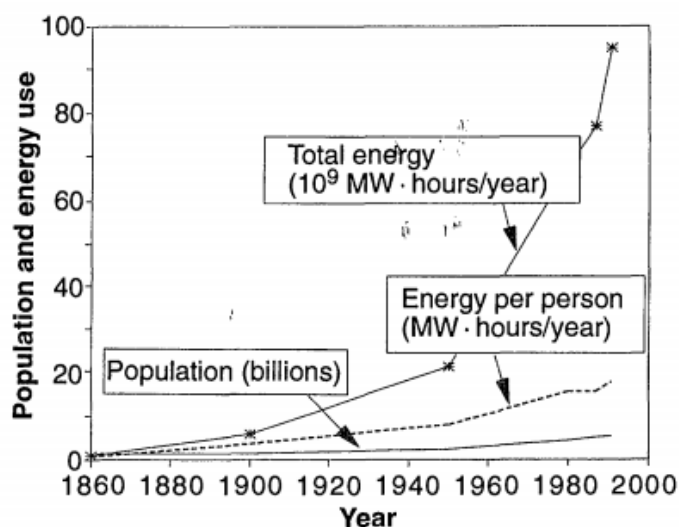


Figure 2.4 Forecasted energy demand compared with rising population numbers [29]

The energy demand of most energy-intensive appliances can be shifted in time without influencing the users comfort level [31]. In South Africa, residential geyser load was shifted by Eskom to reduce the country's peak demand. Eskom encouraged their residential customers to switch their geysers off during peak hours [32]. Most South African residents rely on the less efficient traditional geyser, as replacing them with solar or heat pump systems is simply unaffordable.

In South Africa, the cost of these conventional geysers typically ranges between R1 300 and R3 000 and is clearly the most popular choice for residential use compared to alternatives. Table 2.1 provides the cost comparison between four different water heating technologies available in South Africa [33].

Table 2.1 Cost comparison of four residential water heating systems

Item	Price (R)
Conventional geysers	1 300 – 3 000
In-line heating systems	3 000 – 4 000
Heat pump systems	8 000 – 20 000
Solar water heating systems	12 000 – 25 000

The prices mentioned in [33] and in Table 2.1 were recorded in 2012 and depends on the installation size, and the environmental and system variables. The electricity energy demand of these conventional geysers depends on external factors such as water capacity, ambient temperature and system insulation. These conventional geysers only consume electric energy either through standing losses or through hot water consumption. The alternative, in-line heating systems, only consumes electric energy during hot water consumption while heat-pump technology focusses on consuming less electrical energy to heat the same amount of water.

2.3.3 Heat-pump Technology

Heat pump systems used for water heating can generally be classified into ground source heat pumps, chemical heat pumps, air source heat pumps or electrically driven heat pumps [34]. In South Africa, most heat pump water systems are electrically driven and consists of a scroll compressor, evaporator, condenser and an expansion valve. The only electrical energy used is to drive the compressor unit and a small water pump to circulate water through the condenser unit [35].

As given in Table 2.1, the price of heat pump system can vary widely as the costs directly depends on the heating capacity of the system. For financial advantages, the coefficient of performance (COP) is required to calculate the efficiency of the heat pump system. The COP is a ratio of useful heating or cooling provided to work required. The COP for heating and cooling are different as the heat reservoir of interest is different. The COP ratio for geyser heat pump systems is given by [34]:

$$COP = \frac{|Q_H|}{W} = \frac{|Q_C| + W}{W}$$

where Q_C denotes the useful heat from the cold reservoir and Q_H denotes the heat supplied to the hot reservoir. W denotes the mechanical work performed by the compressor unit.

For the climate conditions in South Africa, the COP ratio of a heat pump water heater varies between 2 and 5. Most researchers and heat pump system providers use an average COP ratio of 3 [34], meaning that 1 kW of electrical power is required to produce 3 kW of heating power. This typically provides an energy saving of up to two thirds of energy consumed by electrical resistance water heaters.

A study aimed at the energy consumption of currently available water heating solutions found that solar heating and heat pump water heating solutions are very similar in terms of energy consumption. Comparing them with electrical resistance water heaters, an average COP ratio

of 3 can be confirmed. Figure 2.5 shows a comparison of the most popular water heating solutions currently installed in the residential sector with regards to annual power consumption [35].

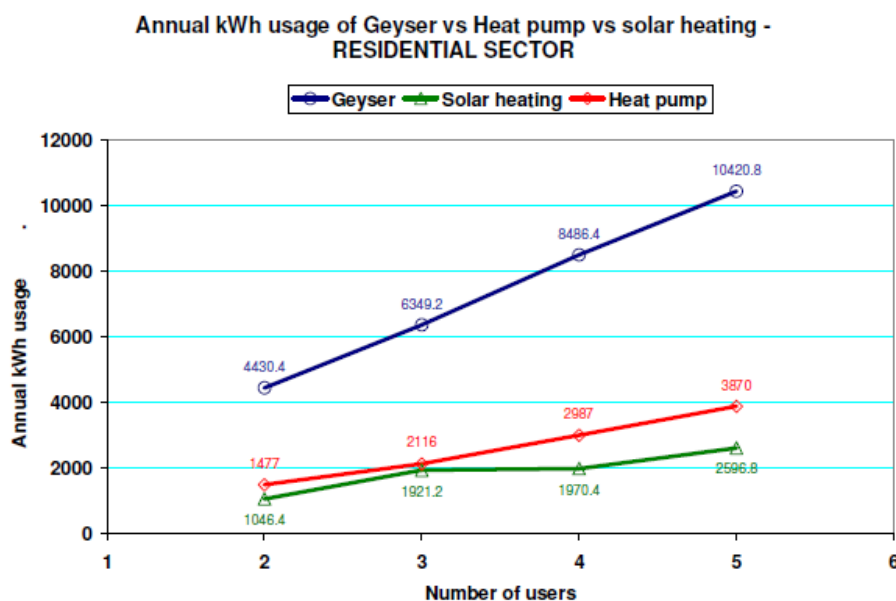


Figure 2.5 Power consumption of a traditional geyser compared to solar heating and a heat pump system [35]

2.4 Micro-grid Systems

2.4.1 Introduction

A micro-grid is defined as a localized grouping or cluster of electricity sources that supply energy to various loads. A micro-grid has the ability to be disconnected and independent from the traditional centralized electrical grid, but can also be grid connected. Therefore, micro-grids typically operate parallel to national electrical grids and should be able to operate at stable operating frequencies and meet grid-code requirements.

Micro-grid systems are typically proposed as a solution to the conundrum of integrating small-scale renewable projects with macro-grids without disrupting the network [36]. This typically reduces the dependency on fossil fuels, and puts more focus on renewable projects. Remarkable research has been done on micro-grid energy systems with major projects underway, for example [37] [38] [39].

The main components of a micro-grid usually contain a combination of energy sources such as mini-hydro plants, solar cells, wind energy, fuel cells and energy storage systems [40] [41]. A common micro-grid topology is given in Figure 2.6.

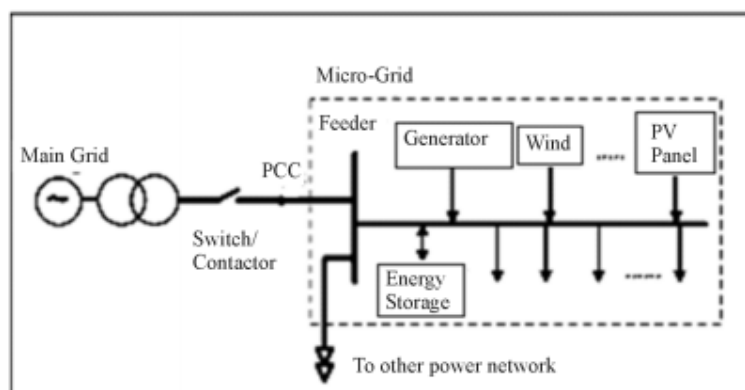


Figure 2.6 Typical micro-grid energy system [40]

Some micro-grid energy systems are classified as remote “off-grid” micro-grids, also known as islanded operation, meaning that these energy systems never connect to a centralized electrical grid. The reasons behind such a system would mostly be economical issue or related to geographic location. An “off-grid” micro-grid generally requires an energy source capable of supplying the baseload and has a maximum rated value greater than the total load. Renewable energy sources are mostly run parallel to diesel generators in “off-grid” micro-grids to reduce the use of fossil fuels and the impact on the environment.

Various methods and control techniques have been introduced and researched to control the multiple energy sources within an islanded micro-grid energy system [42] [43] [44] [45] [46]. Micro-grid control can be classified by means of a hierarchical control scheme. The control scheme consists of three control levels described as follows [47] [48] [49]:

- *Primary control*: Designed to satisfy requirements such as stabilization of operating voltages and frequencies, plug and play capabilities, proper sharing of active and reactive power between sources and to mitigate circulating currents.
- *Secondary control*: Typically used to restore the micro-grids voltage and frequency and to compensate for fluctuations caused by the primary controller.
- *Tertiary control*: This control level considers the optimal financial concerns in the operation. It also regulates the power flow between the micro-grid and main grid.

Controlling of micro-grids is often incorporated with smart controlling technology which is better known as smart grids. A smart grid is defined as an advanced 20th century power grid with two-way flows of electricity and information [50]. It aims to generate an automated and distributed energy delivery network, with more efficient ways to deliver power. This is accomplished by implementing the following technical systems which thoroughly defines a smart grid energy system [50]:

- *Smart infrastructure system*: Defined as the energy, communication and information infrastructure required for advance power delivery and information gathering.
- *Smart management system*: Defined as the subsystem within a smart grid topology to intelligently manage and control the system.
- *Smart protection system*: Defined as the subsystem that provides grid reliability and failure protection. This system is also responsible to provide protection of privacy.

2.4.2 Diesel Generators and Fuel Consumption

2.4.2.1 Overview

Diesel generators are one of the most common energy sources found in an islanded micro-grid energy system. Diesel generators are typically running at full capacity within two minutes from starting, which makes them the ideal standby energy sources. Whilst diesel generators are expensive in fuel and maintenance terms, they are normally only operating for a few hours per week. The greater amount of the baseload is typically maintained by renewable energy sources where diesel generators are mostly responsible to compensate PV and wind system fluctuations. Examples of such systems exist in literature [51] and [52].

Although micro-grids integrate and promote renewable energy sources, the dependency on fossil fuels remains a reality. To further reduce the impact on the environment and prepare for load growth, attempts to reduce fossil fuel consumption persist [53]. Only two options exist to further reduce the dependency on fossil fuels which is either by reducing the load or enhancing the efficiency of the diesel generators.

2.4.2.2 Fuel Consumption

Exact figures are required to determine efficiency figures of diesel generators. The efficiency is typically used to determine fuel consumption figures, leading to fuel cost calculations.

Standard approximations exist to determine the fuel consumption for different sizes of generator sets. The fuel consumption depends on the load of the generator. Table 2.2 shows a typical fuel consumption approximation used in industry [54]:

Table 2.2 Industry diesel generator fuel consumption approximations [54]

Generator Size	Approximate Diesel Fuel Consumption			
	¼ Load [L/h]	½ Load [L/h]	¾ Load [L/h]	Full Load [L/h]
8kW/10kVA	0.9	1.2	1.7	2.1
10kW/12kVA	1.0	1.4	2.1	2.6
12kW/15kVA	1.3	1.8	2.6	3.2
16kW/20kVA	1.7	2.4	3.5	4.3
20kW/25kVA	2.1	3.0	4.3	5.4
24kW/30kVA	2.6	3.6	5.2	6.4
32kW/40kVA	3.4	4.8	7.0	8.6
40kW/50kVA	4.3	6.0	8.6	10.7
60kW/75kVA	6.4	9.0	12.7	16.1
80kW/100kVA	8.3	11.9	16.1	21.4
120kW/150kVA	10.9	17.3	24.1	32.1
160kW/200kVA	14.1	22.9	32.7	42.8
200kW/250kVA	17.4	28.6	40.8	53.5
280kW/350kVA	23.7	39.3	56.0	74.9
400kW/500kVA	33.3	55.6	79.6	107.0

2.4.3 Battery Storage Systems

2.4.3.1 Overview

Battery storage systems are integrated into micro-grid systems to store energy for periods where renewable energy sources are unable to produce energy. Literature unanimously considers batteries as the most viable solution to date, as this form of storage has progressed faster than other alternatives. Reviews of other technologies reveals batteries to be the most mature energy storage solution currently available for the commercial sector [55] [56] [57].

Material availability for mass production of batteries remains a barrier for the energy industry. Various natural elements and their energy storage capability has been studied. Research in the field of technological maturity of energy storage types are summarised in Figure 2.7 [56]. According to this figure, only two elements are mature enough for energy storage usage. However, the majority of elements are in the development stage.

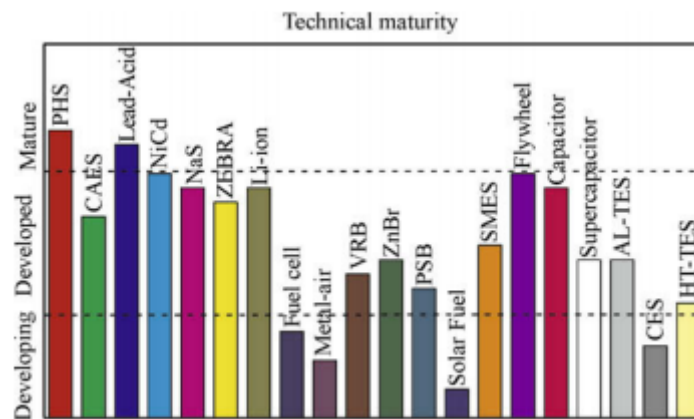


Figure 2.7 *Technological maturity of energy types* [56]

In South Africa, most battery storage facilities contain Li-Ion batteries due to characteristics such as high energy density and their physical light weight. These batteries are also well known for their high discharge capabilities and the ability to withstand overcharge and extensive discharge usage cycles [58]. The use of Li-Ion batteries for consumer electronics, electric vehicles and energy storage banks within small and intermediate renewable energy projects has grown extensively over the last decade [59] [60].

Due to high demand of Li-Ion batteries in the last decade, battery manufacturers produced large amounts of these batteries for the anticipated deployment of electrical vehicles. However, the manufacturing industry suffered from oversupply after lower electrical vehicle sales over this period. This caused a significant reduction in the prices of lithium-ion batteries worldwide. Figure 2.8 shows a survey done by *Bloomberg* of the prices for Li-Ion batteries [61].

Batteries have various parameters and conditions that need to be followed during charging and discharging. The remainder of this section describes research done on the formulation of battery parameters required to control batteries without damaging them.

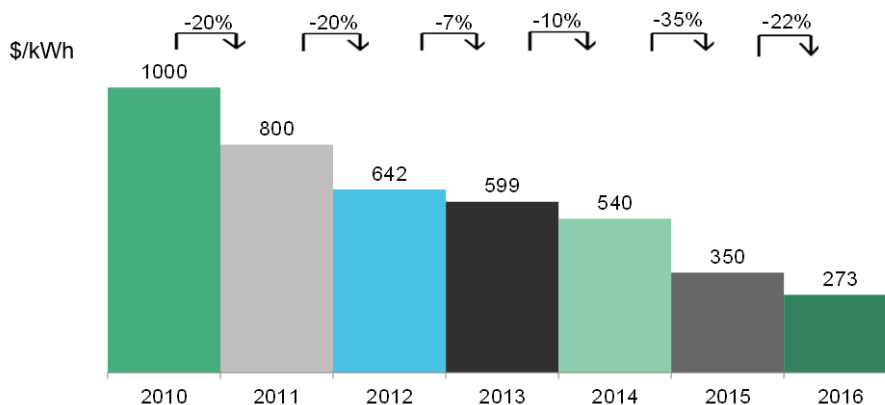


Figure 2.8 *Lithium-ion battery price decrease over the past six years [61]*

2.4.3.2 State of Charge and C-Rating

The current battery capacity is compared to the nominal capacity to provide the State of Charge (SoC) ratio of a battery. The nominal capacity represents the maximum charge capacity which is typically provided by the battery manufacturer. The SoC is defined by [62] as

$$SOC(t) = \frac{Q(t)}{Q_n}$$

where $Q(t)$ and Q_n denotes the current capacity and nominal capacity respectively.

Normally each battery storage system will have its unique SoC due to different battery characteristics and the amount of batteries. However, SoC estimations can be made to predict battery behaviour in renewable energy projects resulting in extended battery service life. Various mathematical SoC estimating formulations are covered in literature [62] [63] [64] [65] [66].

Another parameter, the C-rating, is introduced to govern the charge and discharge rates of a battery as given in [58]:

$$C = \frac{\text{charge/discharge current}}{Q_n}$$

The capacity of a battery is typically rated at 1C, meaning that a battery rated at 1Ah, will provide 1A for one hour. To demonstrate the difference between various C ratings, the performance of a lead acid battery is examined at different loads, thereby generating different discharging times as given in Figure 2.9 [67].

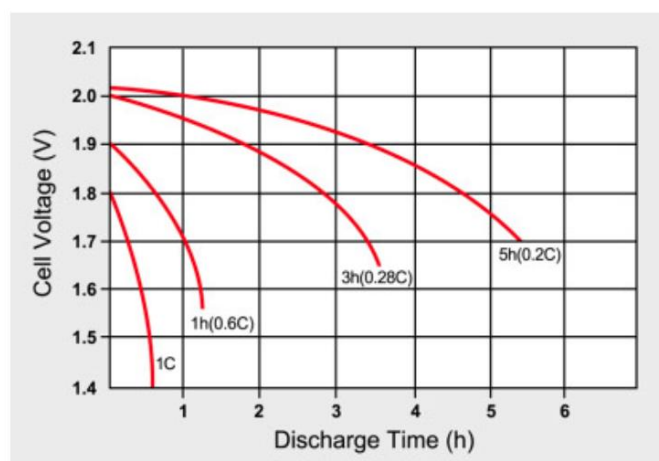


Figure 2.9 Discharging results of a lead acid battery at different loads [67]

Figure 2.9 shows that the voltage of a battery decreases as the battery discharges. This illustrates the reason for battery ratings given in Ah and not Wh which is dependent on the voltage. Using the datasheet and Peukert's research [68], the battery capacity at a given current can be calculated.

2.4.3.3 Charge/Discharge Boundaries

The charging process of commercial batteries typically requires a charge controller. A charge controller will distribute incoming energy to all the individual batteries in the battery storage system. It also observes battery parameters such as voltages, SoC and depth-of-discharge (DoD) to protect the batteries. Battery charging typically occur in three stages. These stages are known as [67]:

- *Constant current charge*: The initial charging phase of a battery. The battery will typically reach a 70% SoC within a period dependent on the type of battery.
- *Topping charge*: The remainder 30% is slowly filled during this stage. The duration of this stage is longer than the constant current charge stage.
- *Float charge*: The battery remains in this stage once fully charged to keep the battery at a 100% SoC. The float charge typically exposes the battery cells to a slight overcharge voltage to maintain an even voltage between all cells.

The battery voltage and charging current of a lead acid battery is shown in Figure 2.10 to illustrate the common three charging stages of a battery [67].

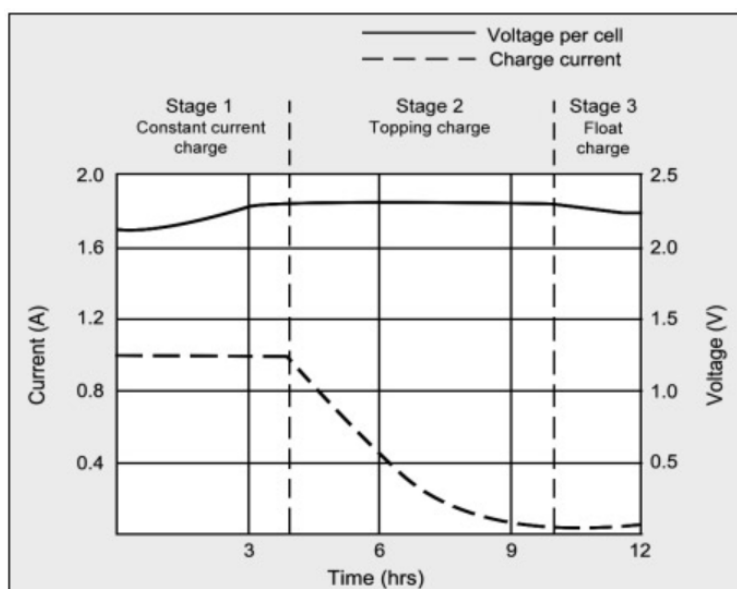


Figure 2.10 Charging phases of a lead acid battery [67]

The DoD represents the percentage of the battery that is discharged and is the complement of SoC, for example if a battery has a DoD of 30%, the SoC is 70%. To increase battery service life and to avoid internal damage, batteries are seldom fully discharged. Most battery manufacturers rate their batteries with a DoD of 80%.

2.5 Software Development Platforms and Applications

2.5.1 Overview

Various development platforms were researched to develop the required software and hardware. This section includes short descriptions of application environments, hardware development environments and simulation software suitable for this project.

2.5.2 Atmel Studio

Atmel Studio is an open-source C-language programming environment for developing and debugging all AVR and Atmel microprocessor products [69]. It offers access to various integrated tools, project examples and software extensions. Atmel Studio interfaces to a debugging tool which connects to the Atmel hardware.

2.5.3 Eclipse

Eclipse is an open-source Integrated Development Environment (IDE) to develop software applications. Eclipse offers extensible frameworks and tools to support various programming

languages, such as C, C++, Perl, Ruby and JavaScript [70]. The environment supports various plug-ins to make it compatible with a wide range of other software platforms.

2.5.4 Qt Creator

Qt Creator is a complete IDE to create computer applications [71]. It is a free open-source framework with multi desktop functionalities. It supports the creation of Windows, Linux and Android based GUI's through C++ libraries. It is also capable of developing web-based applications using Hypertext Markup Language (HTML) 5.

2.5.5 Altium Designer

Altium Designer is a Printed Circuit Board (PCB) development software package [72]. It offers integrated circuit design, embedded software design and associated library and release management functions. It includes a three-dimensional model builder for PCB illustrations.

2.5.6 Matlab

Matlab is an IDE for iterative analysis and design processes. It features its own programming language that expresses matrix and array mathematics directly [73]. It offers the ability to execute analysis on clusters, GPUs and clouds and display advanced graphs and images. It includes a simulation environment called Simulink and toolbox sets for additional features and user like optimisation.

2.5.7 Python

Python is a general-purpose software development language. It aims to reduce the amount of programming required to execute certain commands, which is based on software platforms such as C++ and JavaScript. It features a large standard library with various programming paradigms, such as procedural and object-oriented [74].

3 System Design

3.1 Overview

The use of aggregated load data necessitates the need for individual load monitoring and recording hardware. Designing load monitoring devices, which meets the design objectives, requires an innovative hardware design. The hardware should be designed with the aim to:

- Reduce the cost of acquiring de-aggregated load data with a low-cost design.
- Minimize the size of the physical footprint.
- An optimal design for quick and easy installations.
- Provide a non-intrusive sensing solution for maximum safety.
- Optimise power consumption with the view to extend battery lifetime.

The hardware designed and developed for this project consists of two individual Printed Circuit Boards (PCBs), one acting as the logic core unit and the other as a replaceable sensor unit. The remainder of this chapter focus on the hardware design of these units.

3.2 System Topology

The functional block diagram shown in Figure 3.1 summarises the topology of the implemented system. It can be summarised as four main blocks which include the following:

- *Host Computer*: A personal computer is used to host an application program, which provides a platform to interact with the device and change certain software parameters via a Universal Serial Bus (USB) interface.
- *Generic Logic Core Unit*: The generic logic core unit is designed to host various sensing modules for various types of logger devices, typically measuring parameters such as power consumption, time-of-use profiles, temperature, acceleration, etc.
- *Current Sensor Unit*: The current sensor unit consist of all components required to sense current flow of a targeted electrical appliance. Two sensing circuits, event sensing and analogue sensing, are included as required by various recording capabilities implemented. It also hosts a 3.6 V lithium thionyl chloride battery and a soft on/off latch switching circuit.

- Transducer: A current to voltage transducer acts as measuring instrumentation. It feeds the two sensing circuits situated on the current sensor unit. Both these circuits receive an Alternating Current (AC) signal directly from the transducer.

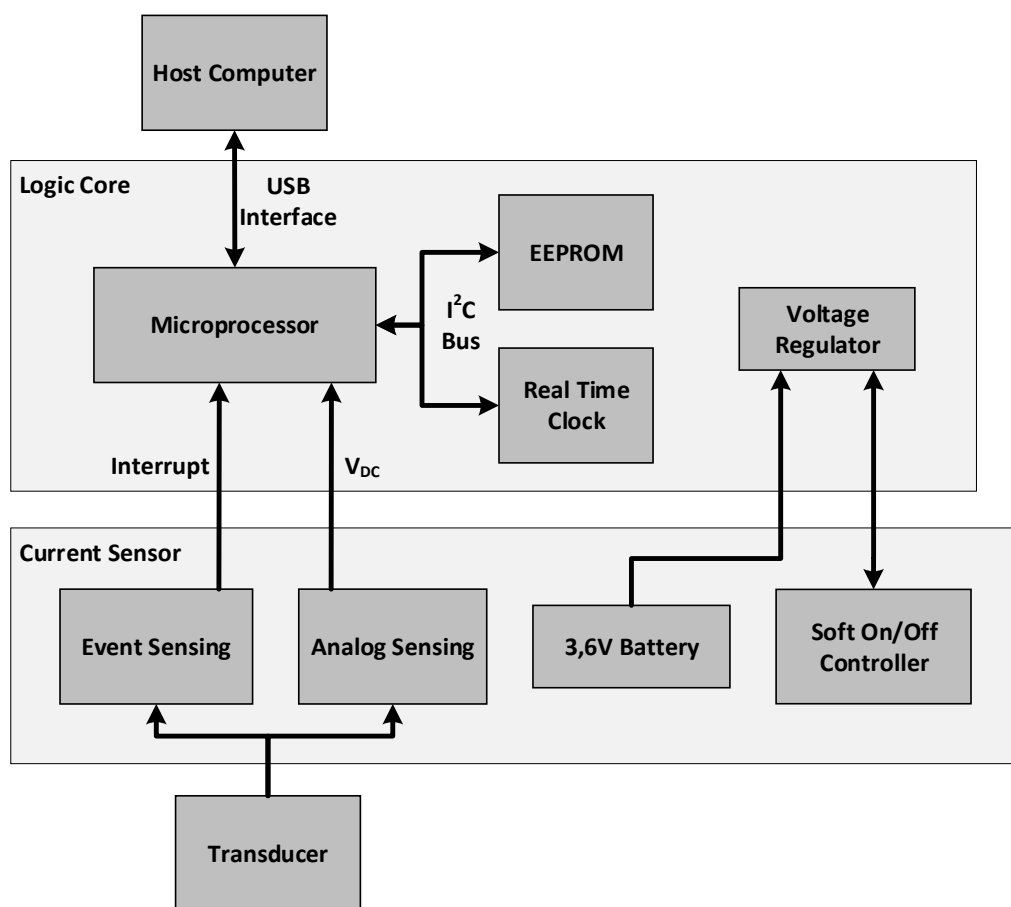


Figure 3.1 Functional block diagram describing the system topology

3.3 Logic Core Design

The logic core unit consists of a microprocessor that interfaces to a Real Time Clock (RTC) and Electrically Erasable Programmable Memory (EEPROM) bank via Inter-Integrated Circuit (I²C) interfaces. The RTC and EEPROM share a 400 kHz I²C interface, while a second I²C interface is routed to the breakout headers for future development.

A B-mini USB connector connects the microprocessor to the Personal Computer (PC), which is closely routed with Electrostatic Discharge (ESD) protection. The USB interface also acts as an additional power source to the system, which automatically disconnects the battery power source to conserve battery power. The USB interface provides a wake-up input signal for the processor to return to a normal operating condition when the USB data lines are connected to a PC.

Data communication between the logic core unit and the current sensor unit is facilitated by two microprocessor General-Purpose Input/Output (GPIO) interfaces. The sensor board consists of two separate sensing circuits, event sensing and analog sensing. Event sensing uses a comparator to provide a digital signal to the microprocessor that is interpreted as a software interrupt. This logic signal reflects the on/off state of the load. For example, if the load is switched on, the comparator will output a digital one which will interrupt the software cycle. The analog sensing circuit includes a RMS to DC converter to generate an analogue signal to the microprocessor which is handled by one of the microprocessors Analog to Digital Converter (ADC) interfaces. This enables the logic core to read analogue voltages with high accuracy without any additional hardware required. Another ADC interface and two Digital to Analogue Converter (DAC) interfaces are routed to breakout headers for future additions.

The logic core unit also features a Serial Peripheral Interface Bus (SPI) and a Universal Asynchronous Receiver/Transmitter (UART) for communicating with compatible communication technologies such as modems, temperature sensors and accelerometers, etc. For simplicity reasons, the additional ADC, DAC, I²C, SPI and UART interfaces are not indicated in Figure 3.1.

The logic core unit implements wake-up procedures to wake the processor during a deep sleep cycle. This is accomplished by using the event sensing interrupt signal or by using the internally routed RTC interrupt. The RTC interrupt provides for pre-programmed timed wake-up functionality. The logic core also features two Light Emitting Diodes (LEDs) as indicators. The one is connected to the RTC unit to indicate clock signals and interrupt triggers while the other is used to indicate system boot-up procedures, over voltage warnings and USB activity.

The breakout headers are orientated in such way to structurally support the PCB at multiple points. On both sides, the headers are divided into two parts, one shorter than the other, to ensure correct orientation when connected to the sensor board. A header on the edge of the PCB acts as a Program and Debug Interface (PDI) to flash program the processor. Figure 3.2 shows the PCB layout and component layout of the logic core unit.

The logic core unit can be fitted to any sensor board designed with the sizing and layout as depicted in Figure 3.2. For this project, only a current sensor is implemented.

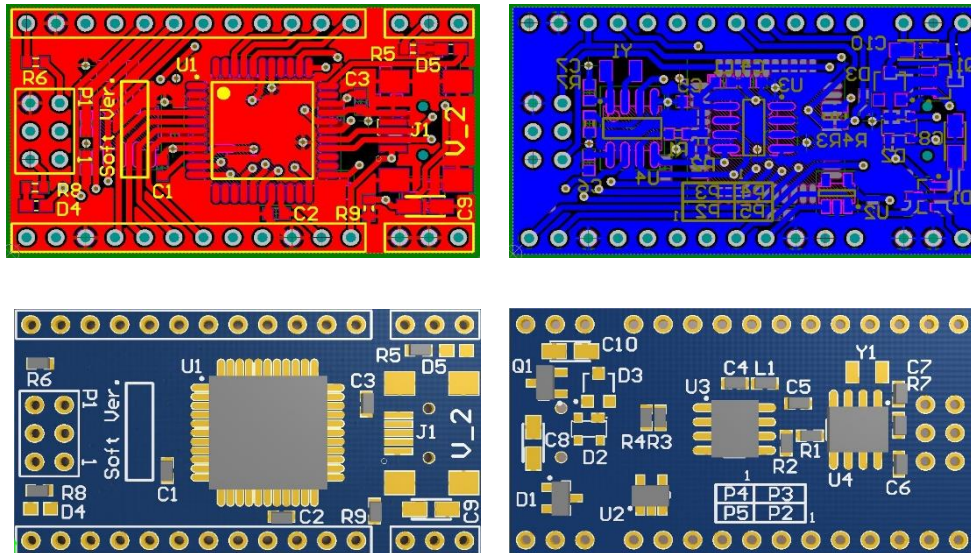


Figure 3.2 PCB designed for logic core unit

3.4 Current Sensor Design

The current sensor unit is designed with the view to facilitate non-intrusive current sensing. To accomplish this, the unit employs a commercially available toroidal current-to-voltage transducer, where the measured current is routed non-intrusively, i.e. without galvanic connections, through the core. The state of a load is measured by the event sensing circuitry shown in Figure 3.3. The design includes a passive low-pass filter, a low power analogue comparator and a rectifier with a ripple filter.

The comparator continuously compares the 50 Hz voltage induced in the secondary winding of the transducer with an adjustable threshold voltage. This produces a bi-polar digital signal in the form of a rectangular wave form, oscillating at a frequency of 50 Hz. To provide the microprocessor with a steady digital value, this signal is rectified and filtered to remove the power frequency ripple component.

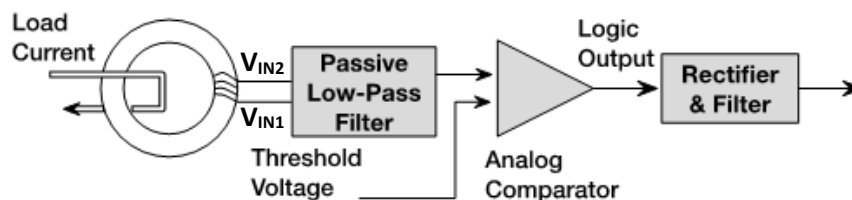


Figure 3.3 Event sensing circuit topology

Unlike the logic core unit, which can go into sleep mode, the current sensor circuitry operates continuously and should contain a minimum number of active components to conserve battery

power. The active components used to generate the threshold voltage of the analogue comparator are chosen to minimize current consumption.

The event sensing circuit should be able to work with a wide range of load ratings. Modern LED lights have current consumption values measured in tens of mA's, while geyser current consumption is roughly between 10 A and 20 A. This poses a challenge to the design, as it needs a broad dynamic range to be able to measure both types of loads. The final design is fully usable for both types of load currents. However, a different set of threshold resistors is required to trigger on loads consuming less than 50 mA.

The analogue sensing circuit, shown in Figure 3.4, consist of an RMS to DC converter to be used for digital readings via an Analogue to Digital Converter (ADC) interface. The 50 Hz AC signal generated by the transducer is routed to the RMS to DC converter. The selected low power RMS to DC converter has an input operating voltage range of 0V to 1V. The input signal from the transducer is first clipped by a Zener diode to ensure a maximum input voltage of 1V. The input voltage to the RMS to DC converter, V_{IN} , is given by

$$V_{IN} = V_{IN2} - V_{IN1} \quad (3.1)$$

where V_{IN1} and V_{IN2} denotes the differential voltages received from the transducer.

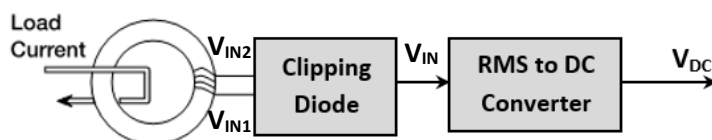


Figure 3.4 *Analog sensing circuit topology*

The RMS to DC converter consist of a summing modulator and a lowpass filter to calculate the Root-Mean-Squared (RMS) value of the input signal, V_{IN} . The summing modulator has a single-bit output whose average duty cycle will be proportional to the ratio of the input signal divided by the output [75]. The lowpass filter performs the averaging of the RMS value determined by the summing modulator. The voltage supplied by the RMS to DC converter is given by

$$V_{DC} = \sqrt{(V_{IN})^2} = \text{RMS}(V_{IN}) \quad (3.2)$$

The converter accomplishes the averaging with a single averaging capacitor. The capacitor is the only additional component required for the RMS to DC converter and is selectable

according to the desired frequency range and settling time. With the processor operating at high frequency and with a confined populated PCB, obtaining an output from the converter with some error is almost inevitable. Choosing the correct averaging capacitor is thus crucial in the design stage. Figure 3.5 plots the DC output error vs the input frequency of the LTC1966 RMS/DC converter used in the design [75]. The targeted loads are all operating at 50 Hz and therefore a 1 μF capacitor is chosen, yielding a peak error in the order of 1.0%. Figure 3.6 shows the PCB layout and component layout of the current sensor unit.

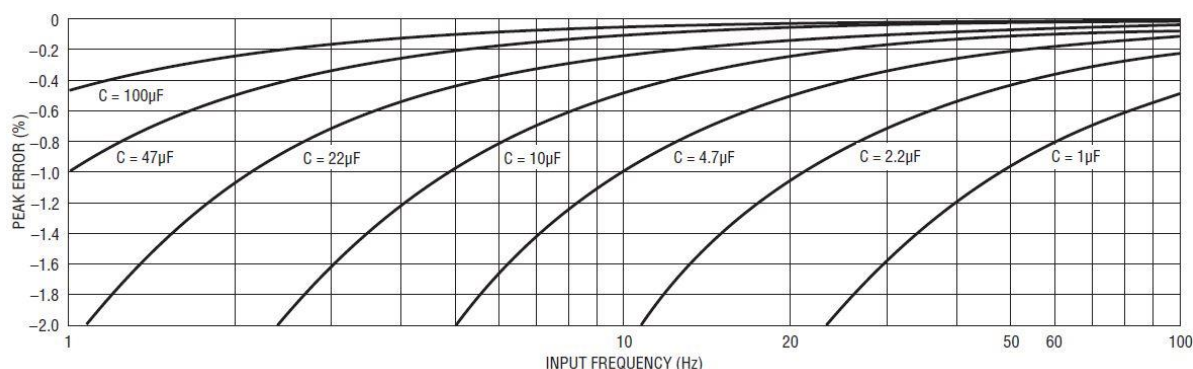


Figure 3.5 DC output error vs input frequency of LTC1966 RMS/DC converter [75]

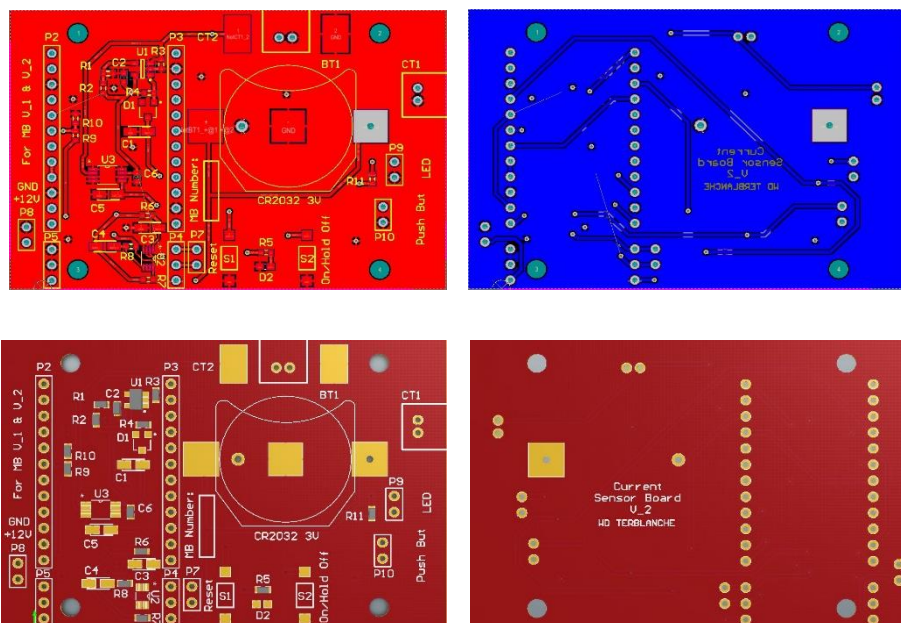


Figure 3.6 PCB designed for current sensor unit

3.5 Power Supply and Power Management

A microprocessor based smart device requires that the power is never inadvertently removed. Consequently, the logger device requires a power switch that can be turned on by a brief button press, but requires a longer, deliberate button hold to turn it off. This prevents accidental

disconnection of the power if the tactile switch is unintentionally touched. To accomplish this with only one tactile switch, a circuit containing a bistable logic low power NAND gate latch is implemented. The circuitry is placed on the current sensor unit and forms part of the voltage regulator circuit as shown in Figure 3.7. This figure is only for illustration purposes, and does not include all components required for implementation.

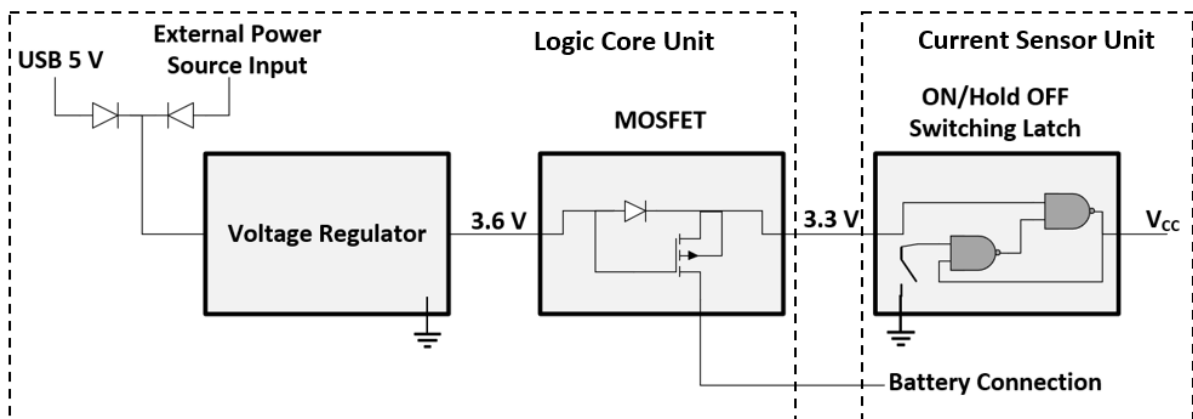


Figure 3.7 Power supply connection overview

The voltage regulator, together with a MOSFET circuit, is placed on the logic core unit which connects the various power sources. The voltage regulator receives its power from either the 5 V USB bus or an external power source input. The battery connection is done after the voltage regulator to reduce energy losses within the regulator when operated from battery power. The voltage regulator is chosen to deliver 0.3 V more to compensate for the voltage drop across the diode used in the battery connection circuit.

Due to size constraints on the logic core unit, the current sensor board hosts the 3,6V lithium thionyl chloride battery, as shown in Figure 3.7. The board can be populated with two types of battery holders, one for a 3V CR2032 lithium-ion battery or for a fixed 3,6V 1/2AA battery. Thionyl chloride fixed batteries are installed due to their high-power output characteristics. These batteries, compared to the traditional CR2032 coin cell battery, typically stores six times more energy. However, the battery selection suitable for the intended purpose depends on the operating duration and location.

Continuously forcing the microprocessor into a deep sleep mode is crucial in battery driven designs. However, for this design the processor cannot be programmed to continuously go into power saving modes as the device can be operated in two modes. These modes are either data downloading mode or recording mode. Distinguishing between them in software, requires an

external input signal to indicate USB presence. The sensor board features a resistor divider circuit to reduce the USB voltage to 3V, suitable for the microprocessor.

In the context of designing a cost-effective logging device for large-scale acquisition of load data, the device is expected to operate from a battery source for an extended period of time. Power consumption therefore represents a key performance parameter.

The power consumption of the logic core is heavily dependent on the clock speed of the microprocessor. In order to determine the system operating frequency with the best energy consumption efficiency, average power consumption measurements were taken for different clock frequencies. Operating the processor at a high clock frequency will let the device return to sleep mode faster, but may consume more power. A lower clock frequency will execute the same tasks over a longer period, but may consume less power. To determine the difference in power consumption and processing speeds, the processor is programmed to write a predetermined number of data bytes to the memory. The processor will take a certain amount of clock cycles to execute the memory write operations. Every time the software is repeated, a software cycle is completed. Figure 3.8 shows a comparison of the microprocessor power consumption at different clock frequencies. Operating at a clock frequency of 32 MHz will consume approximately 56 mW in one software cycle. A clock frequency of 8 MHz will consume less power, but processing one software cycle requires an additional 0.2 s. High speed USB functionality, however, requires a minimum clock frequency of 8 MHz. This clock frequency was therefore selected.

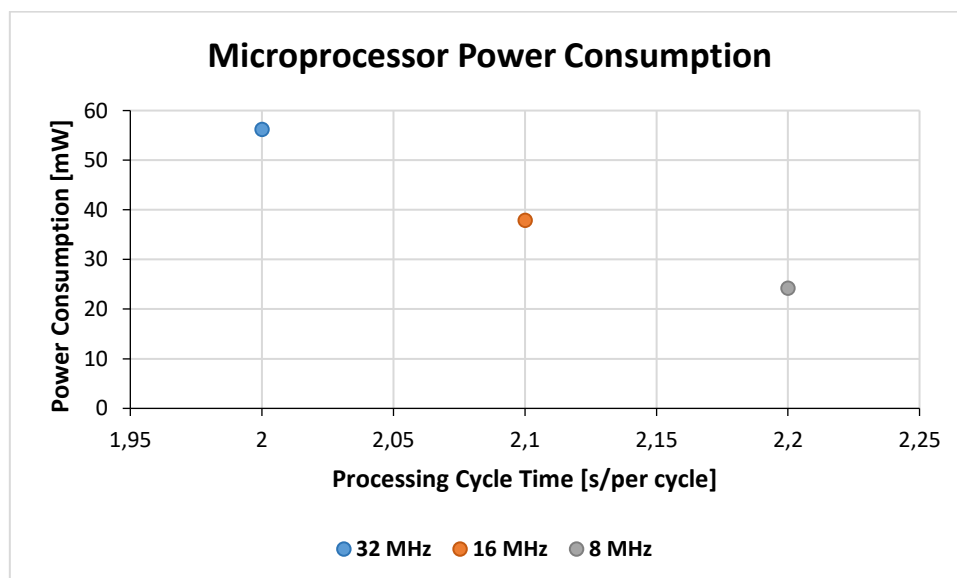


Figure 3.8 Microprocessor power consumption at different clock frequencies [76]

Measuring the current consumption profiles of high-speed logic circuits requires very high sampling rates due to the high frequency nature of the signals. This can be addressed by using the capacitor charge measurement solution shown in Figure 3.9 [76]. The switch is closed repetitively and the source charges the capacitor and supplies the load current during these cycles. The source voltage, switching rate and capacitor value is selected to maintain $v_c(t)$ in a close range around the desired operating voltage. The electric charge, Q_S , supplied by the source during a charging cycle, is given using the relationship

$$Q_S = \int_{t_1}^{t_2} i_R(t) dt = \int_{t_1}^{t_2} \frac{v_R(t)}{R} dt \quad (3.3)$$

where t_1 denotes the start time of the charging cycle, t_2 denotes the start time of the next cycle and R denotes the value of the series resistor [Ω]. The circuit filters the high frequency pulses drawn by the logic core from the measured voltage $v_R(t)$, so that good accuracy can be obtained using a relatively low sampling rate. The total charge, Q_L , supplied to the load during a charging cycle, is given by the relationship

$$Q_L = Q_S - C(v_c(t_2) - v_c(t_1)) \quad (3.4)$$

where C denotes the value of the capacitance [F]. If the ripple voltage associated with $v_c(t)$ is small, $Q_L \approx Q_S$.

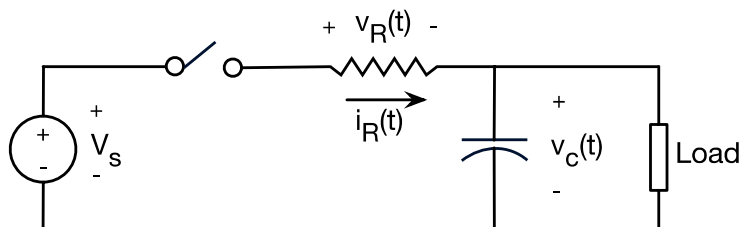


Figure 3.9 Capacitor charge circuit implemented for high frequency current measurements [76]

The charging cycle of the circuit can be readily automated using an active switching element controlled by a switching sequence generator. The test arrangement can be used to determine the energy consumption associated with the various operating modes of the logic core, e.g. idle mode, sleep mode, etc. and to derive the energy consumption associated with any given operation, e.g. executing an event log.

The battery lifetime for a scenario where the device operates in sleep mode, but executes a total of N_e event logs, can be calculated using the following relationship [76]:

$$T_B = \frac{Q_C - N_e Q_e}{I_s} + N_e T_e \quad (3.5)$$

where T_B denotes the battery lifetime in hours, Q_C denotes the battery capacity [mAh], Q_e denotes the charge associated with an event log [mAh], I_s denotes the sleep mode current [mA] and T_e denotes the duration of an event log in seconds.

Figure 3.10 shows typical test results for the device during sleep mode. The device consumes an average current of 94 μA during sleep mode. Figure 3.11 shows the current consumption profile if the cycle includes an event log. The total charge associated with logging an event is of the order of 0.3 μAh , while the event duration is of the order of 0.38 s. Figure 3.12 shows the projected battery lifetime as function of the total number of event logs. For event counts below 10 000, the lifetime is primarily determined by the sleep mode current consumption [76].

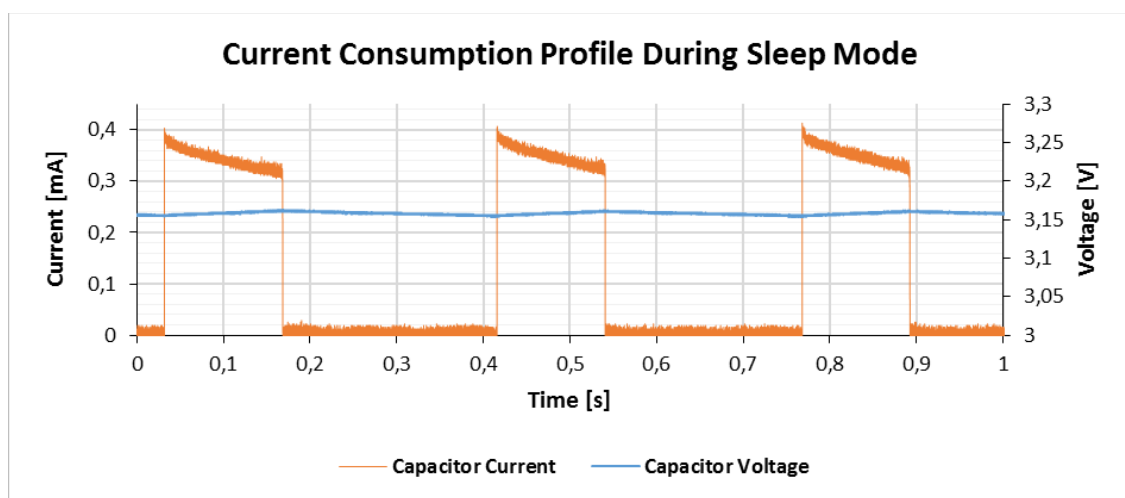


Figure 3.10 Measured logic core unit sleep mode supply current [76]

The power consumption performance of the device shows that the sleep mode current consumption, rather than event count, dominates the battery lifetime for event counts below 10000. An event count of 10000 yields a battery lifetime of 96 days [76]. For a logging period of 1 year, an event count of 10000 translates to 27 events per day, which is ample for most appliance monitoring studies.

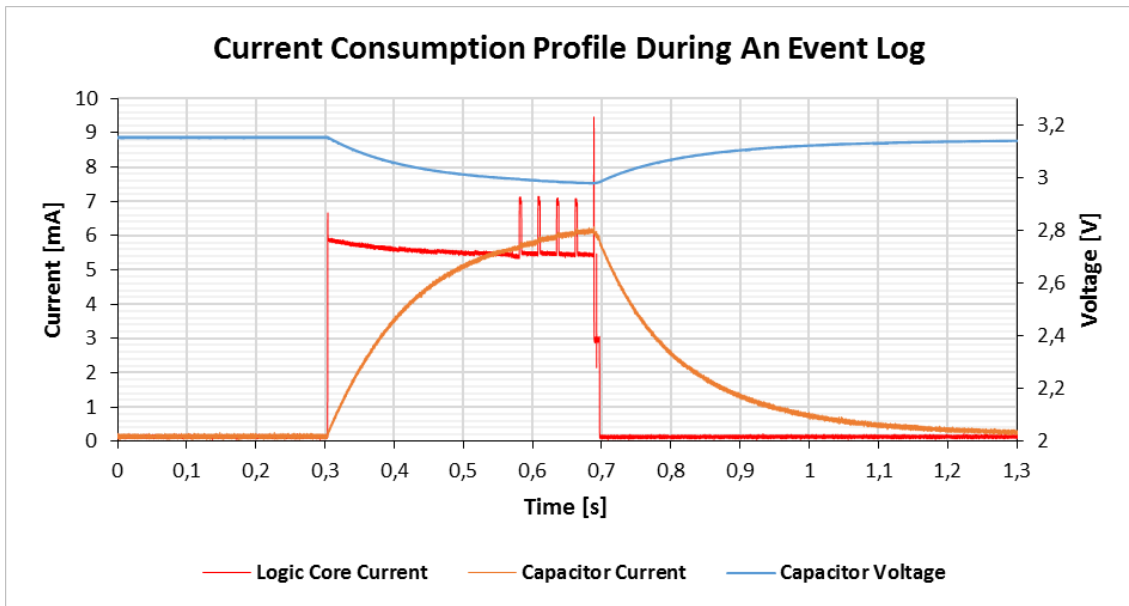


Figure 3.11 Measured supply current of the logic core unit during an event log [76]

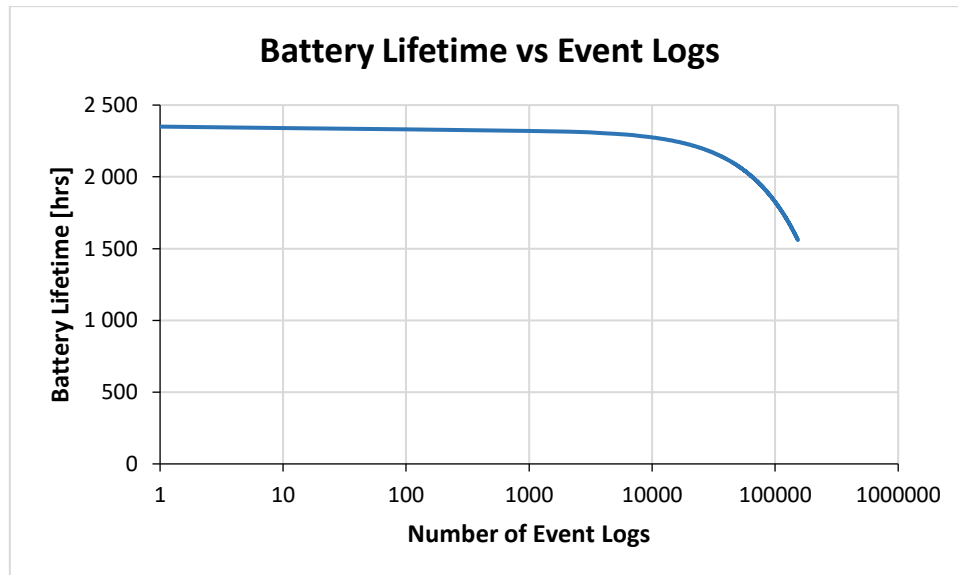


Figure 3.12 Projected battery lifetime of the logger for several event logs [76]

3.6 Cost Analysis

A cost analysis is included in Appendix D, containing a detailed list of components required for the logic core and current sensor unit. The costs listed mostly reflect bulk component placement prices, which are only valid for mass production of these modules. It also includes the cost for circuit boards and transport. The components are chosen according to their local availability and brand type. Manufacturing PCBs in high quantities abroad are more affordable than doing so in South Africa. Both the PCBs were manufactured in China and shipped to South Africa to minimize mass production costs. The manufacturing and transportation costs of the

PCBs are based on an order of 50 boards. Ordering more boards simultaneously will also reduce the total costs.

The costs listed in Appendix Table D.1 and Appendix Table D.2 does not include labour costs. The total cost, excluding labour, to manufacture one logger device is listed in Table 3.1.

Table 3.1 *Total manufacturing costs for one complete logger device*

Device Component	Cost [R]
Logic Core	251.96
Current Sensor	365.66
Total	617.62

With the view to design a cost-effective logging device, the estimated cost of R617.62 per logger is still relatively high. The high cost is due to incorporating all available functionalities. If the functionality is limited to event recording, for instance, components such as the RMS-DC converter can be omitted, reducing the cost by R130.00 per device. Components such as the LEDs and soft-on/off circuitry can be removed to reduce the manufacturing costs even more.

4 Embedded Software Implementation

4.1 Overview

The embedded software is discussed in this chapter. The Atmel Studio IDE is used to implement the embedded code for the Atmel XMega microprocessor. An activity flow diagram and structure overview of each of the important software modules is given. The various embedded software modules facilitate the operations of the RTC, EEPROM, USB communication, interrupt handling and analogue conversions. This chapter further describes the seven possible recording use cases, also defined as modes of operation, as listed in Figure 4.1.

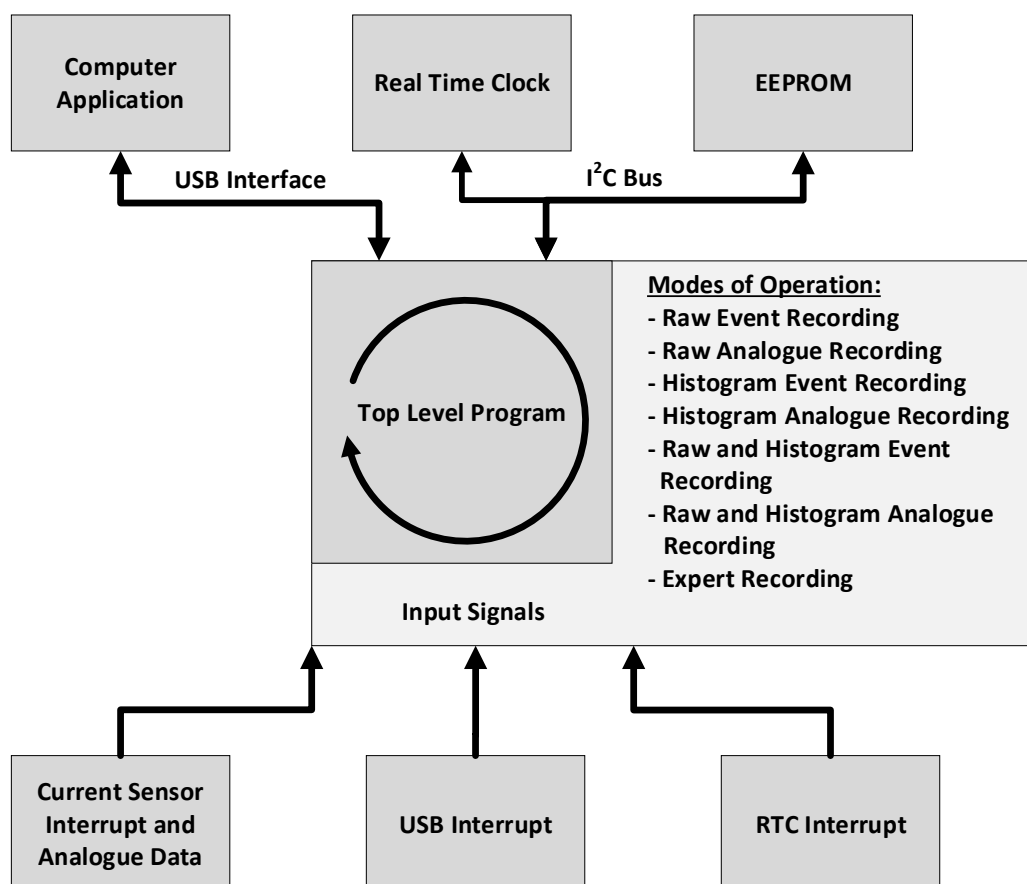


Figure 4.1 Embedded software top level program overview

The seven possible modes of operation include the following:

- *Raw Event Recording*: The time-of-use data of a targeted load is captured by the raw event recording mode. This mode of operation uses the event sensing hardware, shown in Figure 3.3, to retrieve state changes of a load. These state changes are also defined as events. Following an event, the RTC data is retrieved, which represents the time stamp at which the state of the load changed. The data generated by raw event recording is kept in a raw form,

meaning that the data is not converted, simplified or averaged before storing. Raw event recording is typically used for shorter logging periods as a vast amount of data is generated and stored in the memory.

- *Raw Analogue Recording*: Analogue recordings are facilitated by the raw analogue recording mode. As with raw event recording, the data is stored as raw data, which offers all available information to the user during data retrieval. This mode of operation requires the analogue sensing hardware, shown in Figure 3.4, to retrieve the analogue data and to determine the power consumed by the load. These recordings occur at a predetermined interval and is controlled by the RTC interrupt input, as indicated in Figure 4.1.
- *Histogram Event Recording*: Histogram event recording involves translating event timestamps to event start time and event duration histogram bins, instead of keeping it as raw data. Every event start time and event duration are compared to predefined event start time and event duration indices to find the corresponding memory position. The memory allocated for histogram recording can be presented as a 3D histogram memory map, where a single memory position is defined as a histogram bin. This mode of operation aims to reduce the amount of non-volatile memory required for logging operations. It is typically used for longer recording periods, as the data is converted and averaged before stored in memory, allowing much more event recordings compared to the raw event recording mode.
- *Histogram Analogue Recording*: Histogram analogue recording is similar to the raw analogue recording mode. However, the data is not stored as raw data, but rather in the form of a histogram. The timestamp of the recording, as well as the analogue value, is translated to analogue start time and analogue value histogram bins. As with histogram event recording, the corresponding memory position, to increment for each recording, is found by comparing the retrieved data with predefined timestamp and analogue value indices. Histogram analogue recording is typically used to obtain average power consumption data of loads with varying power consumption values over the period of operation.
- *Raw and Histogram Event Recording*: Raw and histogram event recording mode is a combination of raw event recording and histogram event recording. The two modes are executed in parallel, meaning that raw data and histogram data is stored simultaneously. The histogram data is stored on the microprocessors onboard memory, while the raw data is stored on the EEPROM device connected via an I²C bus.

- *Raw and Histogram Analogue Recording*: Raw analogue and histogram analogue data is simultaneously recorded during this mode of operation. The data is also kept separately in the memory to avoid data overwrites and losses.
- *Expert Recording*: Expert recording is a mode of operation during which event and analogue data is stored. This mode uses the same software sections as used to record the event and analogue data as mentioned above, however, the data is only stored in raw format. It is the most power intensive mode in which the device can operated, as it requires both the sensing circuits shown in Figure 3.1 to be active. This mode is named expert recording for the remainder of the document to avoid confusion with the various recording combinations.

4.2 Top Level Program

4.2.1 Start-up and Initialization

The top-level software program continuously monitors the interrupt input, USB communication and power management possibilities. The software executes a start-up sequence during every start up process, i.e. after every power-up cycle or system reset. The start-up sequence executes a number of initialization routines, including the following:

- *Sleep manager initialization*
- System clock initialization
- Analog to digital conversion initialization
- Two-wire interface start-up for EEPROM and RTC
- Start RTC wake-up interrupt
- USB initialization (including USB interrupt)
- LED ports declaration
- Start system interrupts
- Load memory stored variables
- Sensor board identification
- Switch off all unused ports and interrupts

A successful start-up is signalled by flashing sequence of the external LED. If any of the modules fail to successfully initialize during start-up, the processor will reset and repeat the process. If the initialization function fails three times consecutively, the processor will continue without that module operating.

4.2.2 Main Program

A successful initialization process is followed by a software cycle where only a system reset or power down state can exit the cycle. This cycle contains the following three routines, of which one can be active at a time:

- USB command service routine
- Sleep/Power saving routine
- Data recording service routine

The USB command service routine continuously monitors the USB data receive flag. This flag indicates that data has been received by the USB interface sent from the computer application and will activate this section in the software cycle. During a triggered receive flag, the USB line is primed to receive the data from the UART line in an 8-bit format. USB data are always sent and received in data packages containing multiple 8-bit unsigned integers.

The top-level program parses the data received from the USB interface according to the message structure summarized in Table 4.1. Each byte received is either classified as a command byte, which identifies the command routine to be executed, or as an information byte, which typically form part of the parameter set associated with the given command. After receiving the full command message, the top-level program activates the command software section followed by certain software functions.

The switch case statement is activated on the command first byte received. The top-level program will continue to complete certain software functions specified under each case statement (command byte). The command message structures and associated functions are described in Table 4.1.

Table 4.1 *Command message structure*

Group	Command Byte	Function	Data Direction	Data Bytes
Information	0xA0	Send ID, Software Version, Flashed Date, Board Version, Sensor Type, Recording Settings	Out	12
Expert Recording	0xAB	Send Expert Analog Data	Out	Variant
	0xAC	Send Expert Event Data	Out	Variant
Extra Features	0xAD	Update Device ID	In	1
	0xAE	LED Control	None	n/a
	0xAF	Send Single ADC Result	Out	2
Memory	0xE1	Reset Memory Position	None	n/a
	0xE4	Overwrite Memory	None	n/a
	0xE5	Stop When Memory Full	None	n/a
	0xE6	Show Memory Usage	Out	2
Calendar	0xD0	Set Device Date	In	3
	0xD1	Set Device Time	In	3
	0xD2	Return Device Date	Out	3
	0xD3	Return Device Time	Out	3
Clock Frequency	0xD4	Set Clock Output to 32.768kHz	None	n/a
	0xD5	Set Clock Output to 1.024kHz	None	n/a
	0xD6	Set Clock Output to 32Hz	None	n/a
	0xD7	Set Clock Output to 1Hz	None	n/a
	0xD8	Set Clock Output Off	None	n/a
Analog Histogram	0xE0	Clean Map Data	None	n/a
	0xE7	Send Variable Data	Out	132
	0xE8	Send Magnitude Data	Out	1728
	0xE9	Set Map Variable Data	In	132
	0xEA	Set Map Magnitude Data	In	1728
Raw Event	0xEB	Send Raw Event Data	Out	Variant
	0xEC	Send Raw Event Duration Data	Out	Variant
	0xED	Send Raw Event Time-of-Use Data	Out	Variant
Raw Analog	0xEF	Send Raw Analog Data	Out	Variant
Recording Mode Selection	0xEE	Analog Trigger Selected (By Clock)	None	n/a
	0xFF	Event Trigger Selected	None	n/a
	0xAA	Expert Trigger Selected	None	n/a

Acquisition Selection	0xF0	Raw Form Selected	None	n/a
	0xF1	Histogram Form Selected	None	n/a
	0xF2	Both Forms Selected	None	n/a
Reset and Wake-up Functions	0xF3	Reset Device (With Software)	None	n/a
	0xF4	Enable and Set RTC Alarm Function	In	3
	0xF5	Disable RTC Alarm Function	None	n/a
Event Histogram	0xFA	Send Variable Data	Out	116
	0xFB	Send Magnitude Data	Out	1920
	0xFC	Clean Map Data	None	n/a
	0xFD	Set Map Variable Data	In	116
	0xFE	Set Map Magnitude Data	In	1920

Functions that take some time to execute often needs to send a return command byte after successful completion. These return commands are always the same as the specific command byte and are used by die computer application to know when the processor is done with certain tasks. For example, if the histogram memory map gets overwritten with new values, the application must halt any further user interactions until the processor is ready to execute a new command.

The sleep/power saving routine is activated only when there is no USB connection present, which is detected by monitoring the voltage on an input pin. The routine configures the logic core for the lowest possible power consumption state, whereby the processor is placed in a “power down” mode. In this mode:

- All clock sources, except external RTC clock, are stopped.
- External LEDs are switched off.
- USB functions are disabled.
- All peripherals, except asynchronous port interrupts, are disabled.

Only the USB connection interrupt, current sensor event interrupt and RTC interrupt can wake the processor from this sleep mode. On wakeup, the processor will execute the interrupt subroutine and return to the top-level program. Depending on the interrupt triggered and mode of operation, recording flags will be set during the interrupt subroutines.

The last part of the top-level software loop contains the recording service routine. Each type of recording will be activated using the set recording flags. Recording functions are executed which returns to the top-level loop upon completion. If no USB data received flags are triggered and no pending recordings are found, the processor will continue to sleep and reduce power consumption. The top-level program flow diagram is shown in Figure 4.2.

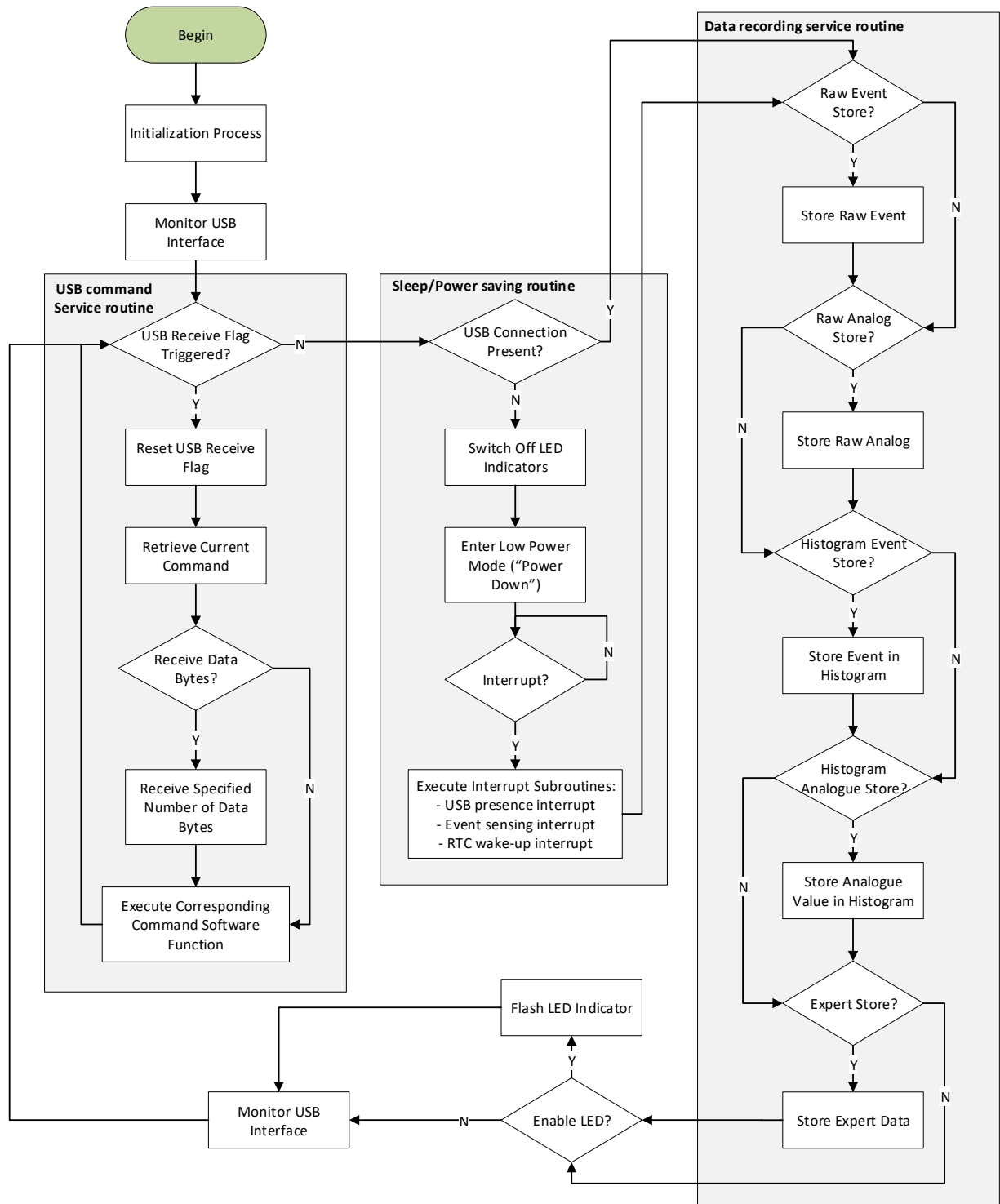


Figure 4.2 Top level software flow diagram

4.3 USB Communication

4.3.1 Overview

Many modern microprocessors feature USB interface functionality, which can be used to connect the processor to a host computer. The XMEGA128A4U microprocessor used in this design features a USB CDC interface. For this project a UART interface was used to send and receive data over the USB line. The following section describes the configuration steps.

4.3.2 Configuration

For the USB interface to operate correctly, certain key configuration steps are necessary. To start the USB device, the system clock and interrupts are first enabled and stabilized. The initialization process is shown in Figure 4.3.

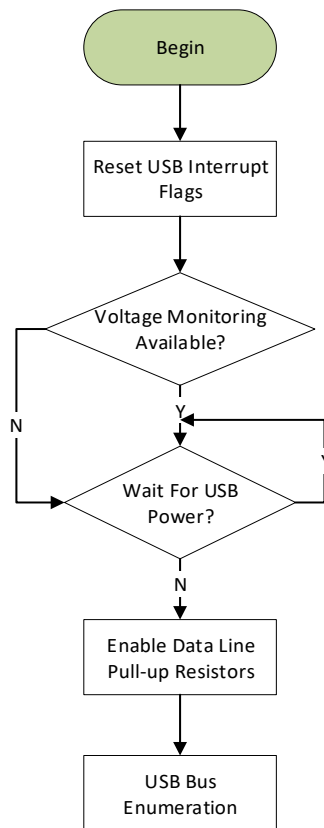


Figure 4.3 System initialization software flow diagram

A UART interface is then initialized and software connected to the two USB data lines, i.e. D+ and D-, when a voltage is detected on the USB bus, followed by the device enumeration step. After the device enumeration (detecting and identifying the USB devices), the USB host starts

the device configuration. When the USB CDC interface from the device is accepted by the host, the USB host enables this interface.

When the USB device is unplugged or reset by the host, the USB interface is disabled and the UART is detached. The UART also gets detached every time the processor goes into a sleep mode, and reattached after wake-up and clock stabilization. This ensures that the USB device does not go into an unstable state every time the system clocks are stopped.

4.4 System Frequency and Clock

4.4.1 Overview

The XMEGA microprocessors can be configured with a range of settings to suit the needs of the specific application. The choice of the system clock mostly depends on considerations such as power consumption and the clock frequency requirements of peripheral components. When using the USB interface functionality, the minimum system frequency must be high enough so that the processor can keep up with processing the incoming data. For the ATXMEGA128-A4U, the minimum CPU frequency is 8MHz for slow USB implementations. For high speed USB implementations, a USB clock frequency of 48MHz is required for a system baud rate of 115200. This section discusses the system clock frequency configuration and the real-time clock implementation.

4.4.2 System Clock Frequency

The microprocessor has a maximum rated CPU frequency of 32MHz. The fastest clock speed is preferred for this battery-driven design, so that the processor executes the data acquisition tasks at maximum speed with the view to return to sleep mode faster. A thorough system frequency vs. system power comparison is detailed in Chapter 3.

The maximum system frequency of 32MHz is not ideal for the closely routed tracks of the compact four-layer PCB design. Thus, in order to eliminate drifting clock frequencies, the main system clock is configured to run at 16 MHz, using the internal 2 MHz RC oscillator calibrated against the internal 32 kHz oscillator and multiplied with a constant of eight. The peripheral bus clocks run at the same speed as the CPU clock, and the USB clock is configured to use the internal 32 MHz (nominal) RC oscillator calibrated to 48 MHz with the USB Start-of-Frame (SOF) as the calibrated reference.

4.4.3 Real Time Clock

The onboard real-time counter of the microprocessor cannot be used for time keeping, as the system clocks are switched off during sleep mode. The design, furthermore, does not include an external oscillator, which makes the internal clock frequency unreliable for accurate timekeeping. In view of the above considerations, the logic core design features a discrete low power RTC device that communicates via an I²C interface.

The RTC has a number of internal registers that can be accessed via the I²C interface. These registers hold the values that make up the timestamp data, such as seconds, minutes, hours, etc. as shown in Figure 4.4, which shows the internal data flow for the device. The different registers are updated based on the 1 Hz interval generated by the external crystal. When overflow occurs on one register, the next one is automatically incremented or updated. The EEPROM and RTC are daisy chained on the same I²C-bus of the processor. It follows that each device requires a device-specific slave address. During a read and write operation, the slave address of the target device is transmitted on the I²C-bus after a start condition, together with a send or receive bit. The slave will respond with an acknowledge signal, after which the relevant register address is sent. The data for this register is then transmitted on the I²C-bus. For the RTC, the lowest register address is the “seconds” value of the timestamp. The device automatically increments the active register to the next register upon successful send or receive of data at the current register. The process is stopped by the I²C master controller when a stop condition is transmitted on the I²C-bus.

During read and/or write operations to the RTC, the automatic timestamp update operations are blocked in order to prevent faulty readings of the clock and calendar data during changes to the timestamp registers. After a read or write operation is completed, these update operations are enabled and any pending updates to the timestamp registers that occurred during the read or write sequence are serviced. All read/write operations must be completed within one second as a maximum of one pending update request can be stored [77].

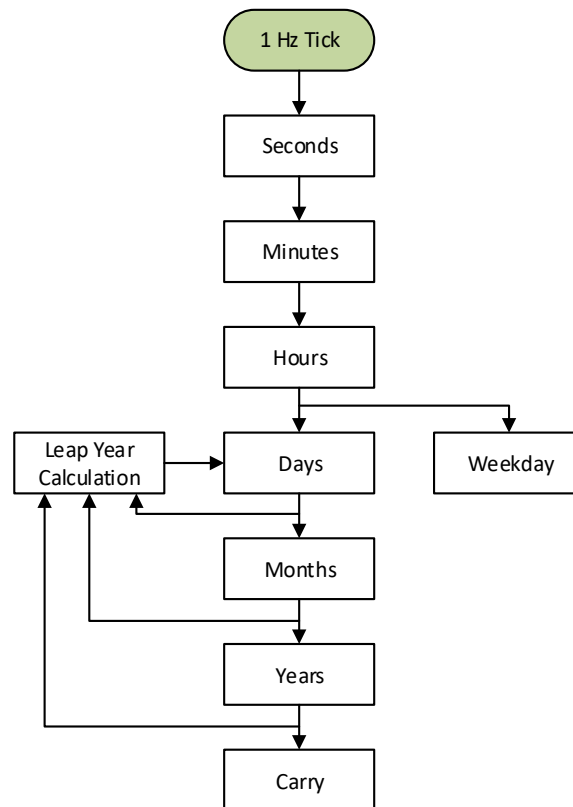


Figure 4.4 Real time clock flow diagram [77]

To accomplish the required I²C communication speed, the I²C-bus is configured to operate at 400 kHz. I²C-bus interrupts are also used to receive the transaction acknowledge signal transmitted, which ensures fast transmit and receive transactions on the line. The data stored in the RTC registers are mostly in Binary Coded Decimal (BCD) format to optimize internal calculations. The embedded software program, however, includes the following software routines to convert between BCD and Decimal format before and after data is send and received:

```

int bcdToDec(int value)
{return ((value / 16) * 10 + value % 16);}

int decToBcd(int value)
{return (value / 10 * 16 + value % 10);}

```

Timed processor wake-up routines are accomplished by using the RTC's alarm interrupt function. The alarm registers are set in the same way as the time and date. The RTC automatically compares the alarm register settings to the current time and date, and an interrupt signal is activated when the alarm register setting corresponds to the current time registers. The interrupt signal is cleared by disabling the alarm function via the I²C-bus. For automatic

repetitive interval-based data acquisition modes, the embedded software program will reset the alarm registers following each wake-up interrupt in accordance with user specified time intervals.

4.5 Analogue to Digital Conversion

Analogue to digital conversions are only required for analogue recording modes. This means that the ADC interface, as well as the RMS to DC converter, can be disabled and switched off during other recording modes. The ADC is configured during the initialization process for a signed, 12-bit resolution and manually triggered conversion process.

The input signal from the RMS to DC converter is limited to 1V maximum. In order to use the full ADC 12-bit resolution, the input signal is conditioned through a software programmable gain stage with a gain of four. This, however, also amplifies input noise. The RMS to DC converter has a small 50 Hz ripple component, which causes a varying measurement result. To compensate for this, an oversampling method is used. Each time an analog reading is requested, 5000 readings are acquired within one second. The 5000 recorded readings are then averaged. This makes the analogue recordings less sensitive to input noise.

The recorded analogue reading is stored in the 12-bit raw format and is also sent to the host computer application program in this format. The calibration values are incorporated in the application and all further conversions are performed in the host computer application program.

4.6 System Memory

Atmel provides a software framework to access and control the microprocessor internal non-volatile 2 kbit memory bank. This storage is situated in the internal EEPROM and is accessed by using the byte addresses between 0x1000 and 0x17FF. With the software framework, this memory is easy accessible through single byte or word read and write operations. The software framework also features a page write option as well as a memory clear function. The rest of the internal storage space is dedicated or reserved for I/O register values and application software as shown in Figure 4.5.

It follows from the memory map, shown in Figure 4.5, that the memory available for data recording purposes is limited. The recorded data is therefore predominantly stored in the external EEPROM. However, with both the event recording and analog acquisition modes active, one of them is recorded on the internal memory to avoid memory overwrites as detailed in the recording use cases.

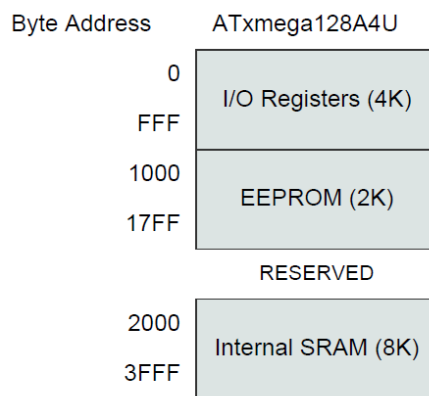


Figure 4.5 Internal storage memory allocation [78]

The external 1 Mbit EEPROM is internally organized as 512 pages of 256 bytes, each of which can store more data than the internal memory. The external EEPROM, which shares an I²C bus with the RTC device, is set up during the initialization process to operate at 400 kHz.

Global read and write operations for the EEPROM uses the same protocol used for the RTC, but with a different device address, 0xA0 for write and 0xA1 for read. A write operation requires the write-bit (zero), two 8-bit data addresses and an acknowledge bit. Upon receipt of this address, the EEPROM will respond with a zero and prepare the device to receive the data word. This process is terminated by responding with a stop bit after the acknowledge bit is received from the EEPROM.

A random read operation requires an initial byte write sequence to load the data address. It is also known as a “dummy write” operation. Once the device address word and data word address are clocked in and acknowledged, the master will generate another start condition. After receiving the device address with the read bit set, the EEPROM will automatically respond with the data at the start address selected.

4.7 Data Recording Use Cases

4.7.1 Overview

The recording capabilities of the logger can be classified by two mode categories. There are two primary acquisition modes, namely the *Raw* acquisition mode and *Histogram* acquisition mode, which can be combined to operate simultaneously. In practice, the usage of combined acquisition modes are subject to memory availability and power consumption constraints.

Table 4.2 summarises the recording capabilities of these two categories. The data acquisition routines are optimally programmed by incorporating functions that can be used by multiple acquisition modes.

Table 4.2 *Recording capabilities offered by the implemented software*

Data Format	Acquisition Mode		
	Raw	Histogram	Both
Event data	✓	✓	✓
Analogue data	✓	✓	✓
Expert data	✓	✗	✗

4.7.2 Raw Event Recording

Raw event recording is the simplest recording form introduced by the smart logger. Events are triggered based on the on/off switching state of the targeted load. Each event recording includes the exact date and time of the state change, as well as the status of the targeted load itself. It also holds the ability to record the sensor number on which the event was triggered for applications where multiple appliances are being monitored.

Recording a single event in raw format typically requires a few bytes to store all the components of the calendar and time. Allocating a byte for each component, that is for the year, month, day, hour, minute and seconds, will assign six bytes for each event. Another two bytes are added for the sensor number and the status of the event.

To reduce the number of bytes needed for each event, the components were bit compressed and added together to form a combined byte. First, the maximum number of bits needed to represent the maximum possible number of each component had to be calculated as listed in Table 4.3.

Table 4.3 *Bits allocated for each variable contained in a single raw event data packet*

Variable	Maximum Value	Bits Required	Data Range with Bits Selected
Year	4	2	0-3
Month	12	4	0-15
Day	31	5	0-31
Hour	24	5	0-31
Minute	60	6	0-63

Second	60	6	0-63
Sensor Number	8	3	0-7
Event Status	1	1	0-1

The year-component only has four bits instead of 16 bits which is actually needed to represent the current year and years to come. This component is, however, used as a counter, where zero represent the year when the software was flashed. The device will be able to keep an accurate calendar for a maximum of four years if the software is not updated during this time.

Compressing all 32-bits assigned to each component leads to a total of four bytes per event. The bit-compressed storage format is illustrated in Figure 4.6.

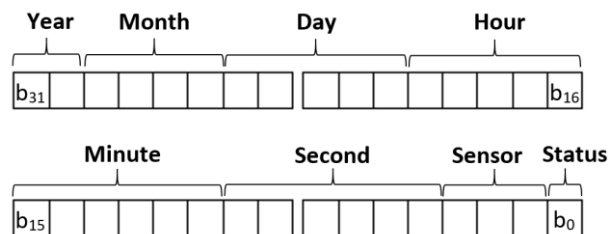


Figure 4.6 Event data compressing format used

The event data is stored sequentially in the external EEPROM, yielding a maximum storage capacity of 32 768 events. A global event counter is used to keep track of the number of bytes currently stored on the EEPROM. It is easy for the computer application to analyse the bytes received when downloading the data as the number of events can be determined by dividing the event memory counter by four. This event memory counter is updated after every event recording by writing to the internal EEPROM which allows the device to retrieve the previous counter in the event of a power failure. The event memory counter is constantly monitored to indicate a possible memory shortage and to react appropriately by either: overwriting the memory when it is full; or cease recording completely. The event memory counter is automatically reset when trigger modes are changed as new data is not necessarily in the same format as the raw event data.

The software flow diagram in Figure 4.7 shows the process of recording an event in raw format. This process is activated by the interrupt and recording flag in the top-level program as shown by the top-level software flow diagram in Figure 4.1.

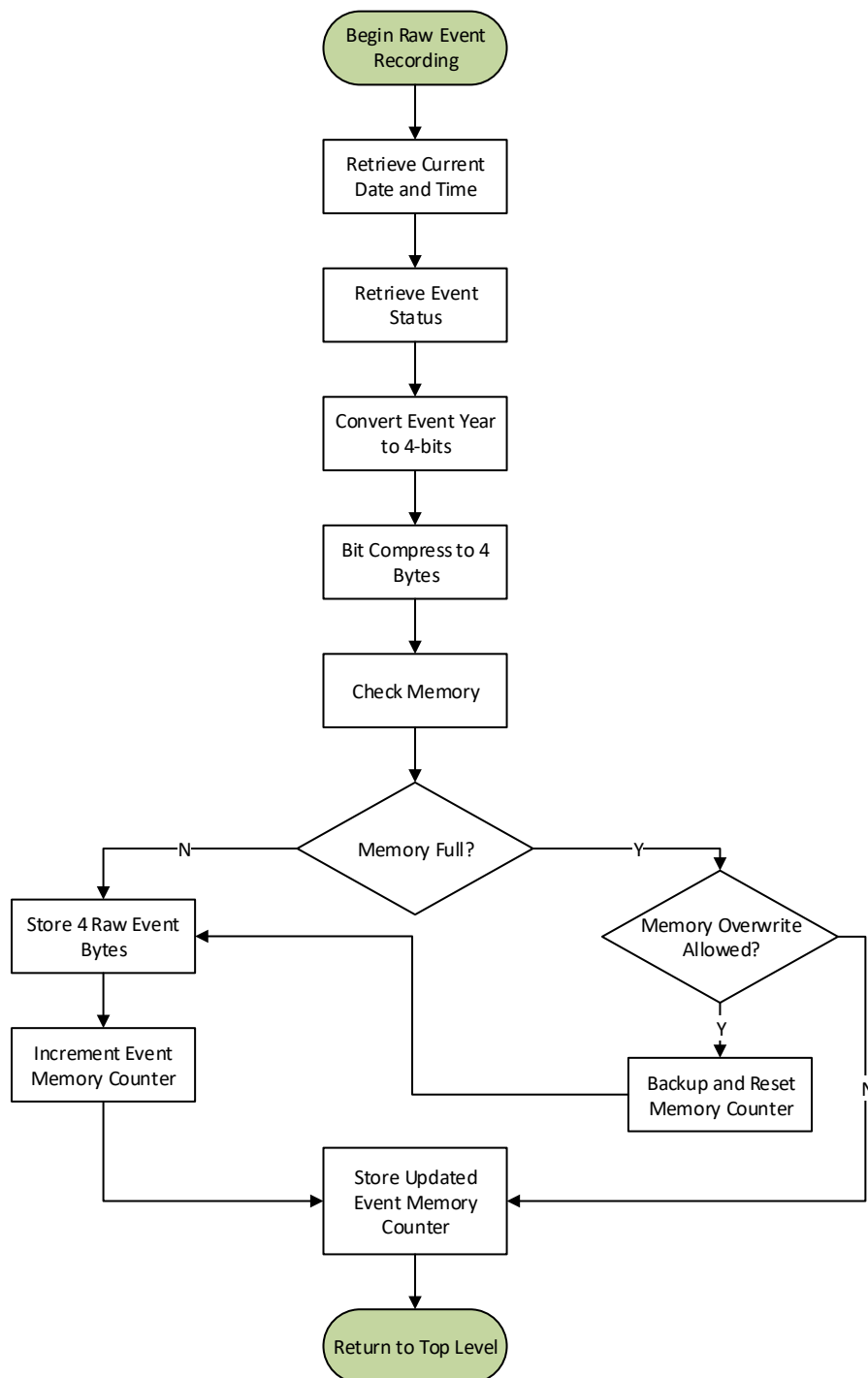


Figure 4.7 Raw event recording software flow diagram

4.7.3 Raw Analogue Recording

Raw analogue recordings provide a timed analogue reading capability, which also records the date and time of occurrence. Recording an analogue value, date and time at a regular interval generates excessive amounts of data, especially with short timed intervals. To limit the amount of data generated, raw analogue mode recording only stores the month, day, hour and minute components of the timestamp.

This recording mode also monitors the event status to limit the number of analogue recordings by not recording when the load is switched off. Raw analogue recording will start as soon as an ON-state is detected and will set the next recording time determined by the user defined interval. When the OFF-state is detected, the repeated wake-up RTC procedure will be disabled.

During raw analogue recording, the current date, time and analogue value will be stored. Bit compression was again implemented to reduce the number of bytes needed per recording. With fewer date and time components needed for analogue recordings, the compression structure differs from the structure used in raw event recording. Table 4.4 lists the number of bits allocated to each component.

Table 4.4 *Bits allocated for each variable contained in a single raw analogue data packet*

Variable	Maximum Value	Bits Required	Data Range with Bits Selected
Month	12	4	0-15
Day	31	5	0-31
Hour	24	5	0-31
Minute	60	6	0-63
ADC Value	4096	12	0-4095

The number of bits required as listed in Table 4.4, to represent all the necessary components of analogue recording is 32 bits. Bit compressing of all five components leads to four bytes in total. An analogue memory counter is used to store these four bytes sequentially in the EEPROM as indicated by Figure 4.8. The memory counter is updated to the internal EEPROM after every increment, at the same location as the raw event recording memory counter.

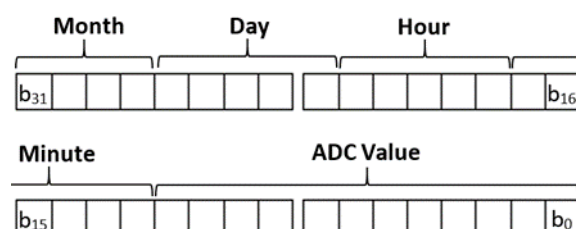


Figure 4.8 *Analogue data compressing format used*

The RTC device does not provide an automatic repeat interval wake-up function, and therefore a software function had to be implemented. The software has to constantly set the RTC alarm by adding the user-specified interval to the current time. Figure 4.9 shows the software flow

diagram which automatically sets the next alarm date and time and increments overflow components accordingly.

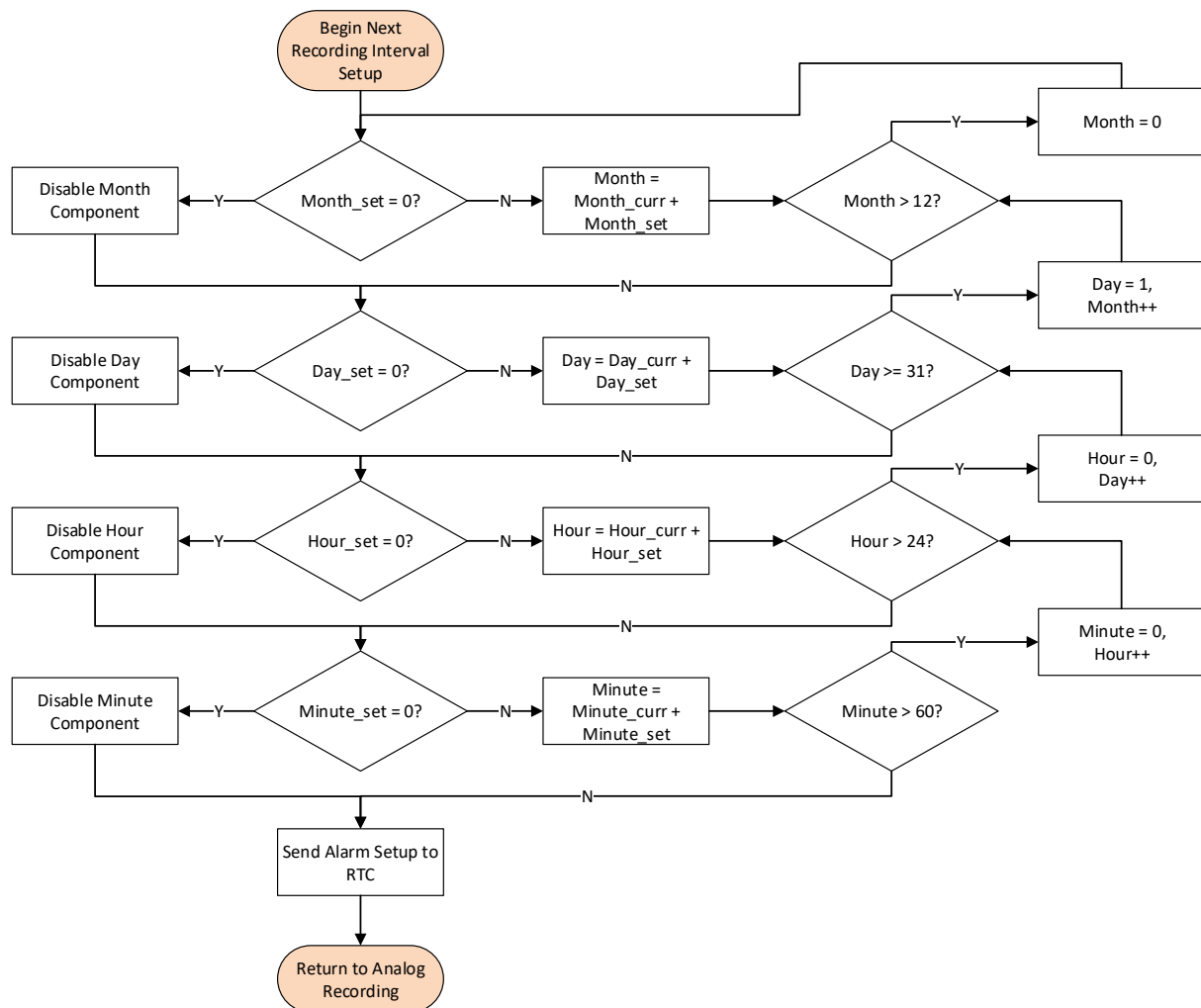


Figure 4.9 Repeated analogue recording wake-up time software flow diagram

Each component of date and time used in the alarm function is compared with the maximum of each component. In the case of a component reaching its maximum value, the software will increment the previous component and will zero the current one. For example, if the minute alarms maximum is reached, the minute component has to be zeroed and the hour component incremented. User-defined interval components are monitored and if not set by the user (equal to zero) the software will disable that component function of the RTC.

The software flow diagram illustrated in Figure 4.9 fits into the analogue recording software flow diagram as indicated by the colour indications in Figure 4.10.

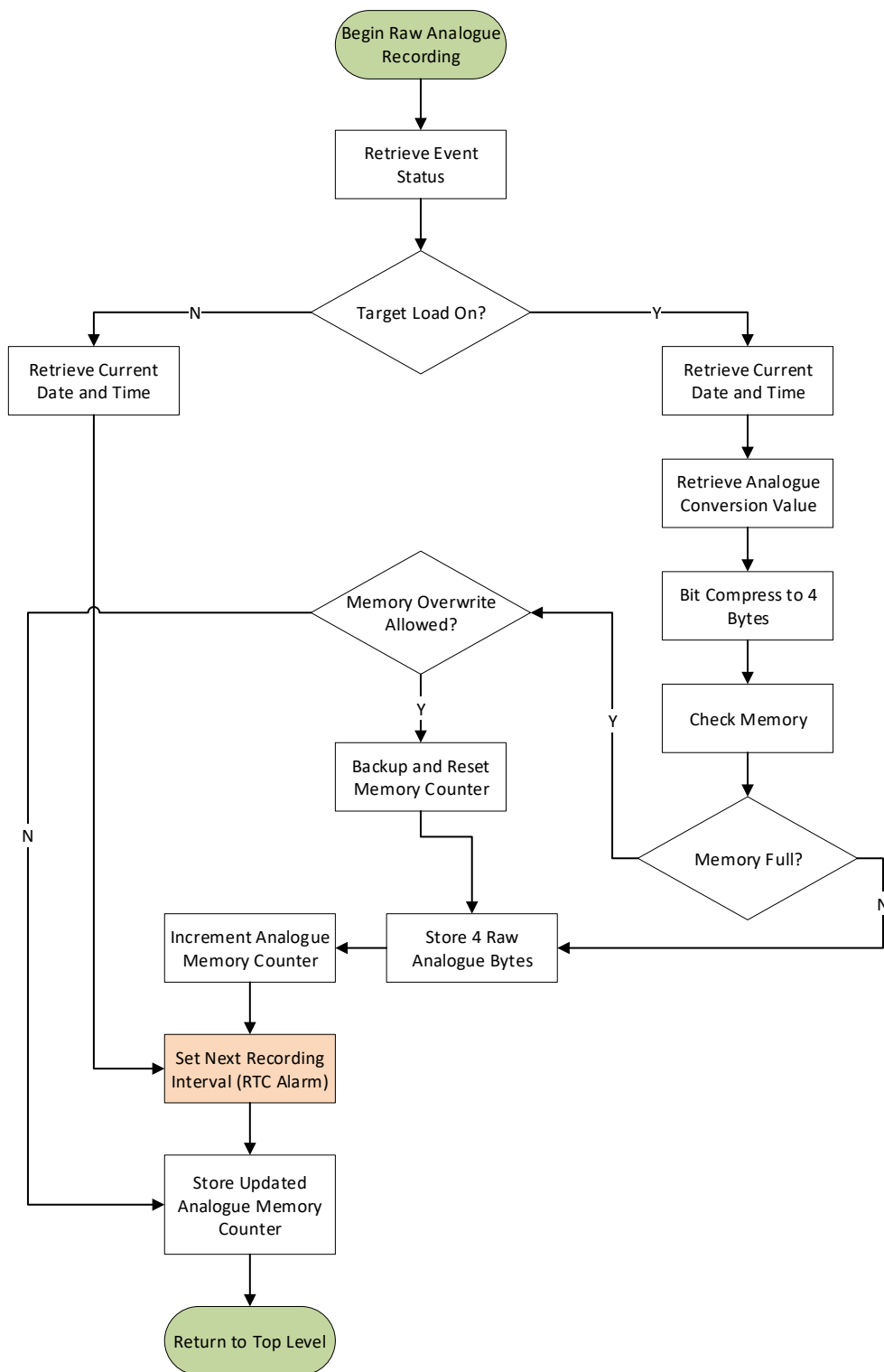


Figure 4.10 Raw analogue software flow diagram

4.7.4 Event Histogram Recording

Event histogram recording involves translating the event timestamps to start time and duration bins. The start time and durations of each event are compared to pre-set bin definitions to

establish which corresponding bin to increment. A histogram is constructed by producing a histogram distribution of all the data collected in the bin memory map.

Histogram event recording reduces the on-board storage requirements of the logging device and the associated data retrieval overheads dramatically. However, histogram event recording memory requirements are directly related to the number of bins defined for each histogram. With limited on-board storage available, the software has a pre-defined bin map set out for histogram event recordings. The definitions of the map, however, is still programmable by the user, but the maximum map size is fixed. The memory map allocated for histogram event recordings is situated in the internal EEPROM as less memory is needed for this recording mode. This further allows multiple recording modes to operate at the same time, like raw event recording and event histogram recording. Figure 4.11 shows the event histogram mapping to the on-board EEPROM.

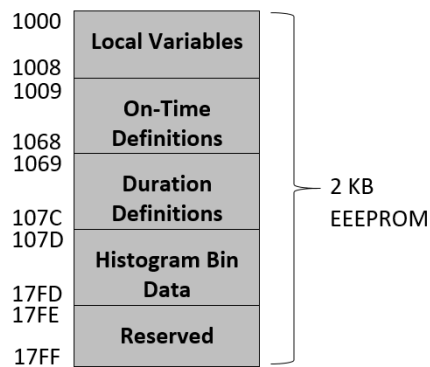


Figure 4.11 Event histogram memory mapping on internal memory

Using all the available memory of the on-board EEPROM, the event histogram memory map consists of 1920 bytes and the bin definitions a total of 116 bytes. The bin definition, On-Time, has 20 available parameters, each 8 bits wide while the bin definition, Duration, has 48 available parameters, each 16 bits wide. The histogram bin data have 20 x 48 possible bin positions where each bin is 16 bits wide resulting in 1920 bytes of bin data. All 2036 bytes are fitted in after the local variables as shown by Figure 4.11. The dimensions of the memory map allow 48 half-hourly daily starting time bins and any duration needed defined over 20 bins.

The bin definitions are set by the user from the computer application and are loaded from memory each time the event histogram mode is activated. Event histogram recording is initiated by the event interrupt and will execute certain functions based on the event status. First, the current time and date are retrieved from the RTC together with the current histogram bin values.

The Time-on index is determined during the On-event of the targeted load while the Off-event will determine the duration index. The corresponding bin will be incremented and the whole histogram memory map will be updated in the EEPROM.

The memory is generally downloaded to the computer by reading all the histogram bin data from the EEPROM. However, a bin location in the memory map can be accessed using one 8-bit index and one 16-bit index, namely the start time bin index I_T , and the duration bin index I_D . For example, to retrieve only one bin position, the memory address is calculated using Equation 4.1 in the memory map shown in Figure 4.12 [76].

$$P_X = P_{Start} + (I_D - 1)N_T + I_T \quad (4.1)$$

where N_T denotes the number of start time bins.

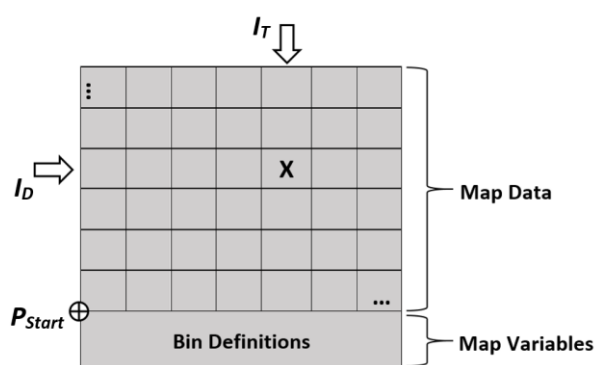


Figure 4.12 Memory map used for histogram recording modes [76]

It is also possible to implement multiple memory maps consisting of different bin definitions and bin sizes. When recording weekdays and weekends separately, for example, the memory address for bin position Y in the second memory map is determined using Equation 4.2 [76].

$$P_Y = P_{Start1} + N_{T1}N_{D1} + (I_{D2} - 1)N_{T2} + I_{T2} \quad (4.2)$$

where N_{T1} and N_{D1} denote the number of start time bins and duration bins of the first memory map respectively and N_{T2} denotes the number of start time bins of the second memory map.

Figure 4.13 shows the software flow diagram implemented for event histogram recording. This code is executed after interrupt execution in the top-level software and not in the interrupt routine itself.

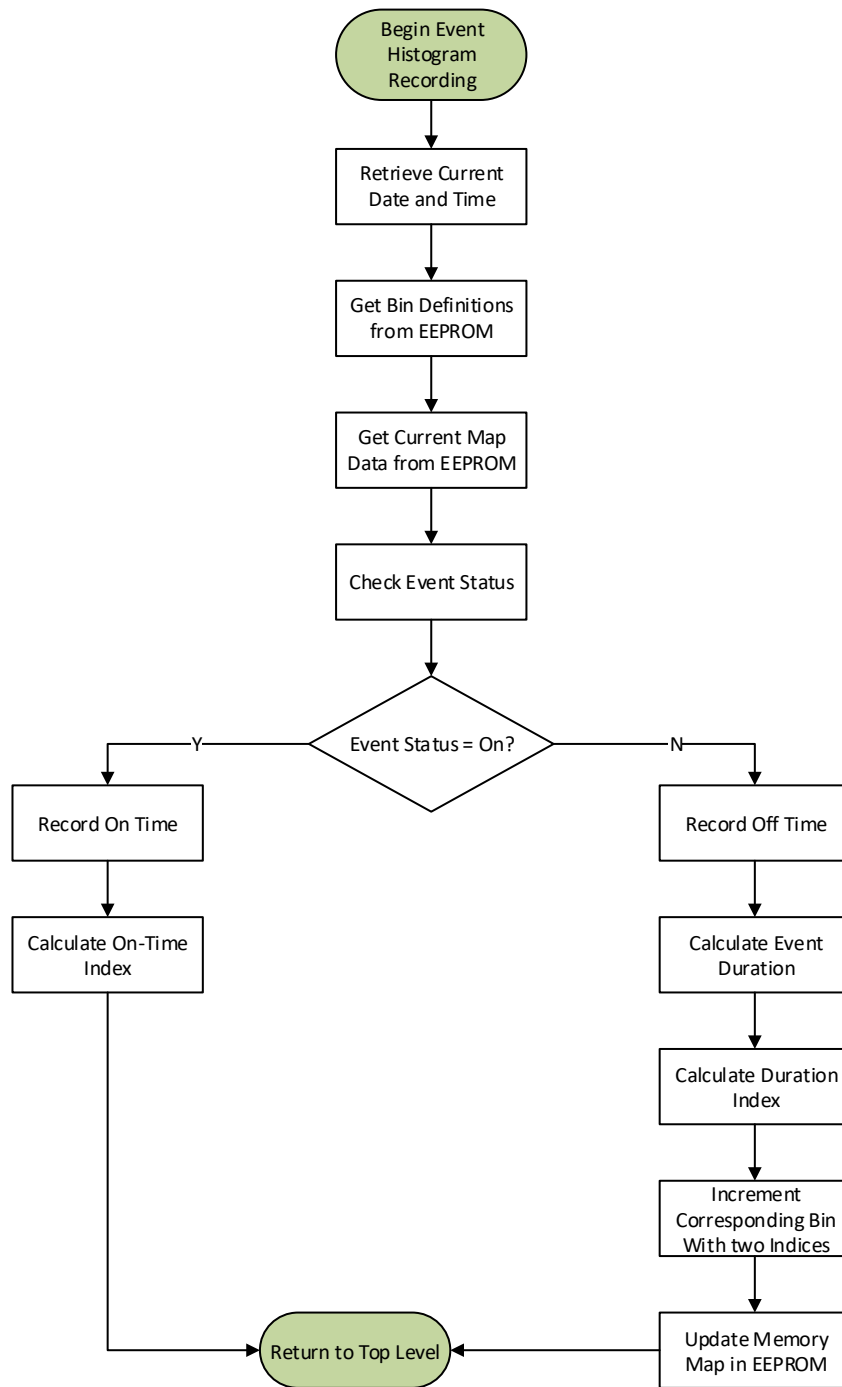


Figure 4.13 Histogram event recording software flow diagram

4.7.5 Analogue Histogram Recording

Analogue histogram recording involves translating the analogue recordings to start time and analogue value bins. As with event histogram recording the time and date of the recording are compared with user-defined time bin definitions and the analogue value is compared with analogue bin definitions. The corresponding time and analogue value index will be incremented in the analogue memory map.

Analogue recordings can generate a lot of data if the recordings are short timed which makes this recording mode a better solution for short interval analogue recordings. Only one histogram recording mode can be active at a time which is why the on-board EEPROM is used for both. When analogue histogram recording is selected by the user, the memory counter is reset, and all data currently stored in memory will be overwritten. The start address of the analogue memory map in the 2 kB EEPROM is the same as the event histogram recording. The length of each definition index for analogue histogram recordings is, however, not the same. Figure 4.14 shows how the 2 kB EEPROM is used during this recording mode.

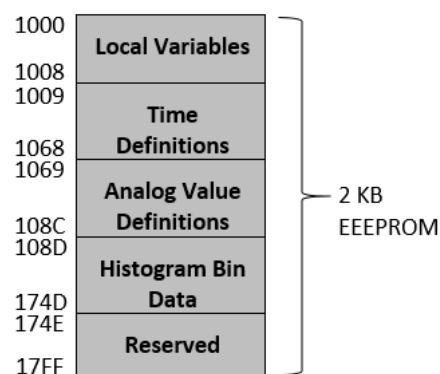


Figure 4.14 Analogue histogram memory mapping on internal memory

The time definitions are situated exactly at the same point in memory as with event histogram recording. These definitions are loaded from the EEPROM by using the same software function, starting at memory address 0x1009. The analogue value definitions, however, have fewer bins than the duration definitions used in event histogram mode. This is due to the size of the analogue readings, where a maximum value can be 12 bits in size. Therefore, two bytes are allocated per analogue value definition which cause the memory constraint and leads to a maximum of 18 bins for analogue value definitions. The analogue histogram data bins are given by multiplying the maximum bin index of the two definitions, resulting in 864 16-bit bins (1728 bytes).

Generally, the EEPROM data are requested by the application in storage sequence and are sent to the computer by reading all the data from the memory. It is again possible to retrieve a single-bin value by using the two indices, the time index and the analogue value index. The software flow diagram presented in Figure 4.15 shows the process of recording analogue histograms. The software executes the repeated interval wake-up software just before returning to the top-level software loop to set the next recording time. This is indicated by the orange block in the flow diagram.

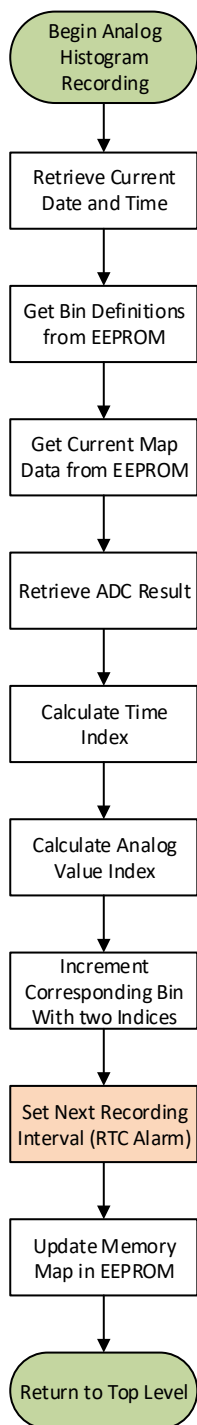


Figure 4.15 Histogram analogue recording software flow diagram

4.7.6 Expert Recording

It is often required to record multiple recording and acquisition modes. Raw and histogram recordings are available to use together only in one mode. However, the expert recording feature provides a combination recording capability to record event and analogue data together.

Expert recording is triggered by the event interrupt and fixed interval analogue readings are measured during the on state of the targeted load. This feature allows the user to observe the energy usage of a certain load as the load's environment or condition changes throughout its on-state. The raw data mode is generally a good acquisition mode to collect both event and analogue data for bigger projects as all data are still available to download. Histogram data will only include distribution based or normalised data and is therefore not implemented in the software.

Raw data has a high memory demand and recording two types of raw data at once requires a large amount of storage capacity. Only for the expert recording mode, both the EEPROMs are in use to provide a maximum recording time. With short interval analogue recordings, the data generated per event can be far more than the data generated for the event recording itself. Thus, the raw event data is stored on the on-board EEPROM while the analogue data is stored on the external EEPROM which keeps the two sets of data separate and easy manageable.

The user selects the analogue recording interval from the computer application which will be used to schedule follow up recordings within the on state of the targeted load. The storage capacity is direct related to the number of analogue recordings and with event durations being unknown, as well as the analogue recording intervals, the maximum number of expert recordings can't be estimated. The software implemented for expert recording mode uses the same functions compiled for the raw event and analogue recording mode. The only difference is that the raw event recordings are stored in the on-board EEPROM and the raw analogue recordings on the external EEPROM. The software flow diagram in Figure 4.16 shows the functions executed during expert recording.

As seen in Figure 4.16, the two recording modes combined in expert recording mode are executed by the two interrupt signals accordingly. However, expert event recording not only records the current event, but calculates and activates the analogue recording interval based on the interval set by the user. The expert analogue recording software will execute upon the RTC interrupt trigger, recording the current analogue reading and calculating the next recording time. If the event state changes before the next analogue recording, the expert recording code will be halted by disabling the RTC wake-up function and conclude by recording the off-state event. Analogue readings will, however, be recorded for the duration of the monitored load whilst in operation, and can only be terminated by the off-state event. The expert recording mode will continue upon initiation of a new on-state event, and will subsequently resume analogue recordings.

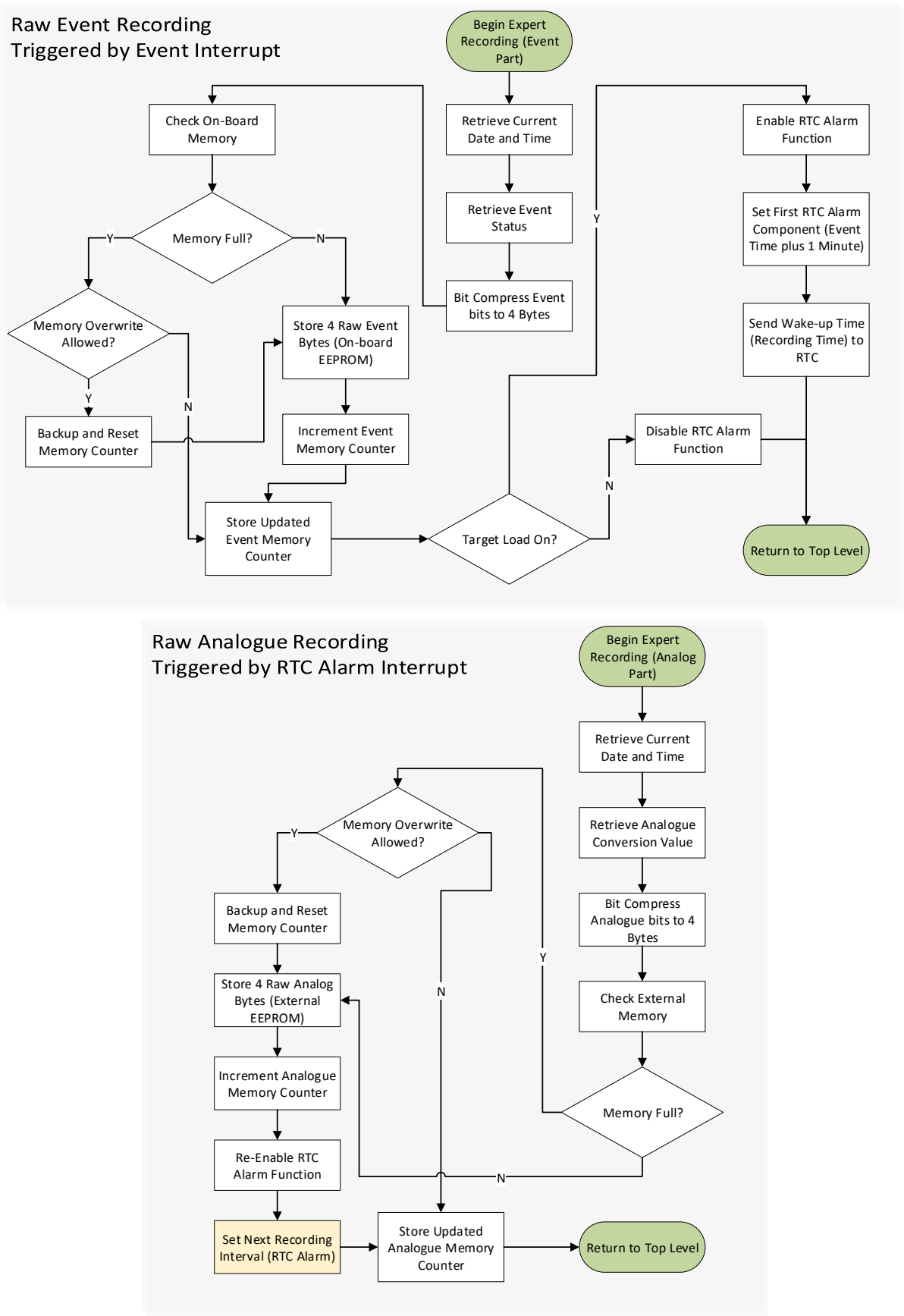


Figure 4.16 Combined raw event and analogue (expert) recording software flow diagram

5 Application Software

5.1 Introduction

The computer application software development is presented in this chapter. The embedded software, as described in Chapter 4, interacts with the computer application software by using the USB interface. An activity flow diagram and structure overview of each important software module is presented. The main objectives of the computer application software are to:

- Manage the real-time clock data.
- Set wake-up intervals.
- Retrieve, display, export and erase data stored on the device memory.
- Configure modes of operation.
- Manage device identification settings.

5.2 High-level Application Software

5.2.1 Overview

In accordance with the project's main objectives, the computer software application is developed to interact with the logger device. The software application is a user-friendly platform to retrieve data recorded by the hardware in a format recognisable by the post mathematical analysis software on the computer. Figure 5.1 illustrates where the computer application fits into the project. The application software is implemented as a GUI using the well supported C++ open-source QT Creator development platform.

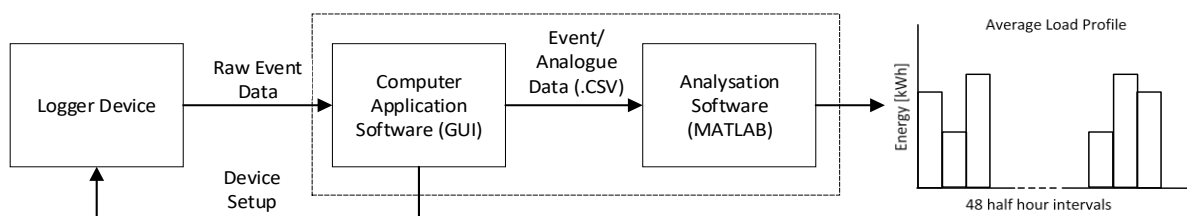


Figure 5.1 High-level application software overview

The application software is developed in parallel with the embedded software, based on the command message structure listed in Table 4.1. The application sends command bytes to the

embedded software to execute certain software functions. It is either sending a command byte to trigger specific software functions, which requires the attached data packet, or alternatively, a single command byte is issued, where after the application receives data sent by the embedded software.

Most of the application software functions are identical to one another but are triggered by different command bytes and requires data packages of different sizes. Therefore, a high-level software program overview of the application is described in this chapter to highlight the non-repetitive software functions. The computer application consists of five device interaction sections, giving access to the necessary settings as given in Figure 5.2.

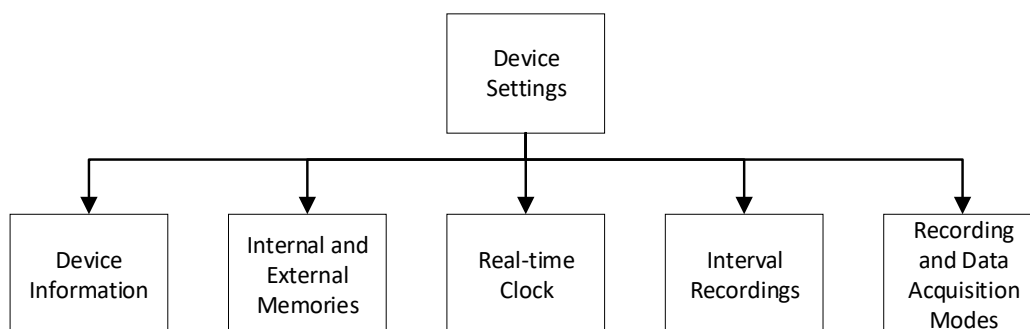


Figure 5.2 *Device settings accessible from the computer application*

The five device interaction sections include the following:

- *Device Information*: This section includes information about the device connected to the computer. It includes information such as USB data transfer speed information, port connection information and device identification number.
- *Internal and External Memories*: Memory data is displayed in this section. The user can manage the device memory settings, including memory overwrite and memory erase functions.
- *Real-time Clock*: Real-time clock information is accessed by this interaction section. The user can use this section to set the current date and time, as well as retrieve and display the clock information on the RTC.
- *Interval Recording Setup*: Interval recording settings for analogue recordings are managed in this section. It also offers an analogue testing interface.

- *Recording and Data Acquisition Modes*: This interaction section is implemented to set up the device in a desired mode of operation as listed in Figure 4.1.

The device interaction sections are only activated when certain recording and data acquisition modes are selected by the user. The device information and real-time clock sections are always active. Each section is thoroughly described in terms of its functionality.

5.2.2 Device Information

The application software executes automatic device hardware identification recognition software to establish a serial communication link via the matching serial port. The embedded software responds by sending device information and the current recording mode to the application. This information is displayed in the device information section, where the user can change the device ID number. Figure 5.3 shows the list of information available to the user for the specific logger device connected.

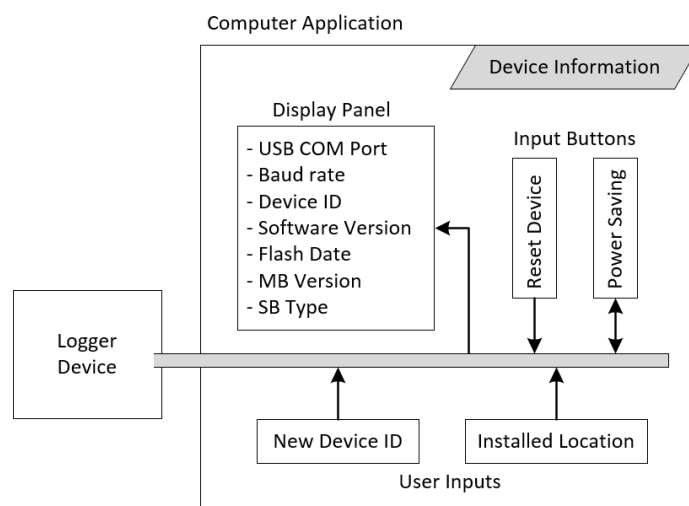


Figure 5.3 Device information available to the user via the computer application

The device information section further includes an easy device installing feature, allowing the user to install the logger without the need to remember where each logger is installed. The installed location is entered during setup and the application will add the installation location, device ID and installed date to a text file stored in the default directory of the computer application.

The section also features an embedded software reset function and a manual power saving feature, which toggles the LED indicators and low power modes of the device.

5.2.3 Memory Information

The same memory information section is visible for all recording and data acquisition modes; however, the memory settings applies to the memory device in use for the selected recording and data acquisition mode. For example, if the user erases the device memory while it is in raw event recording mode, the software will only erase the external EEPROM.

The memory information section controls the memory counter position. The read memory usage function, as shown in Figure 5.4, retrieves the memory counter of the current selected memory device and calculates the percentage memory in use. The user can manually reset the memory counter, which does not reset the memory itself, but instead only resets the memory counter to return to the start position, allowing the device to overwrite the current stored data. The memory information section also features a “memory full” setting, which can either be selected to overwrite the memory or to completely stop the recording process when the memory is full.

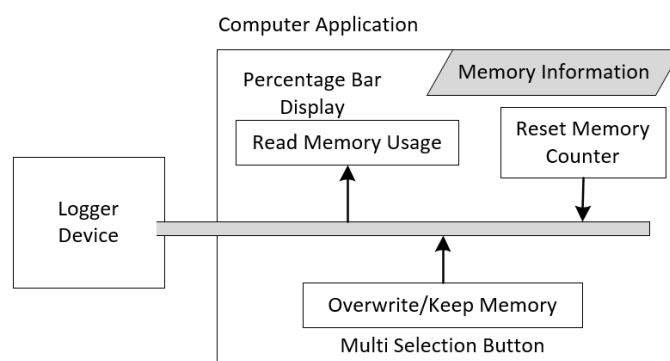


Figure 5.4 Memory information of the logger displayed in the computer application

5.2.4 Real Time Clock Information

Real time clock data can be retrieved or changed by using the RTC information section. The time and date are displayed to the user by using a *time-date display* widget within the application. The time and date of the device is updated by either sending a custom user time and date input from the application or by synchronizing the RTC with the host computer calendar settings. These input parameters are illustrated by Figure 5.5.

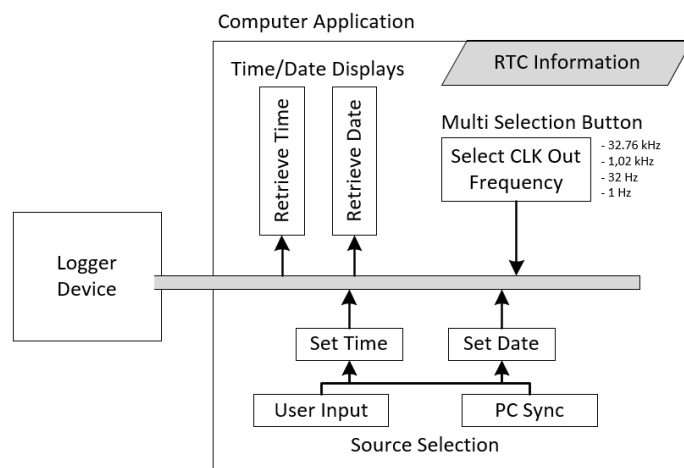


Figure 5.5 Real-time clock interaction options via the computer application

A multi selection button changes the frequency of the RTC device's external clock signal. The feature offers no useful purpose and was implemented for debugging purposes only. For future development, this interface can be used as a reliable clock source for the microprocessor.

5.2.5 Interval Recording Setup

Repeated interval analogue recording configurations are facilitated by the interval recording setup section. The interval recording setup section is only active during analogue recordings and is deactivated in normal event recording modes.

The interval recording setup section receives three time-parameters from the user; days, hours, and minutes, as shown in Figure 5.6. This allows the user to schedule the next analogue recording, based on the user input. In most analogue recordings, only the minute component will be used, as short timed recordings provide more accurate results. For this reason, the day component is limited to three days.

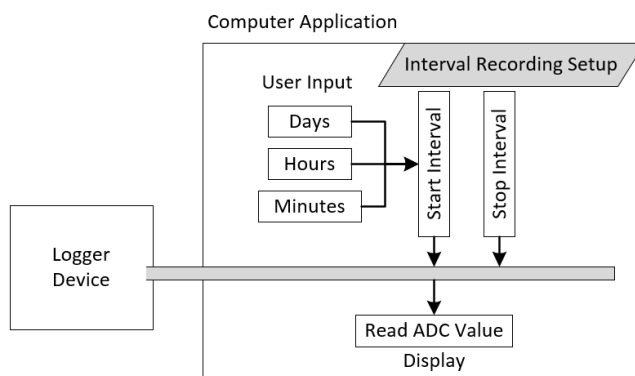


Figure 5.6 Interval recording setup within the computer application

Repeated analogue recordings can be stopped by sending a deactivate command to the device. For expert recording configurations, a user-defined interval is required and saved to the device software. The interval analogue recordings will automatically be activated by the on-event and stopped by the off-event generated by the event sensing circuit.

The interval recording setup section also features a real-time analogue value monitor, which outputs the ADC count result as well as the current consumed by the connected load. The feature can be used for debugging purposes during device installations.

5.2.6 Recording and Data Acquisition Modes

The logger device offers two recording and two data acquisition modes as described in Chapter 4. These modes can be combined, within set boundaries, depending on the type of recording, as well as the method of data storage.

A recording mode configurator is implemented in the form of point buttons, as shown in Figure 5.7. To simplify the recording mode setup for the user, the allowed recording and data acquisition mode configurations have been grouped together. The user will only be able to select a certain data acquisition mode, which depends on the trigger mode selected by disabling the other options. The user can “lock” the settings to activate the selected recording mode.

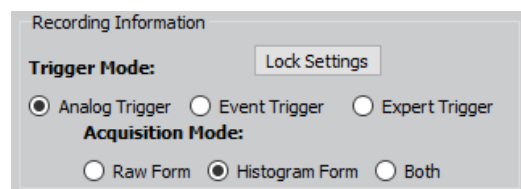


Figure 5.7 Sensor trigger and data acquisition mode setup interface

The updated mode of operation (trigger mode and data acquisition mode settings) will be sent to the device software, where after the mode will be initialized. Each mode of operation is thoroughly explained in Chapter 4. The remainder of this chapter explains how the recording data is retrieved for each data acquisition mode.

Raw event and analogue data retrieval are the quickest way to retrieve the stored data from the device, as there are almost no data conversions necessary to display or export the data. The data packets received for raw data recording modes are ordered and directly exported into a text file. The data is displayed in the application by reading the data from the text file. The data viewer allows exporting of the text file data to a Comma Separated Value (CSV) file format.

Histogram event and analogue recordings are generating less data than raw data acquisition mode. However, setting the mode and displaying the recorded data, requires a histogram map display. This map is only available when histogram data acquisition modes are selected and can be launched by using the *show map* button. A new window will open where the user can adjust the bin definitions. Default bin definitions, for each trigger mode, were calculated based on the amount of data generated and the memory space available. The user can manually adjust these bin definitions and the number of bins can also be reduced. The maximum number of bins for each trigger mode is listed in Table 5.1.

Table 5.1 *Maximum number of bins for different trigger modes available in histogram recording*

Trigger Mode	Maximum Magnitude Bins	Maximum Time Bins	Magnitude Definition Variable Size (bits)	Time Definition Variable Size (bits)
Event Trigger	20	48	8	16
Analog Trigger	18	48	16	16
Expert Trigger	n/a	n/a	n/a	n/a

The histogram bin values are all 16-bit integers and are programmable to change bin values before exporting the data to a CSV-file format. The bin values are cleared when recording modes are switched to avoid memory overwrites and corrupted data.

As mentioned in Chapter 3, and indicated in Table 5.1, expert recording mode is only configurable for raw data acquisition mode. Within the expert recording section of the application, data are downloaded from both memories with two separate commands. The data is stored as two separate text documents. The data viewer can switch between these two files for easy data comparison. However, when using the data exporting function in expert recording mode, the user will have options to export only certain data to a CSV-file format.

6 Data Simulation Software

6.1 Introduction

The main objective of the simulation software is to find energy efficient interventions within a micro-grid system. It aims to calculate possible energy savings by using supplied historical data and real-time measured data as input parameters. Figure 6.1 shows the simulation software execution process. The simulation software executes various software functions to convert the data retrieved from the data logging instrumentation to 48 half-hourly averaging energy profiles. The simulation software is finally used to forecast the payback period of the replacement of the target appliances with energy efficient alternatives.

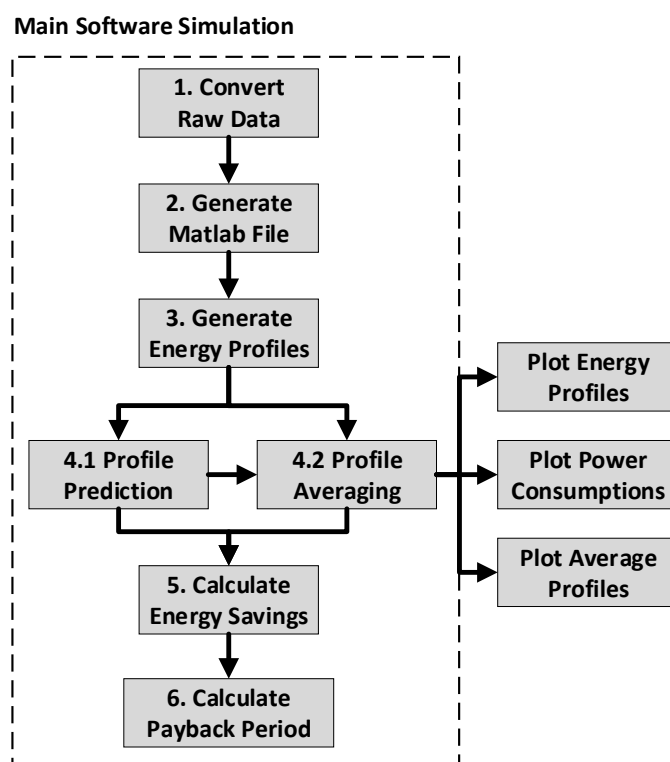


Figure 6.1 Simulation software execution process

The software functions used in the simulation are listed in Table 6.1, together with a short description of each. Each software function consists of various input and output parameters, which is described in detail in the remainder of the chapter. The software data types and profile construction are also explained. The software functions implemented are titled according to the specific energy system defined within the case study, however, the simulation process remains the same for any study.

Table 6.1 Software functions implemented for simulation purposes

Software function	Description
averageGrapher	Plot various energy profiles with averaged data generated by <i>profileAverage</i> for a defined period.
profileGrapher	Plot various daily energy profiles for selectable input data (measured or historic).
convertRawData	Convert historical CSV data to a format suitable for <i>generateMFile</i> .
generateProfile	Generate data matrix for various energy profiles from raw data stored in Excel files.
generateMFile	Generate <i>Matlab</i> recognizable file from raw CSV data for quicker analysis.
profilePrediction	Predict energy profiles of measured logger data using the total appliances measured.
loadBreakUp	Plot different demand profiles in comparison with the total demand profile.
payBackPeriod	Calculate the payback period based on result obtained from <i>energySavings</i> .
powerPlot	Generate a scatter plot of the power consumption of data retrieved from data loggers.
profileAverage	Generate average energy profiles in terms of a matrix.
energySavings	Calculate total energy savings.

Most of the software functions depends on one another and are executed in the order given in Figure 6.1. The graphing software functions are implemented to plot various profiles throughout the software simulation. The remainder of the chapter elaborates on the software functions required to accumulate the payback period, as listed in the main software simulation section in Figure 6.1.

6.2 Software structure design to import measured and historical data

A set of software functions is required to import the data retrieved from the data logger devices. As shown in Figure 5.1, data retrieved are stored in CSV-file format, one file for each logger device. The raw data retrieved from the devices are defined in a format that is easy to analyze, which can be transformed to a *Matlab* file by executing the *generateMFile* function.

A set of input parameters for the *generateMFile* function is defined in Figure 6.2. A short description of the input and output parameters are provided in Table 6.2 and Table 6.3 respectively. The input parameters, introduced in Table 6.1, are a common set of variables used throughout the simulation and is required by most software functions. The output parameters are sometimes required as input parameters for other software functions.

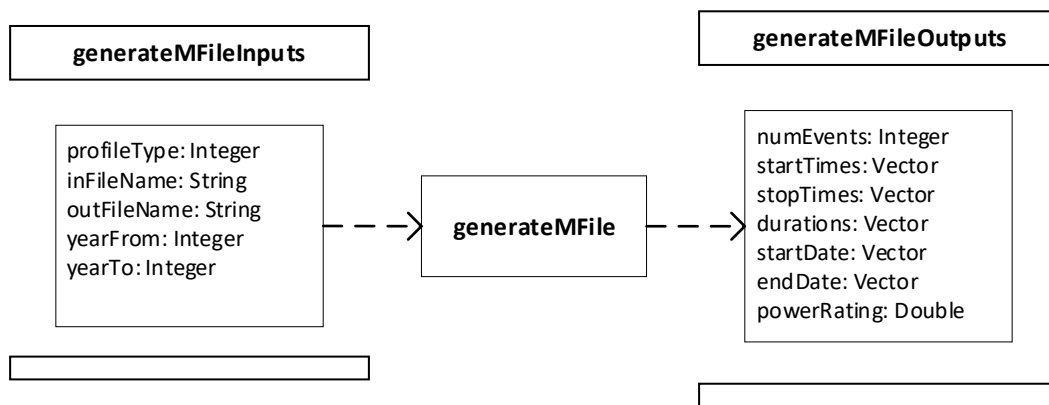


Figure 6.2 Input and output parameter overview for the software function *generateMFile*

Table 6.2 Description of the input parameters for *generateMFile* function

Input parameter	Description
profileType	An integer for profile type as listed in Table 6.4.
inFileName	A string for the input file name, which varies with logger ID numbers.
outFileName	A string for the output <i>Matlab</i> file name, which is recognized by <i>generateProfile</i> functions.
yearFrom	An integer for the year to start the file searching.
yearTo	An integer for the year to end the file searching.

Table 6.3 Description of the output parameters for *generateMFile* function

Output parameter	Description
numEvents	An integer keeping count of the number of events listed in input file.
startTimes	A vector of event on times.
stopTimes	A vector of event off times.
Durations	A vector of event durations.
startDate	A vector of event start dates corresponding with startTimes.
endDate	A vector of event end dates corresponding with stopTimes.
powerRating	A double of monitored appliance power rating.

The *generateMFile* function is executed based on the energy profile type selected. The variable, *profileType*, accepts integers between one and eight, where each value represents a different energy profile type, as required by the case study. Table 6.4 gives a short description of each energy profile type.

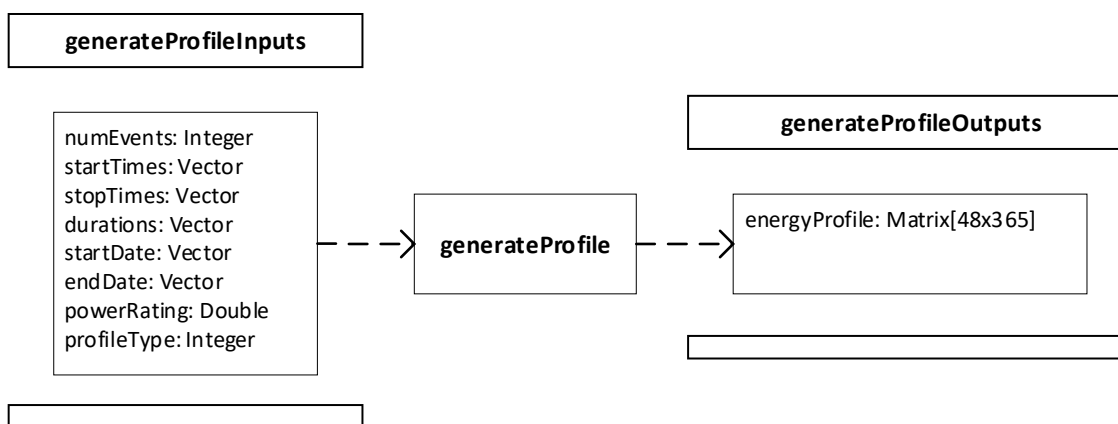
Table 6.4 Descriptions of energy profile types available to generate through simulation

<i>profileType</i> input	Energy profile type description
1	Measured geyser usage data.
2	Historical diesel generation power data.
3	Historical PV plant energy data.
4	Historical battery storage energy data.
5	Historical total demand energy data.
6	Measured cooking load usage data.
7	Historical battery storage charge status.
8	Measured desalination water plant power consumption data.

Historical data is provided in a different format than the format in which the measured data is stored. A common software function is implemented to convert the historical data to CSV-file format. Before the historical data can be analyzed and converted to a *Matlab* file, the function *convertRawData* is executed.

6.3 Software structure design to generate energy profiles

The output parameters generated by the *generateMFile* function is used in the energy profile generation software, as shown by Figure 6.3. The *generateProfile* function is executed to determine the energy profiles. A typical energy profile consists of averaging time intervals with energy values for each, presented as a histogram. The format of the energy profiles presented in the case study consists of 48 half-hourly averaging intervals. This format is used throughout the software simulation to simplify calculations.

**Figure 6.3** Input and output parameter overview for the *generateProfile* software function

Energy profiles are generated based on the profiles available according to Table 6.4, using the *generateProfile* function. Each energy profile is stored in matrix form, consisting of a column for every day of the year and a row for every half-hour of each day. The matrix format used for energy profiles \mathbf{E}_P , is presented as

$$\mathbf{E}_P = \begin{bmatrix} 1 & \cdots & N_C \\ \vdots & \ddots & \vdots \\ N_R & \cdots & N_R \times N_C \end{bmatrix} \quad (6.1)$$

where N_C denotes the total number of half-hours in a day and N_R denotes the total days per year.

The *generateProfile* function first generates a usage profile using the input parameters. The usage profile is then used to determine the energy profile as described in detail in the case study. Figure 6.4 shows a typical timeline for a single day with four events, two on-events and two off-events. First the *startTimes* and *stopTimes* input parameters are converted to timeline event start and stop indices. The event on-time index, I_{On} , is used to find the matching event start half-hour on the 48-half-hour timeline. An upper start index, I_{SU} , and lower start index, I_{SL} , is determined to find the on-duration for the selected on-half-hour, which is given by:

$$n_{on} = (I_{SU} - I_{On}) \times 100 \quad (6.2)$$

where n_{on} denotes the on-duration within the event start half-hour as a percentage [%].

The event off-time index, I_{Off} , is used to find the corresponding half-hour during which the off-event where generated. An upper stop index, I_{EU} , and lower stop index, I_{EL} , is determined to find the on-duration for the selected off-half-hour, given by:

$$n_{off} = (I_{Off} - I_{EL}) \times 100 \quad (6.3)$$

where n_{off} denotes the on-duration within the event stop half-hour as a percentage [%].

All the half-hours between the upper start index and lower stop index are assumed to be periods where the appliance is in an on-state. It results in a value of 100% for each of these half-hours, as the appliance where operating for all the half-hours.

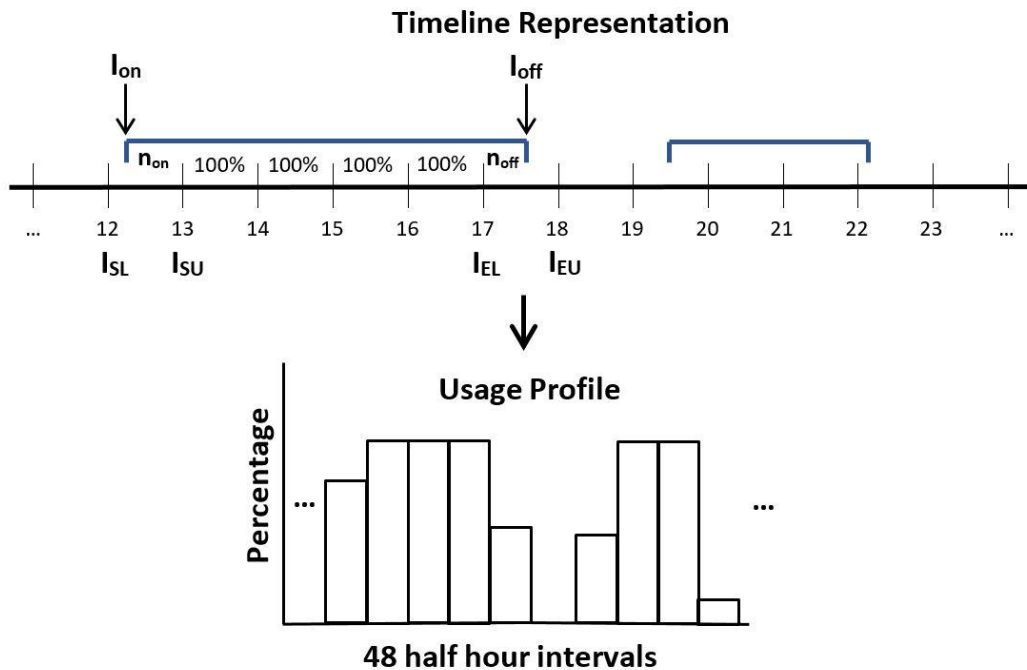


Figure 6.4 Timeline example of an event and the conversion to a usage profile

The daily timeline represents the usage profile of one appliance for a 48-half-hour day. The software function, *generateProfile*, delivers a matrix variable of 365 timelines for each type of profile.

6.4 Software structure design to average and forecast energy profiles

Energy profile averaging and forecasting is facilitated by two software functions, *profileAverage* and *profilePrediction*, respectively. The measured data energy profiles are first used to forecast an energy profile for the specific measured appliances based on the number of appliances present at the site. For instance, the case study elaborates on the installation of 29 data loggers, measuring the energy profiles of geysers, but the site consists of approximately 60 geysers in total. The software function *profilePrediction* derives an average energy profile using all measured energy profiles available. The output parameter represents a per day equivalent energy profile for the specified number of appliances in matrix form. The software function requires the available input files to retrieve the energy profiles for the available sets of data, as given in Figure 6.5 A short description of the input parameters is given in Table 6.5

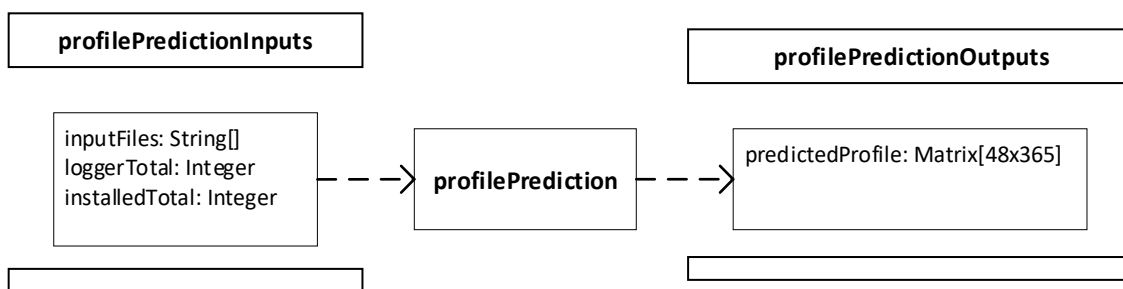


Figure 6.5 Input and output parameters required for profile prediction simulations

Table 6.5 Description of the input parameters for profilePrediction

Input parameter	Description
inputFiles	A string array with all available energy profiles.
loggerTotal	An integer for the total loggers used on a specific appliance.
installedTotal	An integer for the total installed appliances of the type measured by the loggers.

The forecasted energy profiles of the measured data and historical energy profiles are averaged by executing the *profileAverage* function. The software function averages daily energy profiles from the energy profile matrix for a specified period. The type of profile required, and the averaging period, are selectable by an energy profile type, start day and stop day input parameter. The output parameters are separated in multiple energy profiles due to different nature of energy profiles during weekdays and weekends. Figure 6.6 shows the software function input and output parameters. A short description of the output parameters is given in Table 6.6.

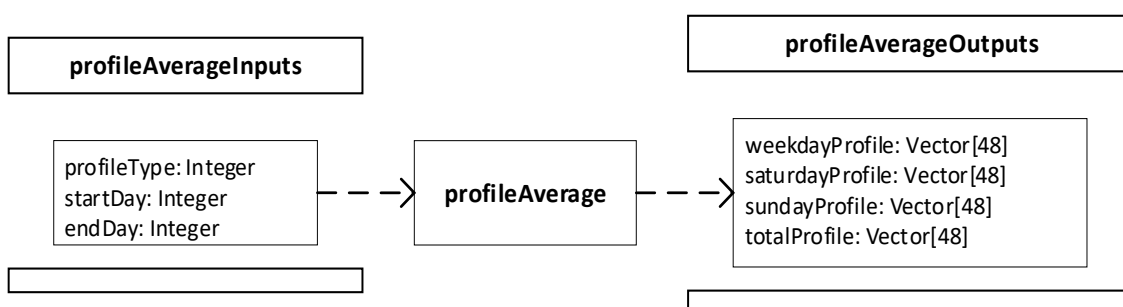


Figure 6.6 Input and output parameters for profileAverage software function

Table 6.6 Output parameters for profileAverage software function

Output parameter	Description
weekdayProfile	A vector of daily energy profile representing the average for weekdays.
saturdayProfile	A vector of daily energy profile representing the average for Saturdays.

sundayProfile	A vector of daily energy profile representing the average for Sundays.
totalProfile	A vector of daily energy profile representing the total average for the period.

6.5 Software structure design to calculate energy savings and payback period

The final two software functions are executed to find the energy savings and the payback period of the installation of heat-pump systems. The energy savings are found by executing a set of energy saving conditions. The mathematical formulation of these conditions is expressed in detail in the case study.

The software function, *energySavings*, accept input parameters based on the selected profile averaging type. The energy savings can be calculated by using the per-day energy profile and average the energy savings at the end, or by using the averaged total energy profile delivered by the *profileAverage* function. Additional input parameters are required by the set of energy saving conditions to determine all possible energy savings as described in Table 6.7. The set of energy saving conditions are applied to the various input profiles to generate a single energy saving value as an output parameter. Figure 6.7 shows the input and output parameters to the *energySavings* software function.

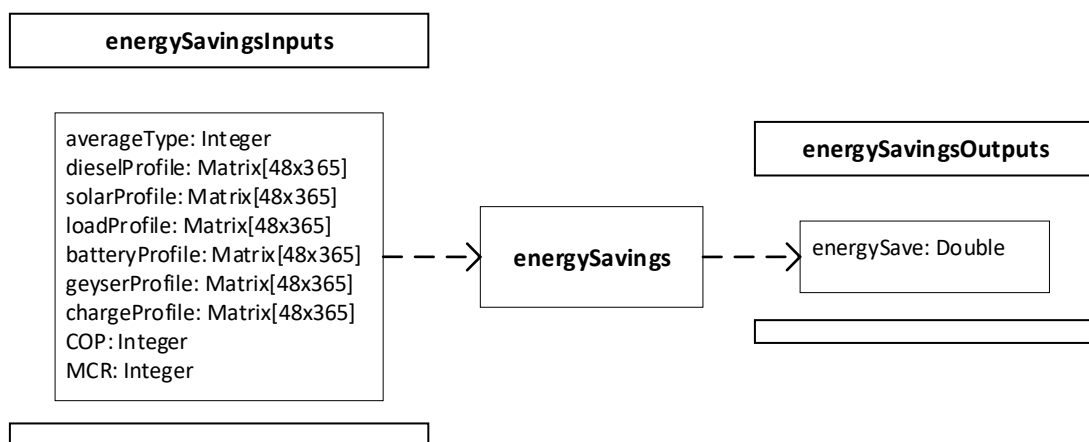


Figure 6.7 Input and output parameter overview of the software function *energySavings*

Table 6.7 Description of the input parameters required by *energySavings* software function

Input parameter	Description
averageType	An integer for profile averaging type selection.
dieselProfile	A vector of diesel generator energy profile as determined by <i>generateProfile</i> .
solarProfile	A vector of solar system energy profile as determined by <i>generateProfile</i> .
loadProfile	A vector of load energy profile as determined by <i>generateProfile</i> .

batteryProfile	A vector of battery energy profile as determined by <i>generateProfile</i> .
geyserProfile	A vector of geyser energy profile as determined by <i>profilePrediction</i>
chargeProfile	A vector of battery charge profile as determined by <i>generateProfile</i> .
COP	An integer for heat pump system's coefficient of performance.
MCR	An integer for the maximum battery system charge rate [kWh].

The calculation of the payback period is facilitated by the function, *payBackPeriod*, which accepts *energySave* as input parameter. The payback period formulation uses predetermined constants for the diesel consumption rate and landed diesel cost. The formulation of the payback period itself is described in the case study. The *payBackPeriod* function delivers the total diesel savings [L] and the accompanied cost savings [R].

7 Case Study and Results

7.1 Introduction

In order to test the functionality and performance of the proposed logging system, a case study was performed at Robben Island World Heritage Site (RIWHS) near Cape Town, South Africa. The case study aims to achieve the following research objectives:

- Performance evaluation of the logger hardware under field conditions, especially with reference to the power consumption performance of the hardware.
- Performance evaluation of the embedded software and computer application software under field conditions.
- Evaluation of the usefulness of histogram recording in comparison to the traditional raw event recording techniques.
- Identification of opportunities for Energy Efficiency (EE) interventions at the site, especially with reference to the sanitary hot water load and cooking load.
- To establish the payback period of replacing the resistive heating elements with heat-pumps, with the view to reduce diesel consumption by generators.
- Investigation of the effects of load profile data averaging over a period of a month compared to per-day load profile data.
- Evaluation of the performance of the Renewable Energy (RE) interventions at the site, especially with reference to the performance of the battery storage system and solar PV plant.

To achieve the above-mentioned objectives, a survey of the electrical loads of a sample set of residential properties at the site is done with the view to identify the load types and power ratings. The usage profiles of high power consuming loads, such as electric geysers and stoves, are logged for a sample set of residences, using the proposed data logger. Diesel generation, solar plant generation and battery storage profiles were obtained, using a five-minute averaging interval, for the period of the project of the field measurements.

7.2 Site Description

7.2.1 Overview

Robben Island is located in Table Bay, about 6.9 km west of Bloubergstrand, Cape Town, South Africa. The island is about 30 meters above sea level and has an area of approximately 5.07 km². Robben Island has been used as prison for nearly 400 years. It was also used as a post office, a grazing ground, a mental hospital and an outpost. Today, it is well-known as an UNESCO World Heritage Site or a South African Heritage Site.

The island houses a wide range of infrastructure, including approximately 90 residential dwellings, a harbour, an air strip, churches, prison buildings, school buildings, hotel, quarries, military installations, a desalination plant, a diesel power plant and a lighthouse. The island is accessible to visitors through tours that depart from the Cape Town waterfront. These tours, which involves ferry trips to and from the island, depart three times a day depending on weather and sea swell conditions. It includes a bus tour of various historical sites on the island, including attractions such as a graveyard, Robert Sobukwe's house, the maximum-security prison, both the bluestone and lime quarries and the army and navy bunkers used during world war two. The island also offers a coffee shop and snack bar located at a location known as Alpha One, where visitors have a view of Table Bay towards Signal Hill. A curio shop is located at the harbour and is available to all visitors arriving at the island.

7.2.2 Building Infrastructure

A partial load survey was conducted in 2015 by Energy Management and Validation Services (EMVS) with the view to compile an inventory of the electricity generation and distribution infrastructure and main electrical load components at the site [77]. The island has extensive building infrastructure that differs in size and have unique individual energy consumption profiles. The water desalination plant was identified as the main electrical energy load on the island, while residential appliances such as geysers and stoves are among the second most power intensive electrical loads present.

7.2.3 Electrical Infrastructure

7.2.3.1 Network Topology

The electrical network topology at the site can be summarised as follows:

- The main electrical power is generated by Low Voltage (LV) Cummins diesel generators at a supply voltage of 400 V.
- Additional electrical power is supplied by a 666.40 kW Photo Voltaic (PV) power plant, operational since April 2017.
- A battery storage bank is charged during daytime and supplies electrical power during night time. The battery storage bank has a nominal capacity of 100 Ah at an operating voltage of 865 V.
- Electrical power from the battery storage bank is fed through a 3 phase, 400 V, 525 kVA ABB cast resin dry transformer to the main electrical network.
- The 400 V main electrical generation bus is connected to an 11 kV Medium Voltage (MV) distribution system through a 400V/11kV step-up transformer. The MV system consists of 11 kV underground distribution cables.
- The MV distribution system forms a micro-grid with a total of 5 mini-sub installations that supply the loads across the island. The ratings of these mini-sub installations are summarised in Table 7.1.

Table 7.1 Transformer ratings at various mini-sub installations at Robben Island [79]

Mini-sub index	Transformer rating
1	315 kVA
2	500 kVA
3	315 kVA
4	200 kVA
5	315 kVA

7.2.3.2 Power Generation Infrastructure

There are three different power sources currently in use on the island, namely diesel generators, a solar PV plant and a battery bank. The diesel generators are located at the power station in the vicinity of the harbour, while additional standby generators are installed at distributed strategic points across the network.

The photovoltaic power plant is situated on the eastern side of the island, about 50 meters from the sea and 300 meters from the Robert Sobukwe House. The solar power plant consists of 1960 PV panels which are group connected to 12 individual ABB 50 kW inverters.

The batteries are installed in an ABB battery storage container, which also houses metering and cooling systems. The battery bank is connected to the 400 V generation bus through a 525 kVA ABB cast resin dry transformer. The 400 V generation bus is controlled by ABB generation controlling technology. The system automatically starts the diesel generators in the event of greater power demand compared to the available power from the battery storage and photovoltaic plant. The 400 V generation bus is interfaced with the 11 kV MV reticulation system via a 400V/11kV step-up transformer. Table 7.2 summarises the ratings, locations and status of the power sources currently installed.

Table 7.2 Summary of power sources at Robben Island [79]

Power Source	Index	Rating	Location	Status
Main Generators	1	500 kVA	Power Station	Operational
	2	500 kVA	Power Station	Operational
	3	500 kVA	Power Station	Operational
	4	500 kVA	Power Station	Operational
	5	1000 kVA	Power Station	Not operational
	6	1000 kVA	Power Station	Not operational
Standby Generators	0	300 kVA	Power Station	Operational
	7	300 kVA	Prison	Operational
	8	300 kVA	Robert Sobukwe House	Operational
	9	300 kVA	Lighthouse	Operational
	10	300 kVA	MPLC	Operational
Photovoltaic Plant	1	666.4 kWp	300m from Robert Sobukwe House	Operational (Since April 2017)
Battery Storage Bank	1	500 kWp	15m from Power Station	Operational (Since April 2017)

7.2.3.3 Load Inventory

A partial load survey was previously conducted at the site in 2015 by EMVS with the view to identify opportunities for EE interventions. The survey focussed on identifying load types rather

than compiling a full load inventory. Their survey relied on approximated power ratings and no detailed usage data was collected. The survey also did not include the load inventories of the residential dwellings. In order to gain insight into the load inventory associated with the residential sector on the island for the purposes of this study, a more detailed survey was conducted for a sample set of 7 occupied residential dwellings. Table 7.3 summarises information gained from the residential survey conducted in August 2017.

Table 7.3 Residential load inventory results from the survey conducted in August 2017

Property index	Number of Occupants	Load Details
8	7	1 x 3 kW Geyser 1 x 2 Plate stove (Hood Only) 1 x 3 kW Kettle 1 x Single door refrigerator 2 x Television sets 1 x Microwave oven 1 x Toaster 1 x 2x58 W FLT lamps 6 x 15 W CFL lamps 4 x 40 W Incandescent lamps 2 x Portable fans
16	1	1 x 3 kW Geyser 1 x 4 Plate stove/Oven (Small) 1 x 3 kW Kettle 1 x Double door refrigerator 1 x Television set 1 x Microwave oven 1 x Toaster 1 x 2x58 W FLT lamps 12 x 15 W CFL lamps
87	5	1 x 3 kW Geyser 1 x 4 Plate stove/Oven 1 x 3 kW Kettle 1 x 2 kW Heater (Bar/oil type) 1 x Single door refrigerator 1 x Television set 1 x Microwave oven 1 x Toaster 1 x 2x58 W FLT lamps 13 x 15 W CFL lamps
82	4	1 x 3 kW Geyser 1 x 4 Plate stove/Oven 1 x 3 kW Kettle 1 x 3 kW Heater (Bar/oil type) 1 x 3 kW Heater (Resistant coil type) 1 x Single door refrigerator 1 x Deep freezer 1 x Television set 1 x 2x58 W FLT lamps 11 x 15 W CFL lamps 1 x Clothes iron
78	5	1 x 3 kW Geyser

		1 x 4 Plate stove/Oven 1 x 3 kW Kettle 1 x 3 kW Heater (Bar/oil type) 1 x Single door refrigerator 1 x Deep freezer 2 x Television sets 1 x Microwave oven 2 x 2x58 W FLT lamps 12 x 15 W CFL lamps 2 x 100 W Incandescent lamps 1 x Washing machine (13 kg Top loader) 1 x Radio/Entertainment system
15	5	1 x 4 kW Geyser 1 x 4 Plate stove/Oven 1 x 3 kW Kettle 1 x Double door refrigerator 1 x Television set 1 x Microwave oven 2 x Toasters 1 x 2x58 W FLT lamps 10 x 15 W CFL lamps 1 x Auto Washing machine 1 x Radio/Entertainment system
89	2	1 x 3 kW Geyser 1 x 4 Plate stove/Oven 1 x 3 kW Kettle 1 x Coffee machine 1 x 3 kW Heater (Bar/oil type) 1 x Single door refrigerator 2 x Deep freezers 1 x Television set 1 x Microwave oven 1 x Toaster 3 x 2x58 W FLT lamps 16 x 15 W CFL lamps 5 x 100 W Incandescent lamps (Bed lamps most) 1 x Washing machine (6 kg Front loader) 1 x Dishwasher

The residential load survey conducted at the site delivered a load inventory with the following general characteristics:

- The residential load component consists mainly of electric geysers and electric heaters. Almost all of the residences surveyed feature a 3 kW 150 l geyser and at least one or two 3 kW resistance or electric oil heaters.
- A few of the residences has four plate stoves with bake and grill functionality, while others only have a small two plate cooking hob.
- All residences have miscellaneous loads such as refrigerators, deep freezers, television sets, computers, washing machines, etc.

- Despite previous EE intervention efforts, some of the residences still have incandescent lamps, which is highly inefficient.

The survey results highlight possibilities for further EE interventions at the site. Apart from the reverse osmosis desalination plant, which has previously been identified as the main load at the site, residential load components such as the geysers, stoves and heaters, can be expected to make a substantial contribution to the overall load profile, especially during periods outside the daytime solar PV generation cycle. All of these load categories qualify for EE interventions in the sense that the conventional geysers can be retrofitted by heat pumps or solar water heating systems, and the cooking and space heating appliances can be replaced by gas appliances.

This investigation focuses on the sanitary water heating and cooking load. The power ratings of these loads are readily available, but usage profiles are required to calculate the load profile of each component.

The remainder of this chapter focuses on the load profile recording procedures that were implemented to characterize the load profiles of the electric geyser and cooking load, using the event and histogram recording technology developed in the study. These load profiles are subsequently used, together with diesel generator supply profiles, PV plant generation profiles and battery storage supply profiles, to determine the potential savings in diesel costs following the implementation of EE interventions.

7.3 Demand Profile Data Acquisition

7.3.1 Overview

A total of 40 histogram data loggers were produced and installed to record the characteristics of the residential geyser and cooking loads. Of these, 29 loggers were installed on geysers, while the remaining 11 were deployed on stoves. The residences targeted in the study were selected based on the number of occupants in order to gain a representative load model.

Power profile data for the diesel generators, PV plant and battery storage were supplied by *Meteo Control, Energy and Weather Services*, which is a commissioning service for monitoring systems and SCADA for PV projects worldwide [78]. Together with the RE installations at the site, a telecontrol and smart measuring system were installed to measure and control the micro-grid remotely earlier in 2017. *Meteo Control* provided access to historical data, measured in 5-minute averaging intervals, such as the following:

- Inverter data which include AC/DC power, voltage, current, temperature and frequency data.
- PV energy generation profiles, irradiance data, system availability data, performance ratios and system efficiency data.
- Wind speed data and environmental indicators.
- Battery system data, consisting of energy profiles, battery voltages, charging status, global battery error conditions and temperatures.
- Diesel generation power profiles. Only generators 1 to 4 are being monitored.
- Total energy consumption demand profile for the island.

Although the PV plant has been operational since April 2017, the historical data is only available from the 10th of August 2017. An additional *PowerTrack* energy analyser was installed at the water plant to retrieve the energy consumption profile and the total energy consumption data.

7.3.2 Installation Procedure

All 40 loggers were deployed on the 20th July 2017 at the site. The residences were selected in a random manner according to their occupancy and accessibility. Only 29 residences were targeted during this study, as the residences equipped with a 4-plate stove were used to install loggers on both the geyser and stove. Each logger was assigned a unique identification number between C1 and C40. The installations are summarized in Table 7.4, which shows the logger ID, house number, appliances targeted and the number of occupants.

Table 7.4 Residential properties used at Robben Island for the study

Logger ID	House Number	Targeted Appliance	Number of Occupants
C1	82	Geyser	4
C2	78	Geyser	5
C3	87	Geyser	5
C4	90	Geyser	4
C5	15	Geyser	5
C6	15	Stove	
C7	16	Geyser	1
C8	10	Geyser	5
C9	10	Stove	

C10	8	Geyser	7
C11	6	Geyser	4
C12	6	Stove	
C13	86	Geyser	4
C14	86	Stove	
C15	11	Geyser	3
C16	11	Stove	
C17	5	Geyser	2
C18	4	Geyser	3
C19	4	Stove	
C20	3	Geyser	3
C21	3	Stove	
C22	42	Geyser	2
C23	44	Geyser	4
C24	56	Geyser	4
C25	59	Geyser	3
C26	60	Geyser	4
C27	57	Geyser	2
C28	63	Geyser	2
C29	63	Stove	
C30	29	Geyser	4
C31	36	Geyser	2
C32	36	Stove	
C33	35	Geyser	3
C34	35	Stove	
C35	89	Geyser	2
C36	72	Geyser	6
C37	80	Geyser	2
C38	7	Geyser	4
C39	Transnet 4	Geyser	3
C40	Transnet 4	Stove	

The loggers were installed non-intrusively at the main distribution board to monitor the supply current of the targeted loads. The loggers were configured using the dedicated computer application developed as part of the project with a specific logger configuration, depending on the targeted appliance.

Regular site visits were conducted to download the recorded data. Due to logistical constraints, data were downloaded in sessions on 16th August 2017 and 23rd August 2017 respectively. The dataset acquired during the first month of the study was only used to test the proposed system, because the power profiles for the diesel generators, PV plant and battery storage

system for the period were not available. The second dataset was retrieved on 15th September 2017 and was used, together with the power profiles for the diesel generators, PV plant and battery storage system for this period, to characterise the energy flow characteristics of the site and to determine the energy saving impacts of the proposed heat pump installations. The data acquired for the last two weeks were used to test the various recording modes of the logging system and to further support the analysis results. The loggers were removed from the site on 4th October 2017.

7.3.3 Logger Configuration

The loggers targeting geysers were configured during the first month in expert recording mode, i.e. recording both the usage profiles and power consumption data. With the power consumption of each geyser known from the first data set, only the usage profiles were recorded during the second data set. The loggers targeting the stoves were also configured to record the usage profiles as well as the power consumption during the first month. These were configured to only record the power consumption values for the second month. With the two datasets, all the recording modes were tested, except for the histogram recording feature. All of the loggers installed for the geysers were configured for event histogram mode for the last two weeks of the study. Table 7.5 summarises the logger configurations for the period of the study.

Table 7.5 *Summary of data recording types and durations for the study*

Period	Geyser Loggers	Stove Loggers
20/07/2017 – 23/08/2017	Expert Recording	Expert Recording
23/08/2017 – 15/09/2017	Raw Event Recording	Raw Analog Recording
15/09/2017 – 04/10/2017	Histogram Event Recording	Expert Recording

7.4 Demand, Diesel Generation, PV Generation and Battery Storage Power Profiles

7.4.1 Overview

The power generation and battery power profiles used in this study consist of five different profiles with five-minute recording intervals. This data is averaged to yield 48 half-hourly averaged values for compatibility with the data gathered by the event loggers. The characteristics of these profiles are mostly explained using two or more daily profiles, indicating the different scenarios. Profile averaging over daily cycles are implemented for comparison purposes and is used as a form of simplification for mathematical formulations. It also provides indication of the differences in the weekday and weekend demand profiles.

A sunny day without cloud cover is compared with a rainy day with plenty cover of clouds, with the view to illustrate the impact of the PV plant and demand profile on the diesel generators, as well as on the battery storage system.

7.4.2 Demand Profile

The demand profile represents the half-hourly averaged total load at the site. The demand profile includes all loads at the site, where hot water cylinders, cooking appliances and the desalination plant represent some of the high energy intensive loads. The demand profile highlights the peak demand periods, typically caused by residential appliances, such as hot water cylinders and cooking appliances. For the detailed analysis done in the case study, the demand profiles are only used to calculate the total demand energy per day. The data retrieved from the logger devices, which represents the usage profiles of the three major loads, namely the geysers, stoves and the desalination plant, as well as energy generation profiles, such as diesel generation profiles, solar generation profiles and the battery storage profiles, are used to determine the impacts of the proposed heat pump retrofits.

The demand profile shown in Figure 7.1 for the 5th of September 2017 represents the total demand for the day, with an operating desalination water plant. Another demand profile shown in Figure 7.2 for the 10th of September 2017 represents the total demand for the day, with the desalination plant operating only for half the day. The numeric values are given in Appendix A, Table A.10 and Table A.11. The demand profile for these two days clearly show that the desalination water plant has a high-power consumption rate that is fairly predictable if operating conditions are known or scheduled.

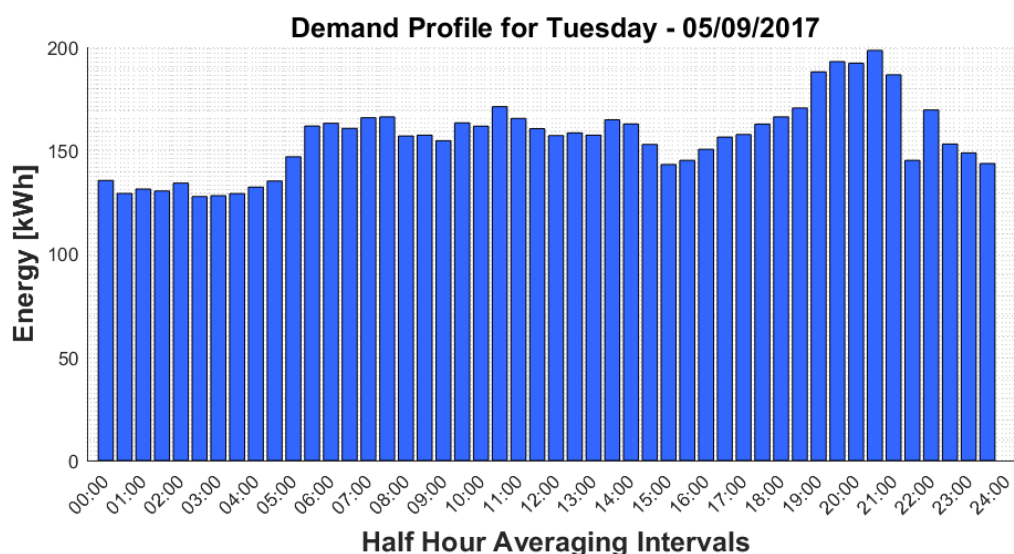


Figure 7.1 Total demand profile with the desalination plant in operation for the whole day

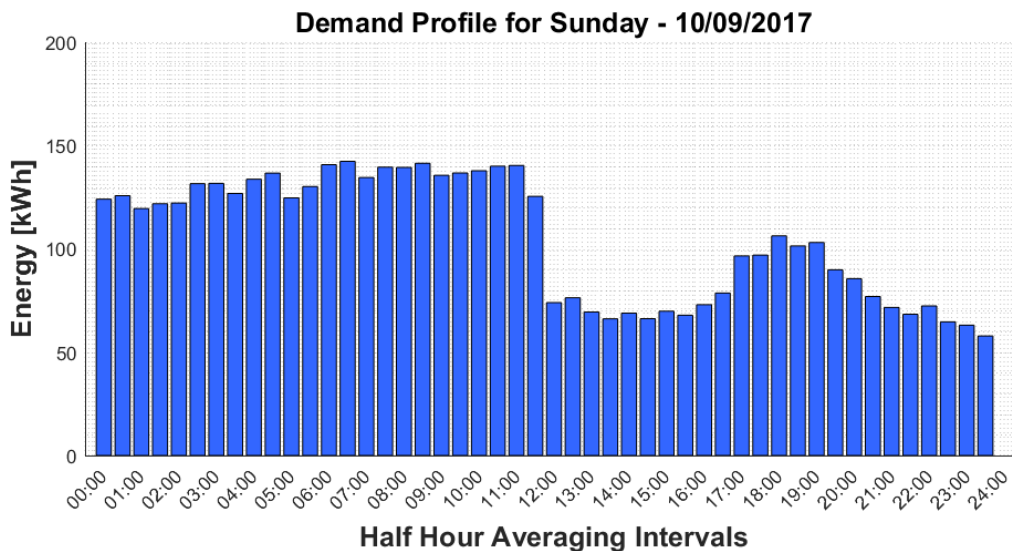


Figure 7.2 Total demand profile with the desalination plant operating for half the day

The overall average daily demand profile for the period of the case study, i.e. 10th August to 18th September 2017, is given in Figure 7.3. The numeric values are given in Appendix A, Table A.12. The overall average demand profile makes it more challenging to derive the desalination water plant operating hours. However, the averaged demand profile exhibits clear peak demand periods, which is between 06:00 and 08:00 and 18:00 and 22:00. The daily peak demand is 155 kWh per half-hour, which is typically caused by residential loads such as hot water cylinders and cooking appliances.

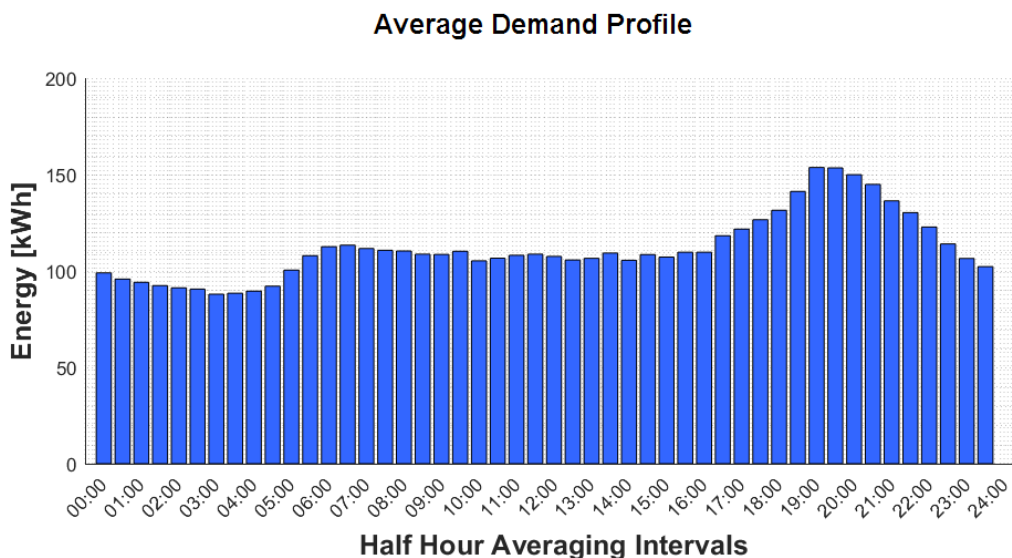


Figure 7.3 Overall average daily demand profile for the period of study

The overall average energy demand is 10 734 kWh per day, which is equal to the sum of the total daily average energy supplied by the diesel generator, PV plant and battery storage system.

7.4.3 Diesel Generation Profile

The diesel generation profile represents the half-hourly averaged energy profile of the four measured diesel generators. The total diesel generation profile is mostly produced by a single generator operating at a time, i.e. generator number 1 or 4. Increased demand automatically starts an additional generator if required. However, for the period of the case study, the demand was mostly in the supply range of a single generator. For the few cases where additional generators were operational, the power supplied from all generators were aggregated to calculate the total energy profile.

The diesel generation profile shown in Figure 7.4 for 1st of September 2017 represents a sunny day where the solar irradiance was sufficient to service the daytime load and fully charge the battery storage system, so that the diesel generators could switch off during the day. For this specific day, only one of the 300 kVA generators were supplying power to the micro-grid during the early morning hours and late evening. Figure 7.4 clearly indicates where the PV plant serviced the full load of the micro-grid. The contribution of diesel generation to the energy consumption is 8 177 kWh for this day. The numeric values for the diesel generation profile on this day are given in Appendix A, Table A.2.

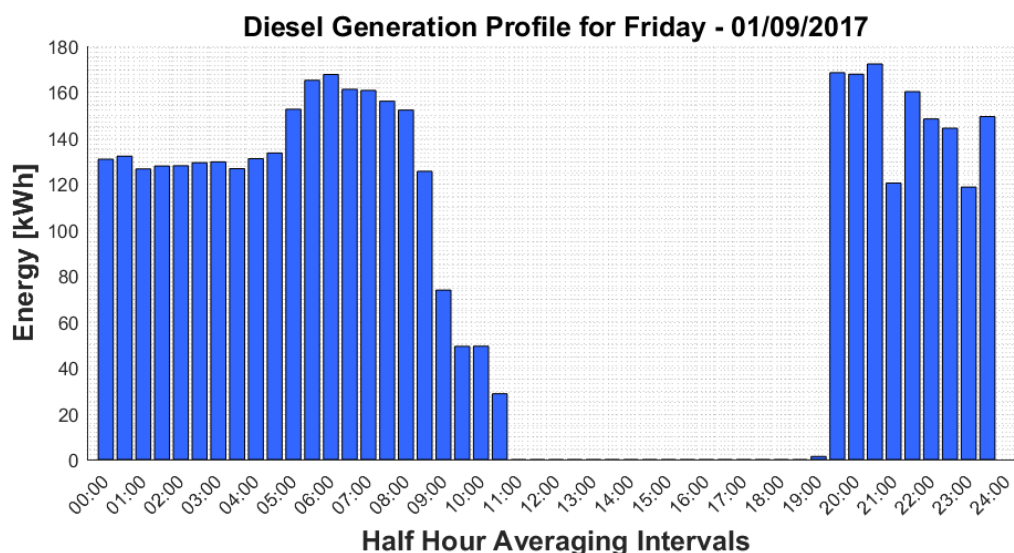


Figure 7.4 Diesel generation profile for a sunny day with no cloud cover

Figure 7.5 shows the diesel generation profile for the 5th of September 2017, which is a typical example of a cloudy and rainy day at the site. These weather conditions have significant impact on the power supplied by the PV plant and also affects the battery charging rate and the diesel generation supply profile. The contribution of diesel generation to the energy consumption is 11 622.4 kWh for this day. The numeric values for the diesel generation profile on this day are

given in Appendix A, Table A.2. By comparing the energy delivered for the profiles shown in Figures 7.4 and Figure 7.5, it is clear that weather conditions can cause a difference of up to 35% in the energy supplied to the micro-grid by diesel generation.

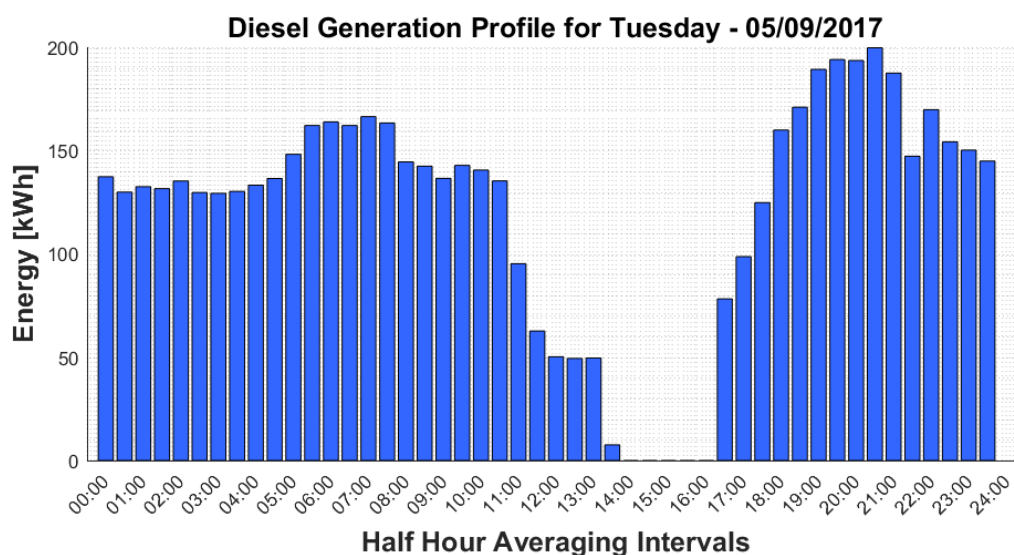


Figure 7.5 Diesel generation profile for a cloudy and rainy day

The statistics for the diesel generation power profiles shown in Figure 7.4 and Figure 7.5 are summarised in Table 7.6.

Table 7.6 Energy contribution and operating timelines of diesel generation for a sunny and cloudy day

Weather condition	Total energy supplied [kWh]	Operation cycle 1	Operation cycle 2
Sunny, high irradiance	8 177	00:00 – 11:00	19:00 – 24:00
Cloudy, low irradiance	11 622	00:00 – 14:00	17:00 – 24:00

The average daily diesel generation profiles for the period of the case study, i.e. 10th August to 18th September 2017, for weekdays, Saturday and Sunday are shown in Figure 7.6, while Figure 7.7 shows the overall average daily diesel generation profile for the period of the study.

Average Diesel Generation Profile

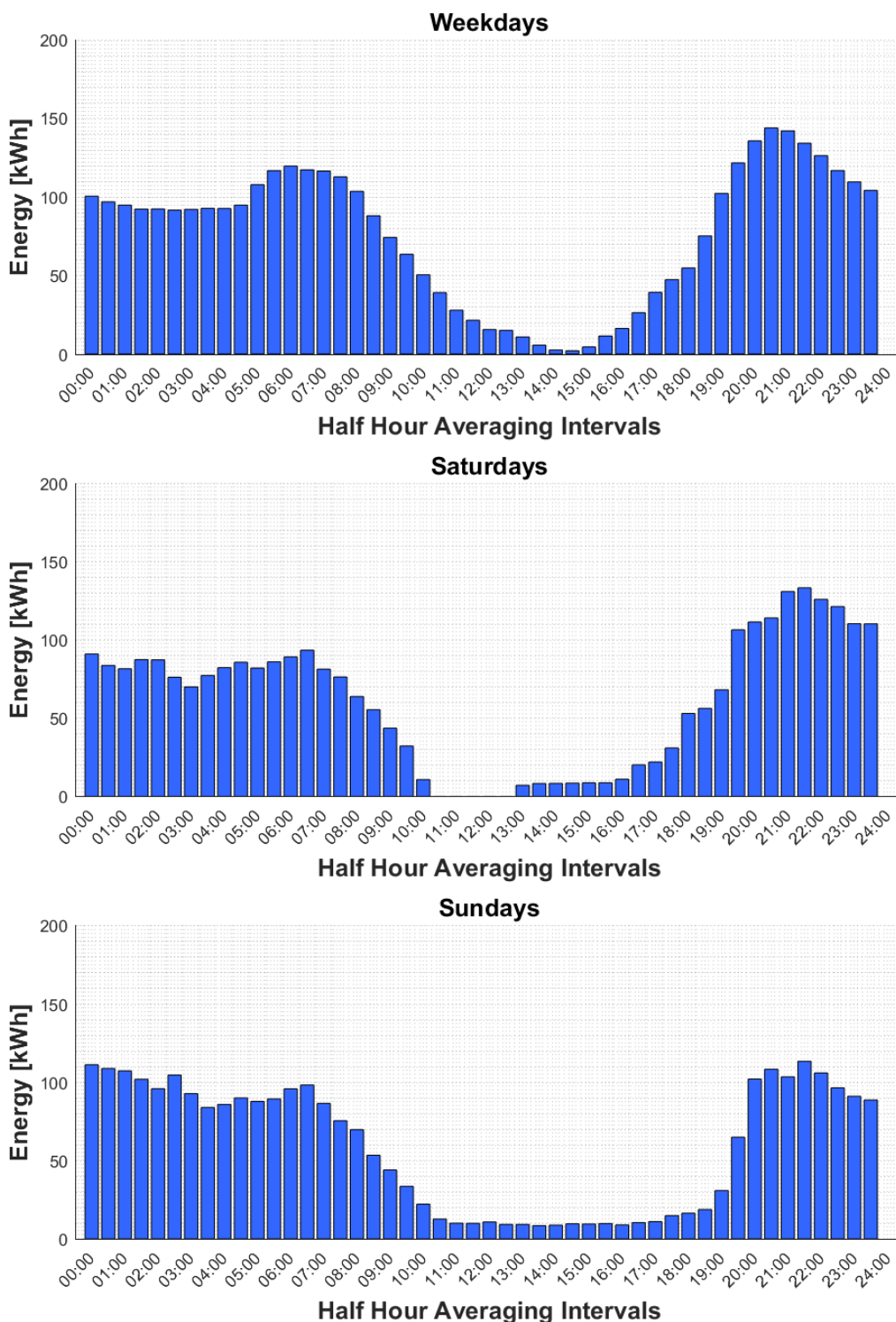


Figure 7.6 Overall average daily diesel generation profiles for weekdays, Saturdays and Sundays for the study period

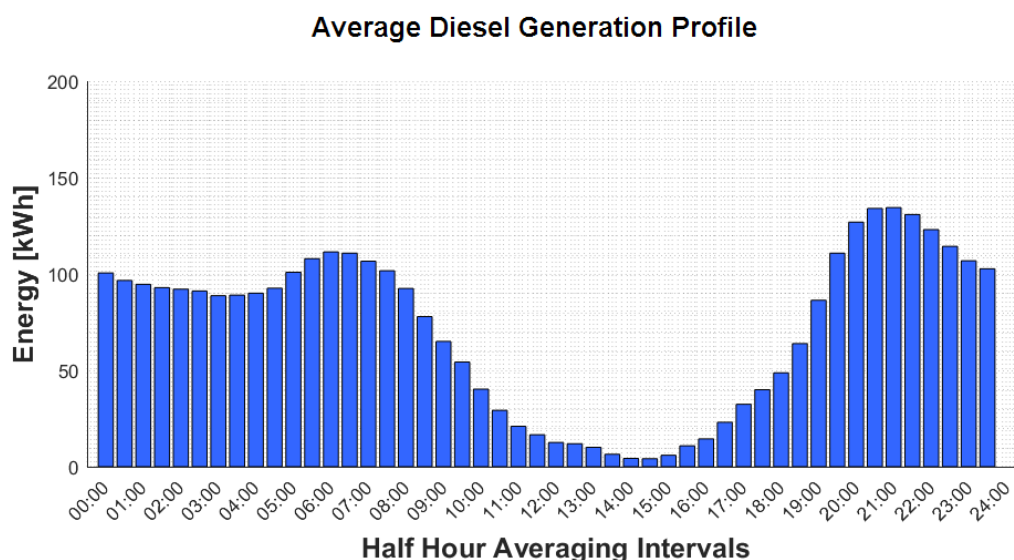


Figure 7.7 Overall average daily diesel generation profile for the study period

The averaged diesel generation profile, shown in Figure 7.7, represents a worst-case baseline profile. As the study was done in the winter season, when most residences used electric heaters and high consumption of sanitary hot water, this model can be seen as the worst possible condition for the year. The numeric values for the averaged diesel generation profile are given in Appendix A, Table A.3. The daily energy contribution is 6 845.6 kWh, with a peak half-hourly energy supply of 135 kWh at 21:00.

7.4.4 Solar Generation Profile

The daily solar generation profile represents the half-hourly averaged energy delivered by the PV plant for a specific day. The profile consists of 48 half-hour energy values measured as the total output from the 12 installed inverters. In order to study the impact of the weather conditions on the solar generation profile, the profile for an ideal sunny day is compared to the profile for a cloudy day. The solar generation profile for the 1st of September 2017, which represents a sunny day with no cloud cover, is given in Figure 7.8. The numerical values are given in Appendix A, Table A.4. The profile has a total cumulative daily energy value of 5 773 kWh, with a peak energy output of 256.2 kWh per half-hour.

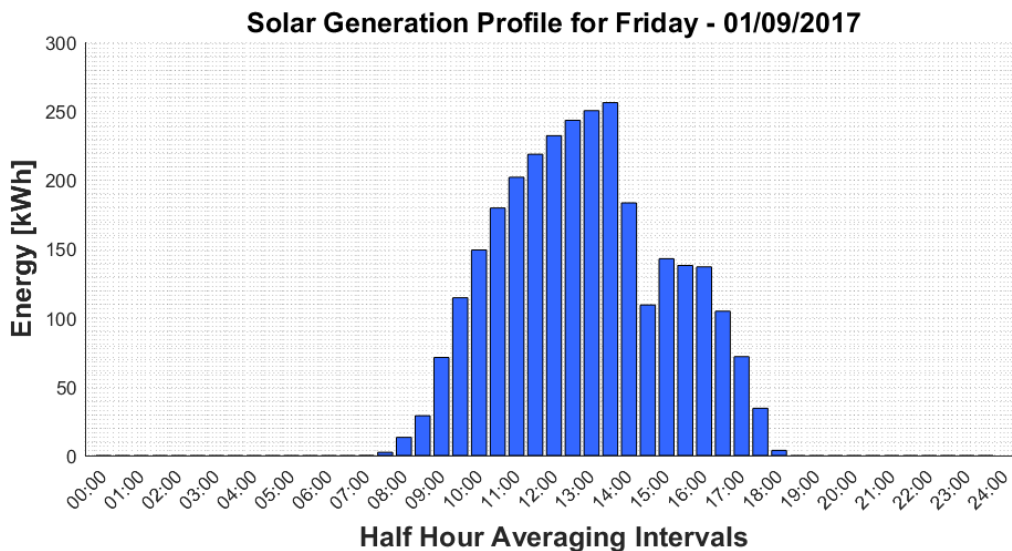


Figure 7.8 *Solar profile on an ideal solar day*

The solar generation profile shown in Figure 7.8, follows the solar irradiance profile closely for the period that the batteries are charging, meaning that all possible energy is retrieved from the PV plant. The batteries reach a maximum charging state at 14:00, where-after the solar generation profile follows the demand profile. For this period, the solar irradiance is high enough to deliver the required power.

A cloudy day have an impact on the charging cycle of the batteries. The batteries may take longer to reach its maximum charging state or don't reach it at all. This have an impact on the subsequent diesel generation profile, which will be required to compensate for the lower energy delivered by the PV plant and battery storage. The solar generation profile for a typical cloudy day is given in Figure 7.9. The numeric values are provided in Appendix A, Table A.5. The profile has a total cumulative daily energy value of 3 474 kWh.

The daily energy delivered by the PV plant for both weather conditions are summarised in Table 7.7.

Table 7.7 *Summary of total energy supplied on both ideal solar and cloudy days*

Weather condition	Total energy supplied [kWh]
Sunny, high irradiance	5 773
Cloudy, low irradiance	3 474

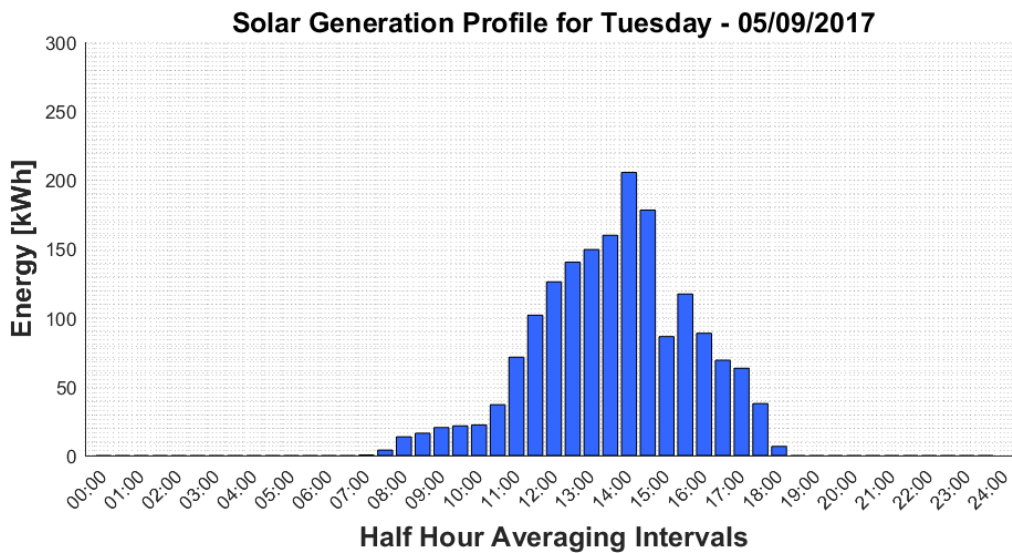


Figure 7.9 *Solar generation profile for a cloudy and rainy day*

The average daily solar generation profile for the period of the case study for weekdays, Saturdays and Sundays are shown in Figure 7.10, while Figure 7.11 shows the overall average daily solar generation profile for the period of the study. The difference between the weekday and weekend profiles are typically due to ideal solar days where the batteries could reach full capacity, as well as a reduction in demand over weekends. The numeric values are provided in Appendix A, Table A.6. While solar generation does not distinguish between the days of the week, the weekday, Saturday and Sunday profiles are useful if interpreted in the context of the demand profiles for a given period.

Average Solar Generation Profile

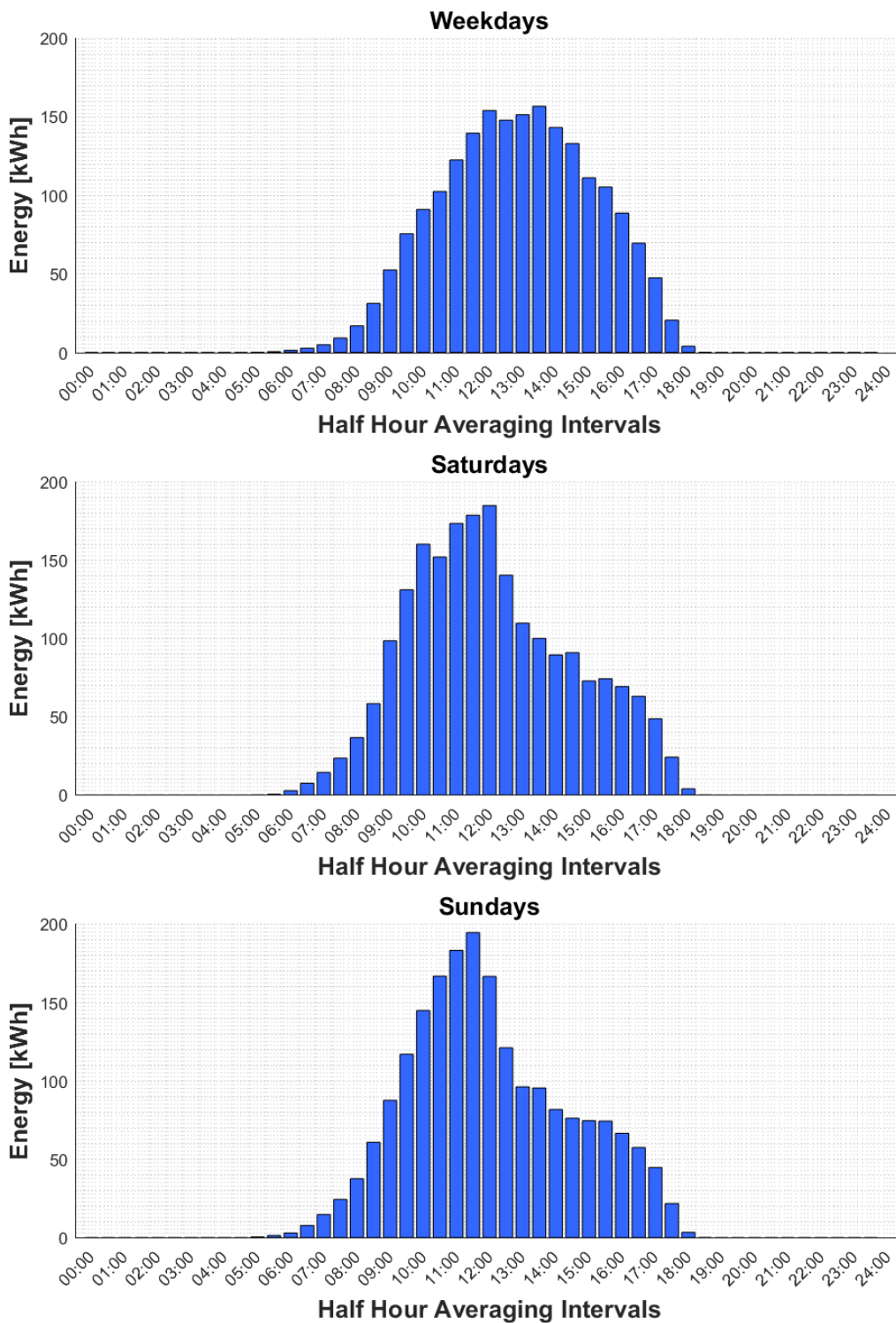


Figure 7.10 Overall average daily solar generation profile for weekdays, Saturdays and Sundays for the study period

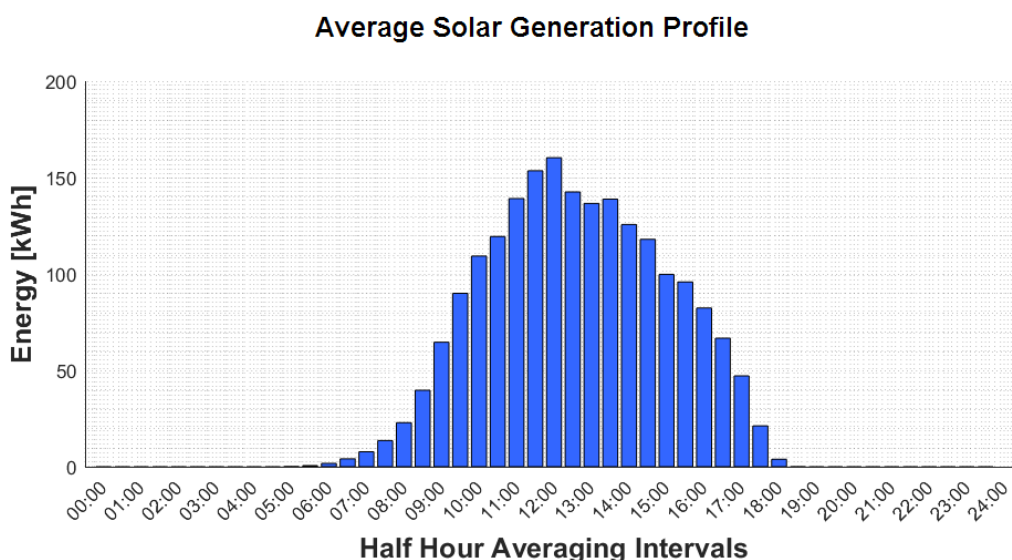


Figure 7.11 Overall average daily solar generation profile for the study period

7.4.5 Battery Storage Profile

The battery storage profile reflects the half-hourly average energy flow to the battery system. Positive values represent energy supplied by the batteries to the micro-grid, while negative values represent energy flowing from the micro-grid to the batteries during charging. The data is recorded every 5 minutes and averaged to obtain 48 half-hourly averaged energy values.

The battery storage profile for 1st September 2017, shown in Figure 7.12, represents a sunny day with relatively high demand where the batteries charged to full capacity before it started to supply energy to the network. The numeric values are given in Appendix A, Table A.7.

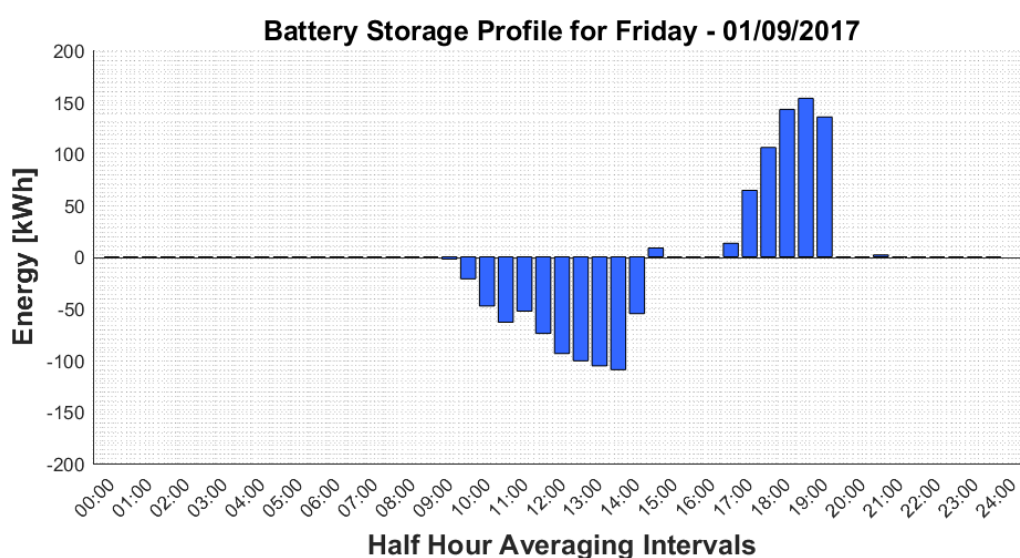


Figure 7.12 Battery storage profile for an ideal sunny day with high demand

The battery storage profile shown in Figure 7.13 for 17th September 2017, which represents a sunny day with excellent solar irradiation and relatively low demand, indicates that the demand profile has a great impact on the charging cycle of the battery system. For the high demand profile, the batteries reached full capacity over a longer period compared to the low demand profile. The batteries also discharged faster for the high demand profile compared to the low demand profile.

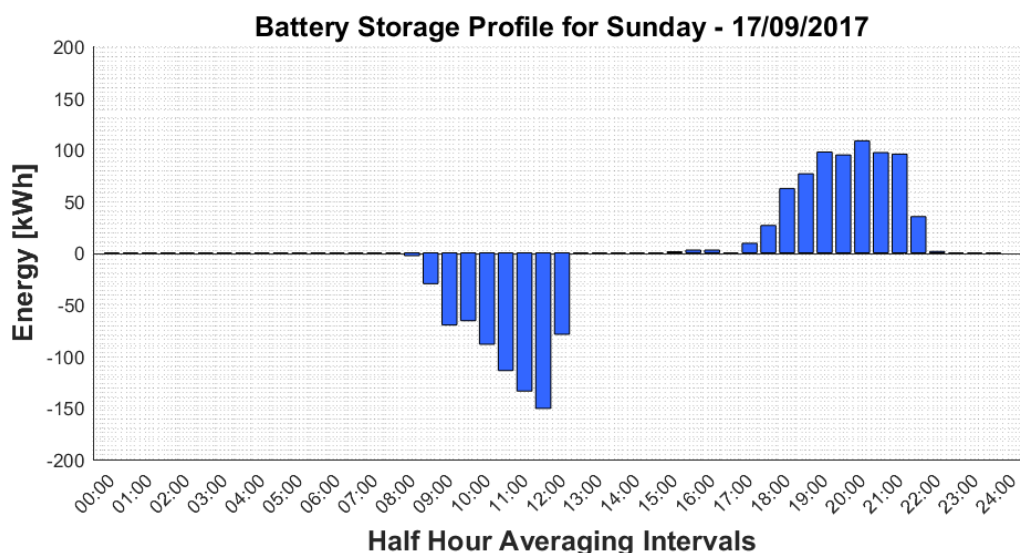


Figure 7.13 Battery storage profile for an ideal sunny day with low demand

The battery storage profiles given in Figure 7.12 and Figure 7.13 have equal total charging energy as well as equal total supply energy, but have various charging and supply durations. The total supply and charge energy is summarized in Table 7.8. For one full battery charging and discharge cycle, about 200 kWh of energy is lost due to internal battery losses. This results that only 86.2% of the energy absorbed from the PV plant will be available to supply to the micro-grid.

Table 7.8 Typical energy consumed and supplied by the battery storage system

Energy direction	Total energy [kWh]
Supplying	1 250
Charging	-1 450

The battery storage profile on 5th September 2017 is given in Figure 7.14. With low solar irradiance, the batteries never reached their full capacity and resulted in less available energy for the evening. The total supplied energy for this day is only 311.8 kWh, i.e. about a ¼ of the energy available on a sunny day. The numeric values are given in Appendix A, Table A.8.

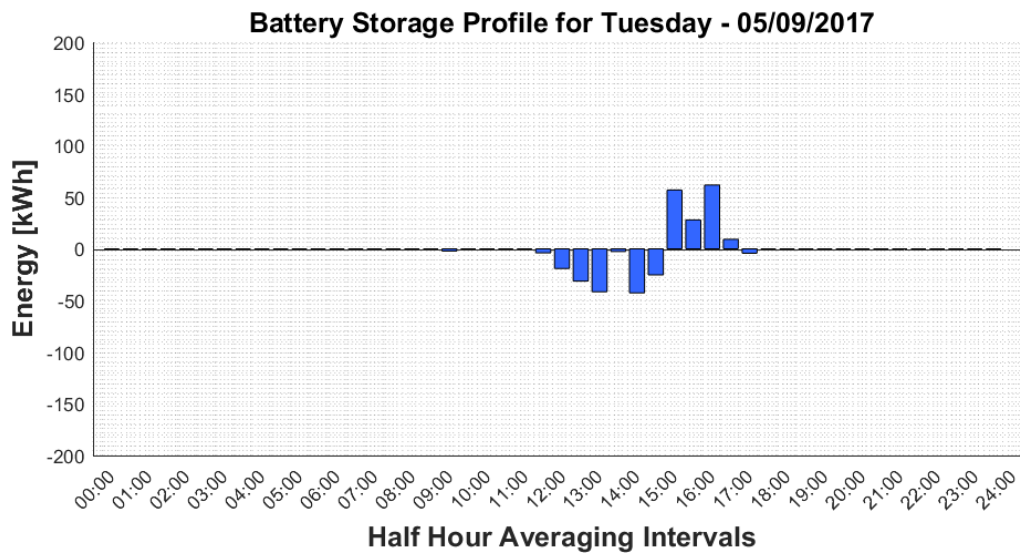


Figure 7.14 Battery storage profile for a cloudy and rainy day

Figure 7.15 shows the overall average daily battery storage profiles for the period of the study for weekdays, Saturdays and Sundays, while Figure 7.16 shows the overall daily average profile for the period of the study. The numeric values are given in Appendix A, Table A.9.

Average Battery Storage Profile

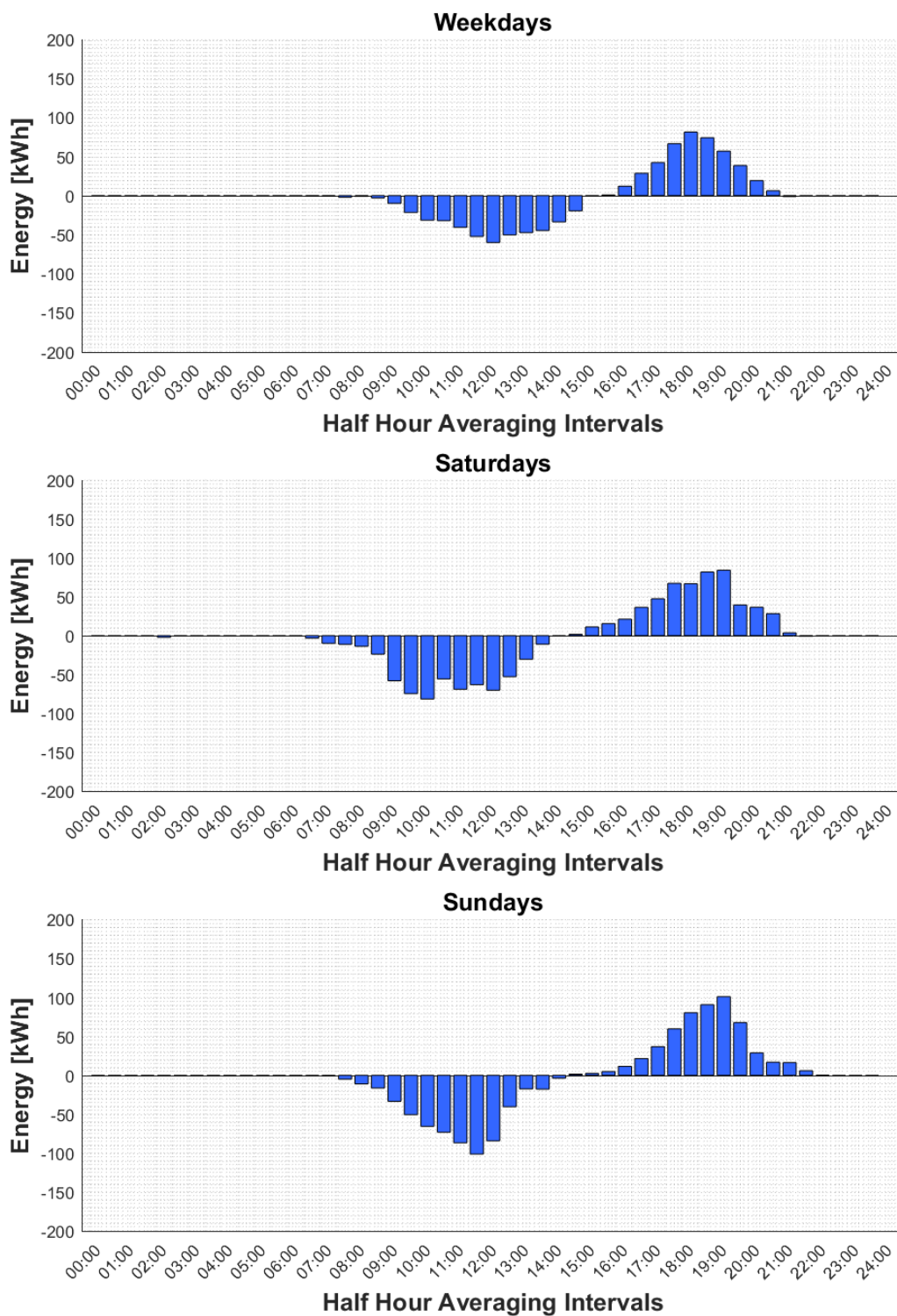


Figure 7.15 Overall average daily battery storage profile for weekdays, Saturdays and Sundays for the study period

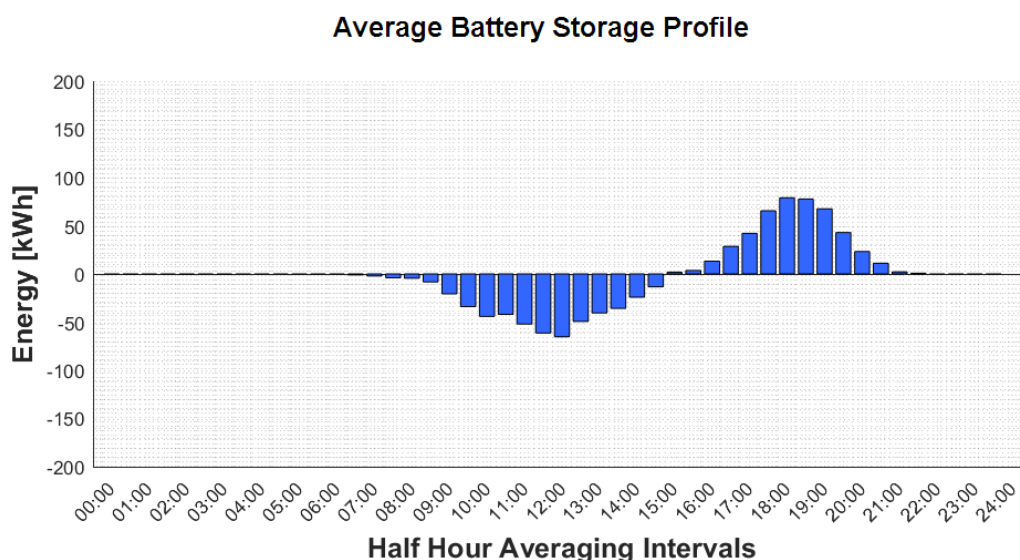


Figure 7.16 Overall average daily battery storage profile for the study period

7.5 Measured Usage Data and Results for the geysers and stoves

7.5.1 Overview

The usage profiles and power consumption data retrieved from the data logging instrumentation are summarized in this section. The usage profiles are obtained from data retrieved from data loggers installed at the following loads:

- *Desalination water plant:* A *PowerTrack* energy analyser were installed at the main supply distribution board situated at the desalination plant.
- *Geysers:* A total of 29 loggers were installed at residential dwellings to measure the usage profiles of hot water cylinders.
- *Stoves:* A total of 11 loggers were installed at residential dwellings to measure the usage profiles and power consumption data of stoves.

The data delivered by the loggers are used to construct a daily energy profile for each day of the study. These load profiles are used in two different methods, namely averaged and non-averaged energy profiles. The average energy profiles represent the overall daily average energy consumed by the targeted load for the period of the study, while the non-averaged energy profiles represent the energy consumed by the targeted load for the individual days of the study period. The mathematical formulation of the demand profiles and some additional data retrieved by other recording modes are presented in the remainder of this section.

7.5.2 Load Profile Formulation

A daily usage profile is generated by each logging device, presented as 48 half-hour averaged timestamps. The value associated with each time-stamp represents the on-duration of the appliance in percentage. To derive the daily demand profile for each individual appliance monitored, the usage profile is multiplied by the power consumption value, as illustrated in Figure 7.17. Using set theory notation, each half-hour, t_i , in the daily usage profile, is assigned to the set for the d^{th} day of the year T_d as follows:

$$T_d = \{t_i\} \quad i = 1, 2, 3 \dots N_p, d = 1, 2, 3 \dots N_Y \quad (7.1)$$

where N_P denotes the total number of daily half-hours and N_Y denotes the total number of days in the year.

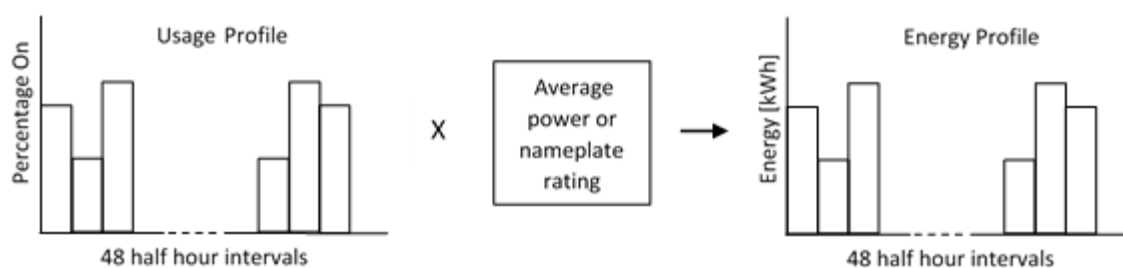


Figure 7.17 Formulation overview of energy profile

The power consumption of a geyser typically varies slightly during the on cycle, while for the stoves, the power consumption constantly changes. In order to derive the energy demand profiles, nameplate power consumption ratings are used for the geyser profiles and a daily average power consumption value is calculated for the stove profiles. The average daily power consumption can be expressed as

$$\tilde{P}_d = \frac{1}{N_K} \sum_{s=1}^{N_K} P_{ds} \quad s = 1, 2, 3 \dots N_K, d = 1, 2, 3 \dots N_Y \quad (7.2)$$

where P_{ds} denotes the power consumption of the s^{th} sample for the d^{th} day of the year respectively. N_K denotes the total number of samples recorded on each day. The samples recorded are only for on-times, meaning that only non-zero samples are used. The daily average power consumption, P_d , will be close to the power consumption rating as stated on the nameplate of each geyser and varying for each stove.

The daily demand profiles in kWh, E_d , for each monitored appliance, can be expressed as

$$E_d = \frac{1}{2} \tilde{P}_d(t_{i+1} - t_i) \quad i = 1, 2, 3 \dots N_p, d = 1, 2, 3 \dots N_Y \quad (7.3)$$

An average daily geyser and stove demand profile, based on the number of loggers, can be expressed as

$$\tilde{E}_d = \frac{1}{N_M} \sum_{j=1}^{N_M} E_{dj} \quad j = 1, 2, 3 \dots N_M, d = 1, 2, 3 \dots N_Y \quad (7.4)$$

where N_m denotes the total number of daily demand profiles received from the loggers targeting the same load. E_d represents an average demand profile for a single appliance. The total daily geyser demand profile, E_{Gd} , and total daily stove demand profile, E_{Sd} , depends on the number of each load component present at the site and is given by

$$E_{Gd} = \tilde{E}_d \times G_T \quad d = 1, 2, 3 \dots N_Y \quad (7.5)$$

and

$$E_{Sd} = \tilde{E}_d \times S_T \quad d = 1, 2, 3 \dots N_Y \quad (7.6)$$

where G_T and S_T denote the total numbers of geysers and stoves present at the site respectively. According to the number of residential properties in use, the quantities for each targeted load are listed in Table 7.9.

The de-aggregated energy profiles presented in the remainder of this chapter are based on the numbers of appliances listed in Table 7.9.

Table 7.9 *Number of appliances in use at Robben Island*

Targeted load	Quantity in use
Geysers	60
Stoves	45

The daily demand profiles retrieved for the desalination water plant are half-hourly averaged power readings presented in 48 half-hours. All three de-aggregated demand profiles can be represented as a set of daily demand profiles for the individual days or as single overall average daily demand profile. Both these methods are used in the calculations and the outcomes compared. The average demand profiles can be expressed as

$$\tilde{E}_G = \frac{1}{\Delta T} \sum_{d=T_0}^{T_f} E_{Gd} \quad d = T_0, T_0 + 1, T_0 + 2 \dots T_f \quad (7.7)$$

and

$$\widetilde{\mathbf{E}}_S = \frac{1}{\Delta T} \sum_{d=T_0}^{T_f} \mathbf{E}_{Sd} \quad d = T_0, T_0 + 1, T_0 + 2 \dots T_f \quad (7.8)$$

were

$$\Delta T = T_f - T_0 \quad (7.9)$$

and T_0 and T_f denotes the start day and end day for the averaging period respectively.

7.5.3 Desalination Water Plant Demand Profile

The desalination water plant demand profile represents the measured half-hourly averaged energy consumption profile of the desalination water plant. The desalination water plant profile is produced by the *PowerTrack energy analyser*, installed at the desalination water plant, from 17th of August 2017 to 15th of September 2017. The desalination water plant demand profile includes the power consumption of all machines, compressors, pumps, heating elements and control system required at the water plant. It does, however, exclude the main sea water feed pump situated at the Alpha One pump station. This water feed pump is rated at 20 kW and is typically operated together with the desalination water plant.

The desalination water plant demand profiles shown in Figure 7.18, Figure 7.19 and Figure 7.20 for the 25th of August, 2nd of September and 5th of September 2017 respectively represent days where the desalination water plant was operating, but with different times of operation. Observation of the desalination plant data also exposed a smaller load, which operates at certain intervals and remains on for constant durations. The load was identified as a standby air compressor, with a small air leakage, causing recurrent energy consumptions. The desalination water plant profile mostly has a constant energy consumption for every half-hour, indicating that the water plant is running at full capacity. The average contribution of the desalination water plant to the total demand energy is 951 kWh per day. The desalination plant operated for 51.2% of the days during the study. The numeric total daily energy values for the desalination water plant are given in Appendix A, Table A.13 for the period of the study.

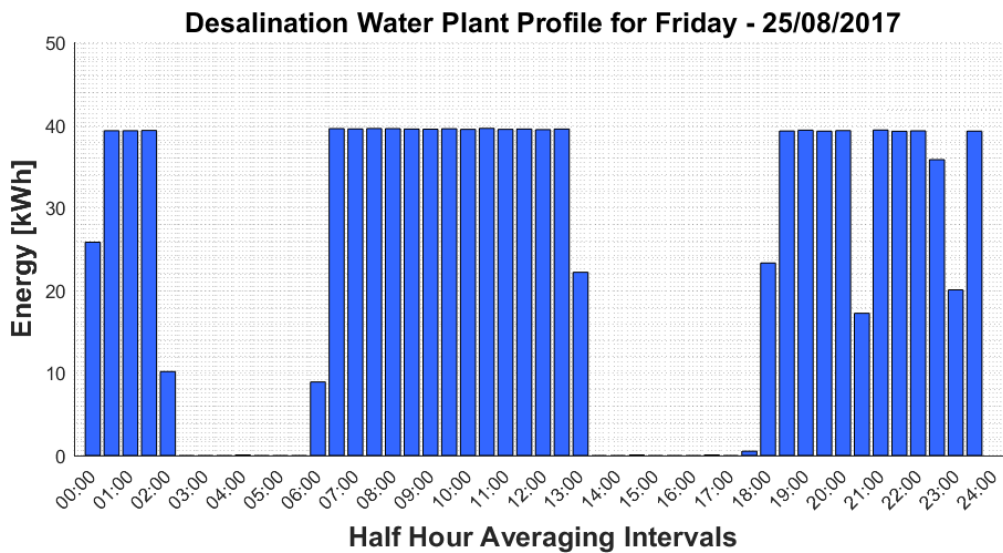


Figure 7.18 Desalination water plant daily demand profile for Friday the 25th of August 2017

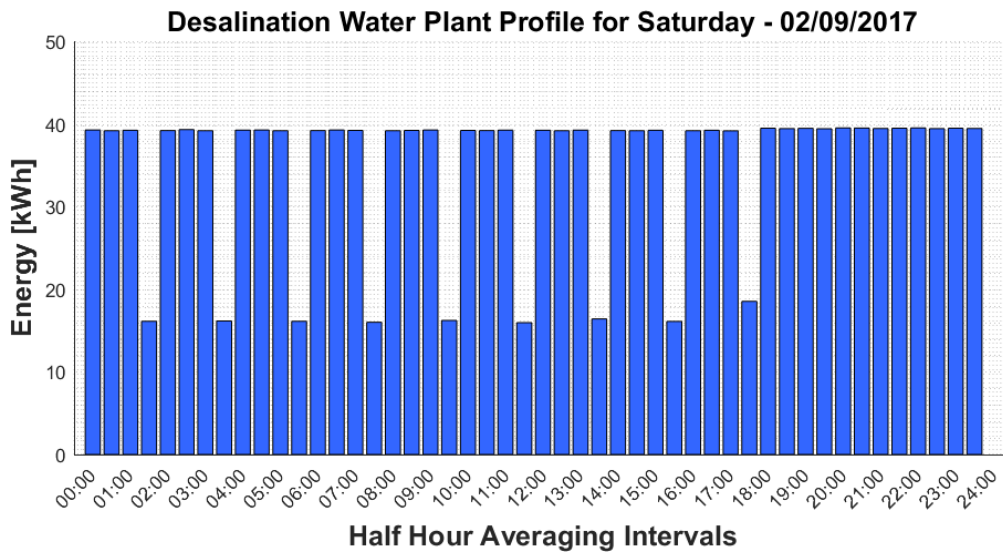


Figure 7.19 Desalination water plant daily demand profile for Saturday the 2nd of September 2017

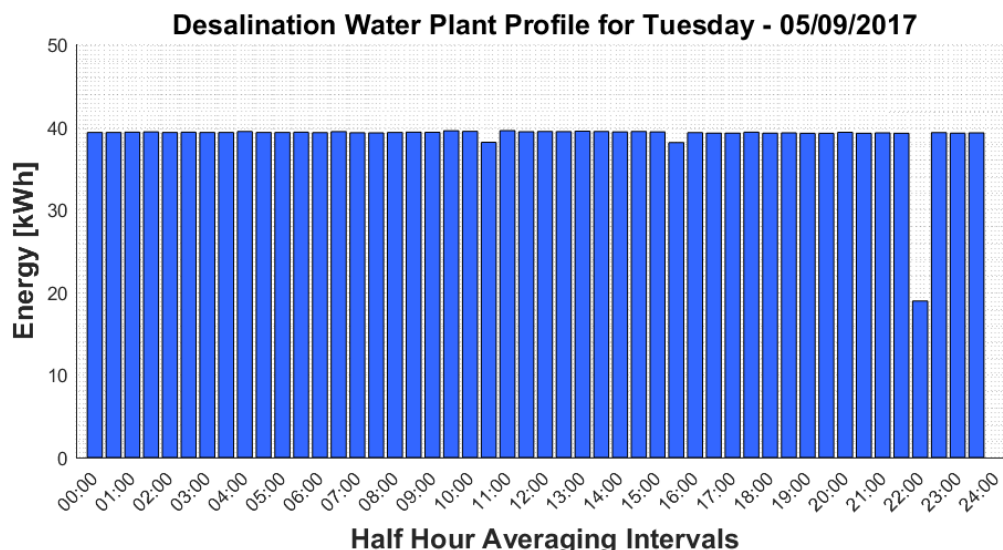


Figure 7.20 Desalination water plant daily demand profile for Tuesday the 5th of September 2017

7.5.4 Sanitary Hot Water Demand Profile

The geyser demand profile is highly dependent on the number of people using the geyser, the water capacity of the cylinder, the power rating of the element, the mounting orientation of the unit and the ambient temperature. The geyser demand profiles delivered by the loggers typically indicate the energy consumed during hot water usage and standing losses. This is illustrated using the data gathered by logger C10, which monitored a 3 kW, 150 l geyser, supplying a household of seven people, as summarized in Table 7.4. The geyser profile for Friday the 8th August to Sunday the 10th August is shown in Figures 7.21 to Figure 7.23.

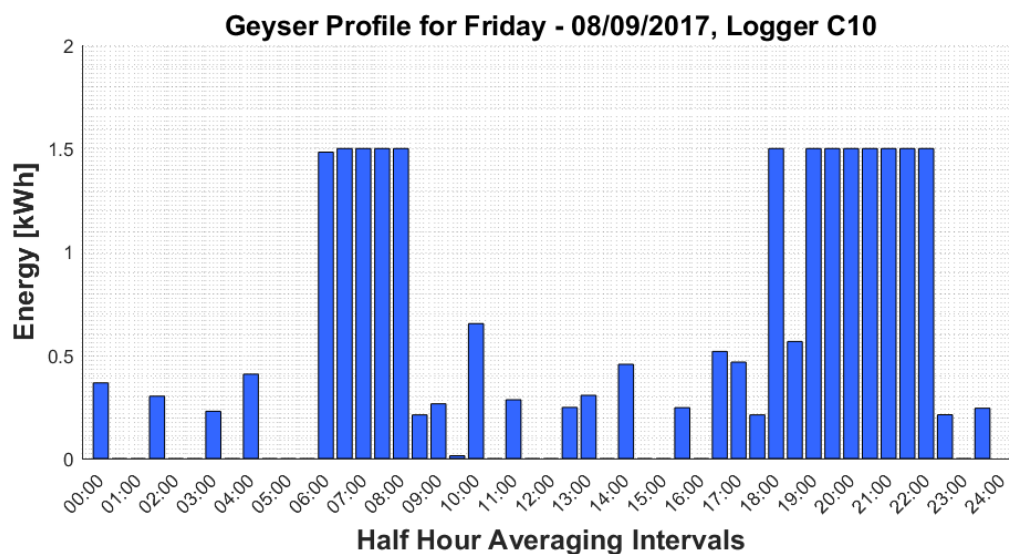


Figure 7.21 Geyser daily demand profile for a residence with seven people – Friday 08/09/2017

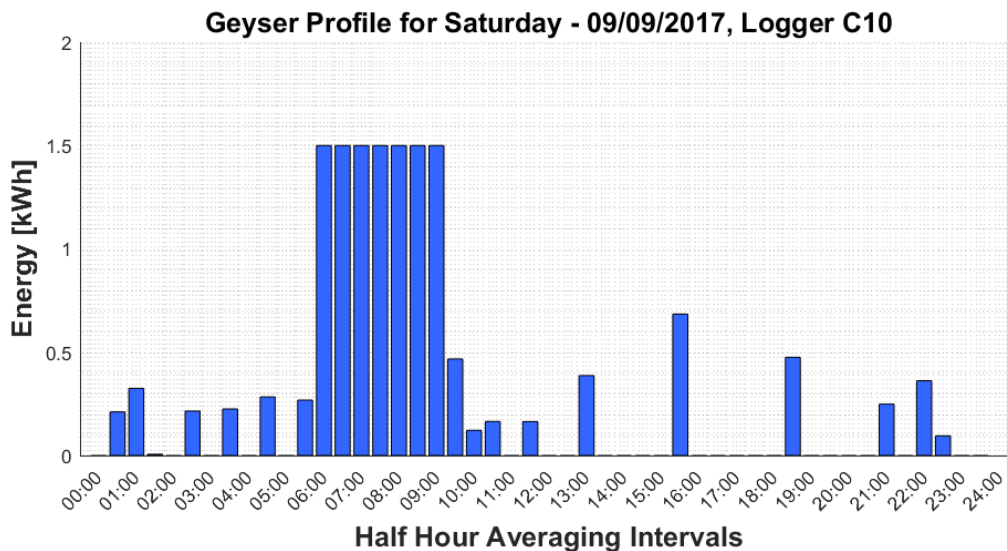


Figure 7.22 Geyser daily demand profile for a residence with seven people – Saturday 09/09/2017

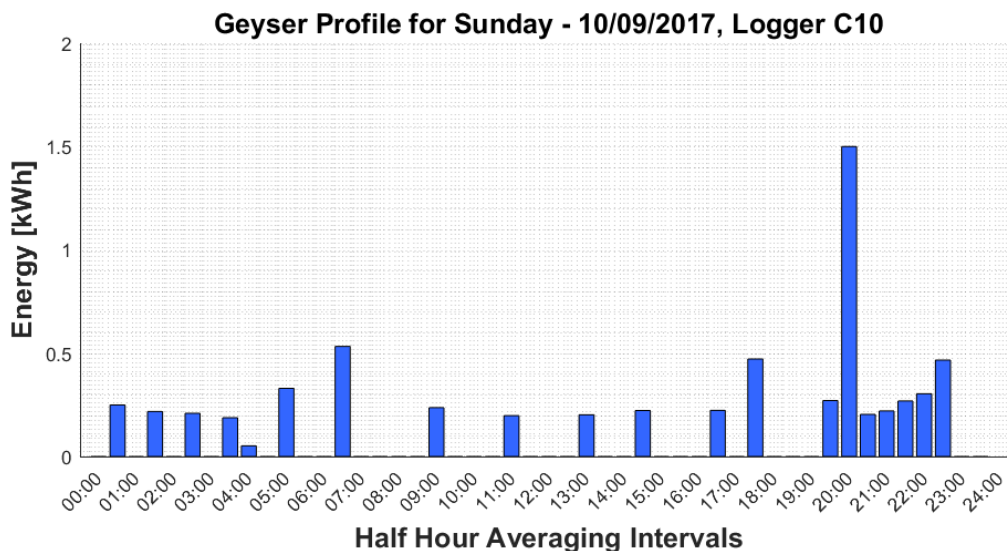


Figure 7.23 Geyser daily demand profile for a residence with seven people – Sunday 10/09/2017

The three geyser demand profiles show clear evidence of hot water draw-off and standing losses, but are all diverse according to the day of the week. The geyser demand profiles mostly show the pattern illustrated in Figure 7.21, which represents the weekday routines of the occupants. The typical geyser demand profile for Saturdays indicates that the occupants use hot water predominantly during the morning peak. The Sunday geyser demand profiles shows that hot water draw-off occurs evenly distributed throughout the day, with no distinct peak demand period.

The geyser demand profiles for this residence also exhibit clear evidence of high standing losses. This can be seen in the demand patterns during the early morning hours, but also from

the repetitive energy usage during the day as shown in Figure 7.23. This possibly due to hot water leakage, high thermostat settings or insufficient heat insulation.

The total energy consumed by the geyser monitored by logger C10 for one week is 145.3 kWh. It is compared with the weekly total energy consumed by a geyser supplying only two people. Logger C28 delivered data for a geyser supplying two people with hot water, resulting in a weekly total energy of 119.6 kWh. The simulated average daily geyser profile for 60 geysers is given in Figure 7.24, categorised by weekdays, Saturdays and Sundays.

Average Geyser Profile

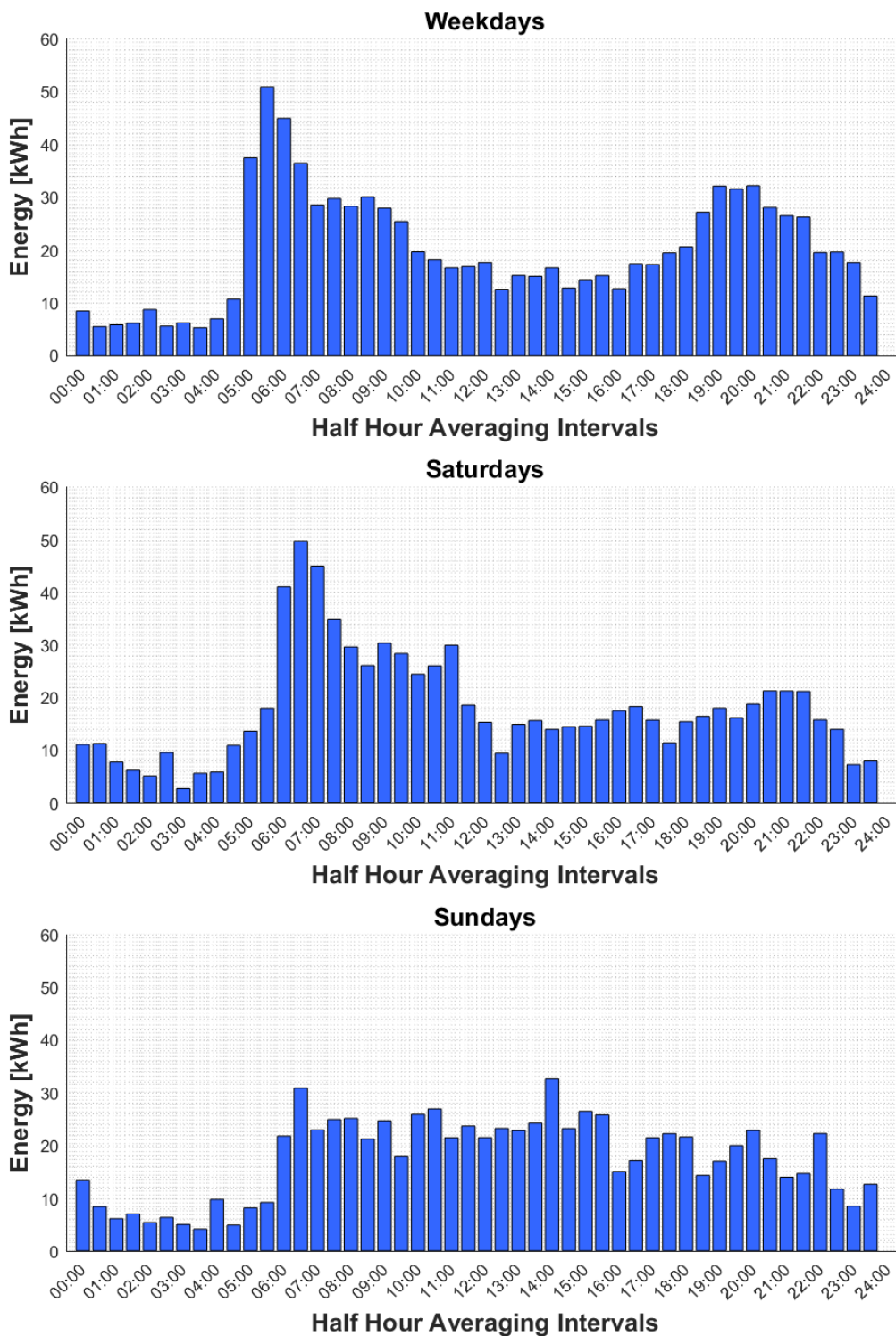


Figure 7.24 Average daily geyser demand profile for weekdays, Sundays and Saturdays for the study period

The daily geyser demand profile, averaged for the study period, given in Figure 7.24, reflects the daily geyser profile retrieved from most geysers. For weekdays, the peak demand periods

are in the early morning hours, from 05:00 to 09:30, while for Saturdays this peak demand only exist once a day, mostly from 06:00 to 11:00. The Sunday averaged geyser profile reflects a more distributed geyser profile and only reaches a maximum demand of about 30 kWh per half-hour. The total average geyser profile is given in Figure 7.25. The numeric values are given in Appendix A, Table A.14.

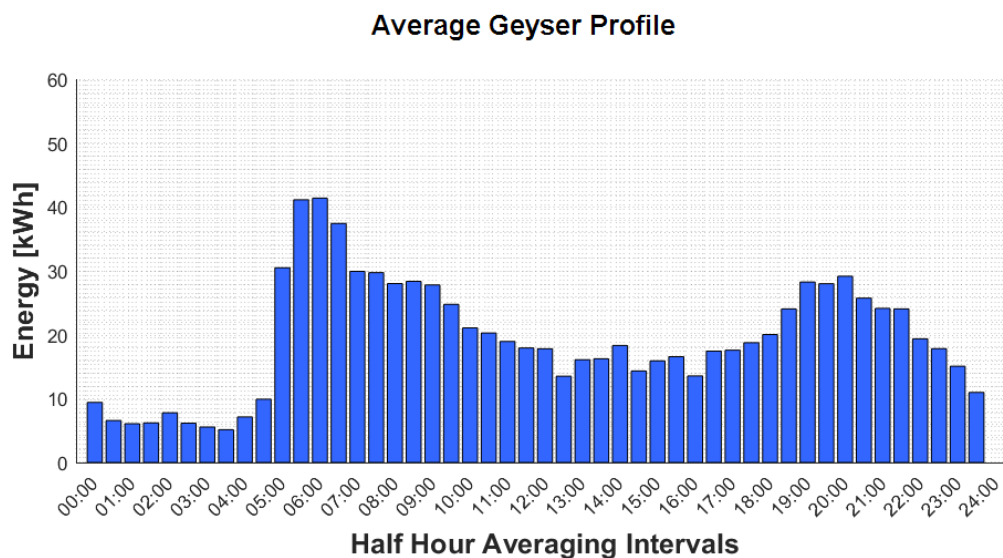


Figure 7.25 Overall average daily geyser demand profile for the study period

The average geyser demand profile has a total daily energy consumption of 929.65 kWh per day for a total of 60 residential properties, with high peak demand of 41.3 kWh per half-hour.

7.5.5 Cooking Demand Profile

Stove demand profiles were acquired by 11 loggers, targeting conventional 4-plate stoves. The stoves were monitored to test the loggers on a different load type, but also to determine the energy demand of the stoves. A stove typically generates considerably more events during the usage period due to multiple heating elements repetitively switching on and off to regulate the temperature.

The demand profiles of cooking loads are less predictable compared to geyser demand profiles, which has a more constant power consumption. Also, the usage data for 11 stoves represents a statistically less significant model. However, the average predicted energy impact of a total of 45 stoves, derived from the measured data, compared to the geyser and other loads at the site, are given in Figure 7.26. The model is built from the logger data retrieved during the trial run in August 2017. The average total daily energy consumption for each type of load category is listed in Table 7.10, as well as the percentage it represents of the total load. The results show

that the geyser load is considerably more significant compared to the cooking load, and represents a significant percentage of the overall demand for the site.

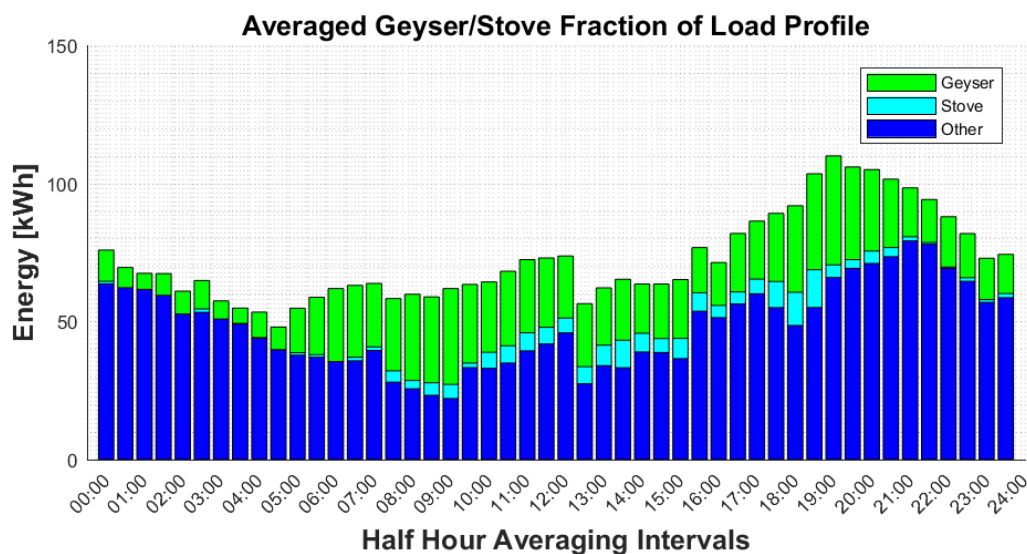


Figure 7.26 Average daily demand profile comparison between the geyser load, stove load and other loads at the site for the study period

Table 7.10 Total average daily energy consumption of the targeted loads

	Geysers	Stoves	Other Loads
Total Energy [kWh]	1 969.2	353.2	4 646.0
Percentage [%]	28.3	5.1	66.6

The results presented in Table 7.10 indicate that the stoves are consuming about six times less energy than the geysers during an average day. The individual stove demand profiles provide more detail regarding the usage patterns of stoves in general. The individual stove demand profiles are derived using the measured usage profiles and daily averaged power consumption. The results recorded with logger C16 is used to illustrate the varying power consumption over a period of a week, as shown in Table 7.11.

Table 7.11 Stove power consumption for a period of a week

Day - Date	Average Power Consumption [kW]
Friday – 15/09/2017	986.0
Saturday – 16/09/2017	0
Sunday – 17/09/2017	1841.4
Monday – 18/09/2017	1783.5

Tuesday – 19/09/2017	2242.9
Wednesday – 20/09/2017	1597.0
Thursday – 21/09/2017	2206.0

The stove demand profile for the 20th of September 2017 is given in Figure 7.27.

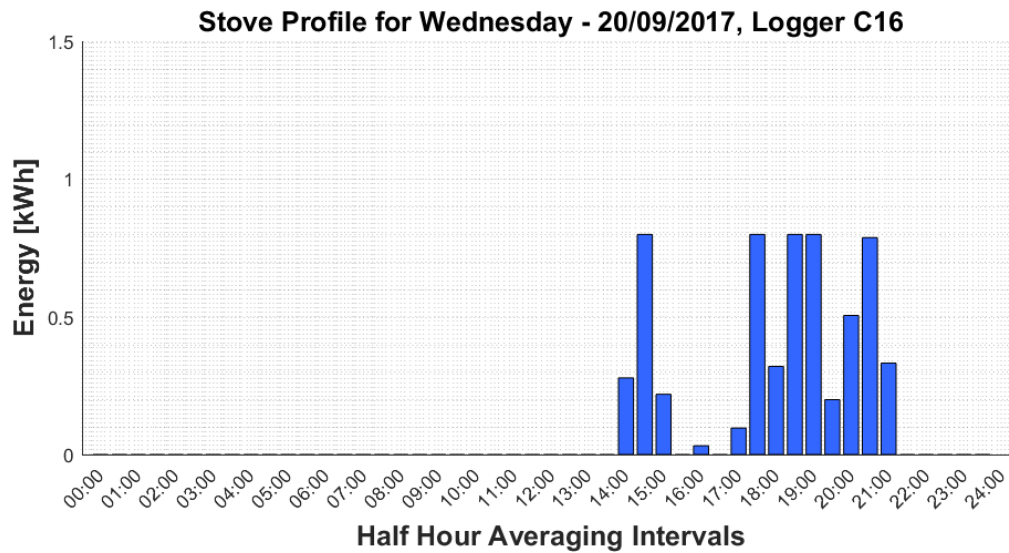


Figure 7.27 Stove demand profile for Wednesday the 20th of September 2017 for one individual stove

The stove demand profile does not show detail of individual heating elements due to averaging of the power consumption profile. Plotting the power consumption profile using the 5-minute analogue current consumption recordings, provide some insight into the power consuming characteristics exhibited by the stove. Figure 7.28 shows a scatter plot of the stove power consumption.

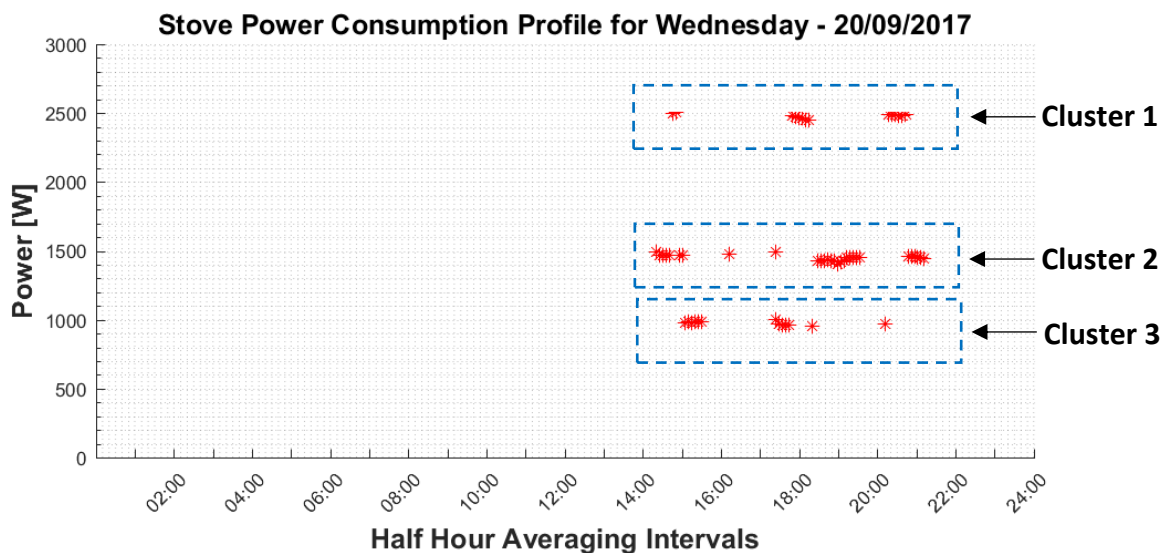


Figure 7.28 Stove power consumption profile clustering example

The power consumption values in Figure 7.28 forms three clearly visible clusters. The clusters most likely represent the aggregated power consumption of simultaneous combinations of various heating elements.

7.5.6 Histogram Recordings

The histogram event recording mode was tested during the last two weeks of the study. A total of eight loggers were set up for raw histogram data acquisition mode and deployed on geysers serving three to four people. The histogram memory maps are set up with duration intervals at 12-minute increments. Each histogram memory map consists of daily 48 half-hourly start time interval bins, resulting in a total number of 960 entries.

The eight histogram memory maps are averaged per bin to represent a histogram. Each bin value represents a percentage calculated based on the total entries across all duration bins for each half-hour. The average bin values are given in Appendix A, Table A.15. The histogram map over the 48 period is presented in Figure 7.29.

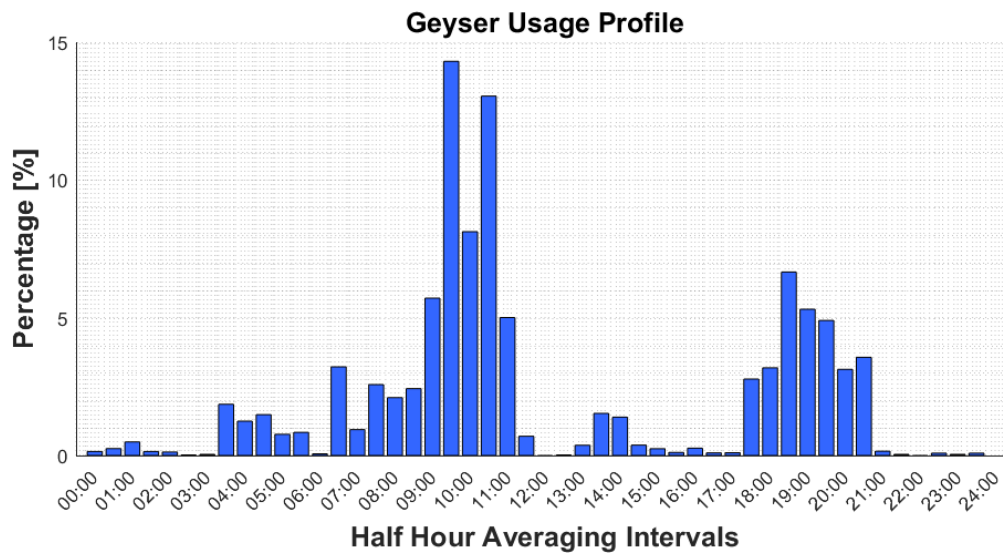


Figure 7.29 Geyser usage profile constructed using duration histogram data

The usage profile, given in Figure 7.29, already adapts to the distribution of the average geyser profile obtained from raw event recording, given in Figure 7.25. The two results are, however, expected to differ to a degree due to different data acquisition periods and number of samples retrieved. However, both profiles show a high usage period between 09:00 and 11:00 in the mornings and between 18:00 and 21:00 in the evenings.

The major advantage of the histogram recording mode is that statistical data on the time of use as well as the duration of use of the targeted appliance are obtained. Figure 7.30 shows a histogram of the on-durations of the geysers targeted in the field recordings.

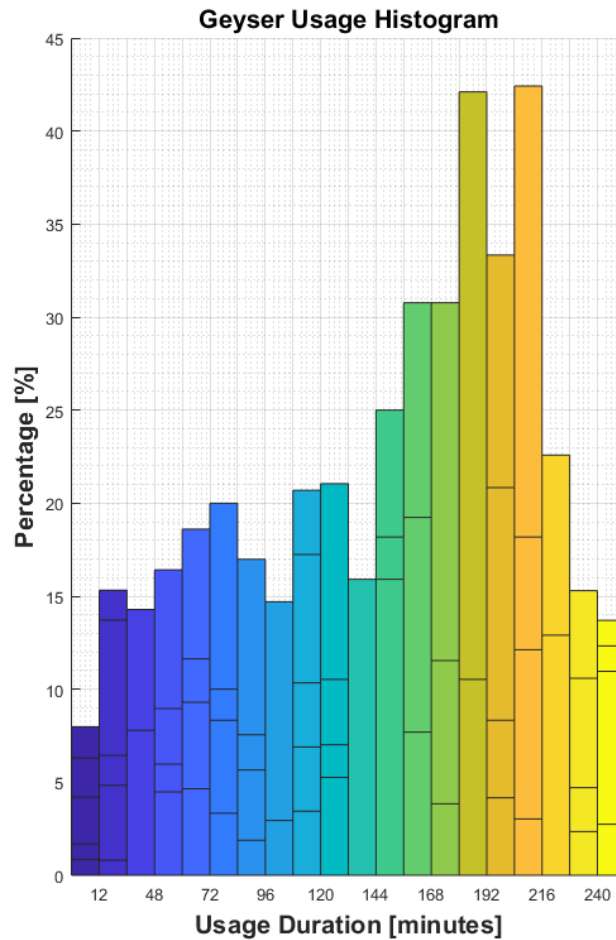


Figure 7.30 Histogram of geyser usage durations for the geysers targeted in the field recordings

Figure 7.30 shows that the most common geyser power consumption duration ranges from 168 minutes to 216 minutes, i.e. of the order of 2.5 to 3.5 hours. Another duration peak occurs for the bin between 48 minutes and 96 minutes.

Figure 7.31 shows a three-dimensional histogram that reflects the usage durations and the half-hourly bins in which the usage events start. Short durations are presented as dark blue bars, while the longer usage durations are presented as green and yellow bars. This histogram clearly distinguishes between short usage durations associated with standing losses and longer usage durations associated with hot water draw-off. The usage durations associated with standing losses are generally less than 24 minutes and occur predominantly during the early morning and late evening hours.

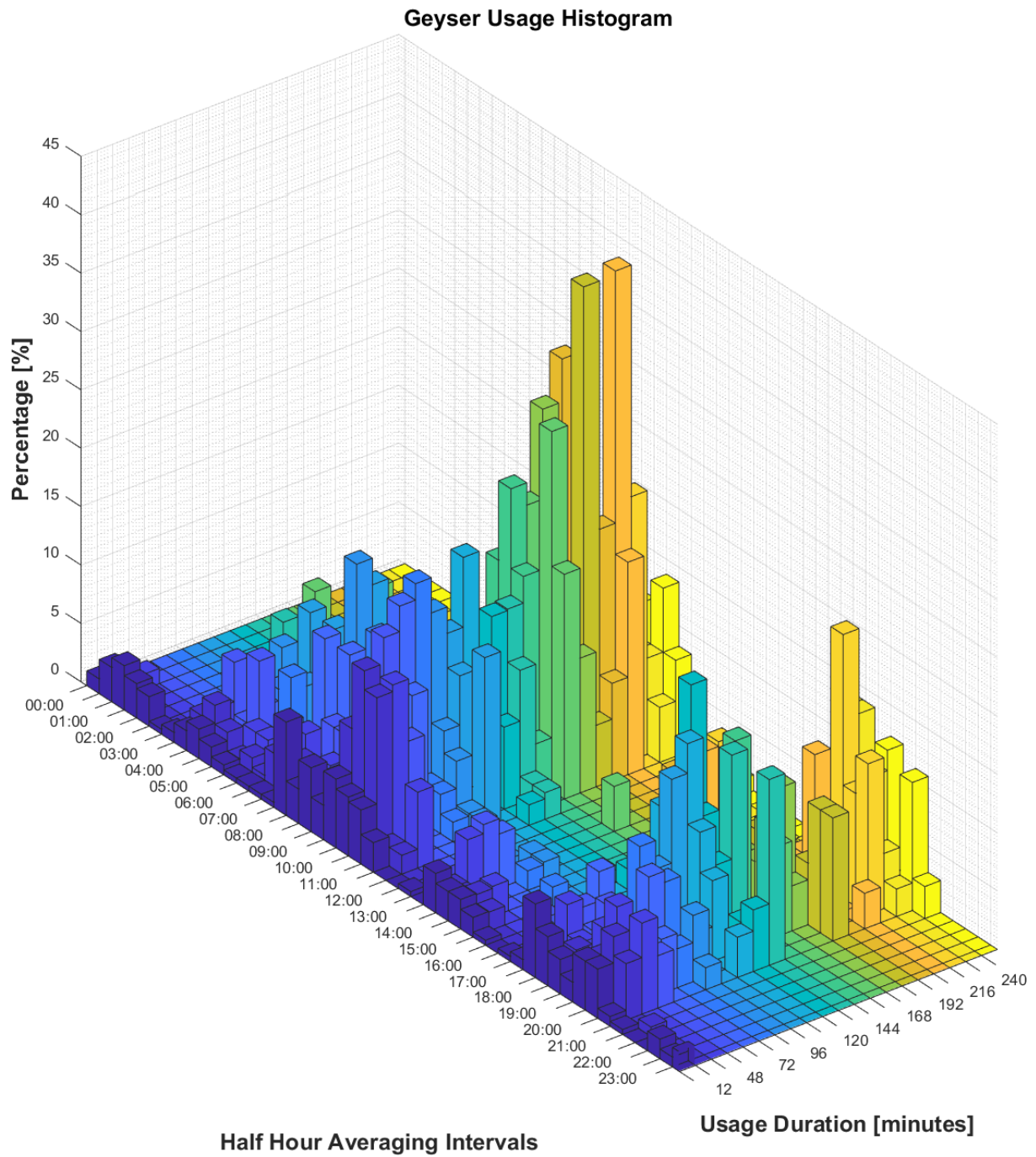


Figure 7.31 Histogram of the geyser usage durations for the geysers targeted in the field recordings, grouped according to the half-hourly daily start-time bins

7.6 Energy System Topology

7.6.1 Overview

The Robben Island energy system represents an islanded micro-grid. The system topology consists of different sub-systems representing generation, storage and loads. The system is analysed using a mathematical model, which essentially implements the principle of

conservation of energy, is used for simulating the performance of the system using half-hourly averaged energy profiles.

7.6.2 Micro-grid Energy Model

The Robben Island micro-grid consists of four subsystems, namely diesel generators, a PV plant, battery storage and loads as shown in Figure 7.32.

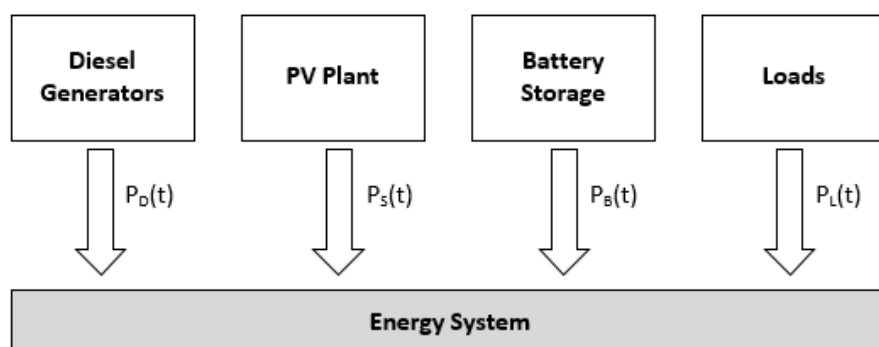


Figure 7.32 Topology of the Robben Island micro-grid energy system

The law of conservation of energy requires that the instantaneous power flowing into the system should be equal to the instantaneous power flowing out of the system. This implies that the total instantaneous power should summate to zero, which for the power flow definitions shown in Figure 7.32 gives rise to the relationship

$$\widetilde{P}_D(t) + \widetilde{P}_S(t) + \widetilde{P}_B(t) + \widetilde{P}_L(t) = 0 \quad (7.10)$$

where $P_D(t)$, $P_S(t)$, $P_B(t)$ and $P_L(t)$ denote the instantaneous power delivered by the diesel generators, PV plant, battery storage or load respectively. This also holds true for the daily and half-hourly averaged energy profiles given by

$$\widetilde{E}_{D_i} + \widetilde{E}_{S_i} + \widetilde{E}_{B_i} + \widetilde{E}_{L_i} = 0 \quad i = 1, 2, 3 \dots 365 \quad (7.11)$$

and

$$\widetilde{E}_D + \widetilde{E}_S + \widetilde{E}_B + \widetilde{E}_L = 0 \quad (7.12)$$

The energy profiles provided as historical data and profiles generated by the proposed system will be used in the 48 half-hour averaging intervals, as given in Section 7.5, in the remainder of this chapter. Demand profile optimisation will be performed by focussing on the geysers and cooking appliances used in the residences to minimise the use of diesel generators as energy source.

7.6.3 Power Flow Constraints

Each subsystem within the energy system shown in Figure 7.32 is subject to power flow constraints. These constraints are needed for the energy profile optimisation as each subsystem has an energy supply or energy consumption limit. The power flow constraints translate to half-hourly energy flow constraints. The power flow and energy profile constraints are listed in Table 7.12, where:

$P_{D\ max}$: Maximum total instantaneous power delivered by total diesel generators.

$P_{S\ max}$: Maximum power rating of the PV system.

$P_{B\ C\ max}$: Maximum battery system charging rate.

$P_{B\ DC\ max}$: Maximum battery system discharging rate.

$P_{L\ max}$: Maximum total power consumption of all loads present at the site.

$i = 1, 2, 3 \dots 365$: Day of the year.

Table 7.12 Power flow and energy profile constraints applicable to the energy system at the site

Subsystem	Power Flow Constraints	Half-hourly Energy Profile Constraints [kWh]
Diesel Generators	$0 \leq P_D(t) \leq P_{D\ max}$	$0 \leq E_{Di} \leq 0.5P_{D\ max}$
PV Plant	$0 \leq P_S(t) \leq P_{S\ max}$	$0 \leq E_{Si} \leq 0.5P_{S\ max}$
Battery Storage	$-P_{B\ C\ max} \leq P_B(t) \leq P_{B\ DC\ max}$	$-0.5P_{B\ C\ max} \leq E_{Bi} \leq 0.5P_{B\ DC\ max}$
Loads	$-P_{L\ max} \leq P_L(t) \leq 0$	$-0.5P_{L\ max} \leq E_{Li} \leq 0$

The battery storage system features of a battery charge monitoring system. The system prevents overcharging and protects the batteries from fully discharging below a given minimum. The State of Charge (SoC) of the batteries is measured every five minutes and compared with the relationship

$$B_{SOC\ min} \leq B_{SOC\ h} \leq B_{SOC\ max} \quad h = 1, 2, 3 \dots N_M \quad (7.13)$$

where N_M denotes the total number of five-minute samples. $B_{SOC\ max}$ and $B_{SOC\ min}$ denotes the maximum and minimum SoC of the batteries as a percentage. The battery monitoring system will disconnect the batteries from the micro-grid when $B_{SOC\ max}$ or $B_{SOC\ min}$ is reached. The

minimum SoC is predetermined for the set of batteries by the allowed Depth-of-Discharge (DoD) rating for each battery. This is given by the relationship

$$B_{SoC\ min} = 1 - B_{DoD} \quad (7.14)$$

where B_{DoD} denotes the allowed DoD of the batteries. The minimum energy charge level is given by

$$E_{B\ min} = B_{SoC\ min} \times B_{PR} = B_{PR}(1 - B_{DoD}) \quad (7.15)$$

where B_{PR} denotes the rating of the battery system in kWh.

The maximum and minimum constraint values applicable to the energy system at Robben Island is given in Table 7.13.

Table 7.13 Maximum and minimum constraint values of the Robben Island energy system

Denotation	Value
$P_{D\ max}$	1200 kVA
$P_{S\ max}$	666.4 kWp
$P_{B\ C_max}$	-510 kW
$P_{B\ DC_max}$	556 kW
$B_{SoC\ max}$	100%
$B_{SoC\ min}$	17%
B_{DoD}	0.88

If the PV plant cannot supply the total demand at a given time, the battery system is added to support the PV plant. However, if the power delivered by these two sources cannot support the demand, the diesel generators supply the shortage.

7.7 Financial Analysis

7.7.1 Overview

One of the objectives for the project is to determine the payback period of heat-pumps as an alternative for the resistive heating elements currently installed in the conventional geysers. This will reduce the dependency on diesel generation and save diesel costs.

The total diesel generator energy savings profile is derived, leading to the total energy savings per day. This figure is then used to forecast the financial savings as well as the payback period of the heat-pump systems.

7.7.2 Potential Energy Savings

The replacement of the conventional geysers with heat-pump systems give rise to a new set of energy profiles. These profiles forecast the daily energy generation or consumption figures when the geyser profile is reduced by the energy saved from the geyser replacement. The half-hourly energy savings obtained by the heat-pump retrofits, $E_{G_{save}k}$, can be expressed by the relationship

$$E_{G_{save}k} = E_{Gk} - \frac{E_{Gk}}{COP} = \frac{(COP-1)}{COP} E_{Gk} \quad k = 1, 2, 3 \dots 48 \quad (7.16)$$

where E_{Gk} denotes the baseline geyser energy consumption for the k^{th} averaging interval and COP denotes the coefficient of performance ratio of heat-pump systems.

Not all of the half-hourly demand savings represented by $E_{G_{save}i}$ necessarily contribute to diesel savings. For instance, for a half-hour with unused PV generation capacity, only part or possibly none of the geyser demand savings translates to diesel savings. Whether $E_{G_{save}i}$ contributes to diesel savings is determined by a complex rule-based model that encodes the possible energy exchange scenarios between the various subsystems for that particular half-hour. These scenarios are summarised in Table 7.14, where E_{Dk} , E_{Sk} and E_{Bk} denote the energy of the daily diesel generation profile, PV plant profile and battery storage profile respectively for the k^{th} half-hourly averaging interval.

Table 7.14 Summary of energy exchange scenarios

Condition	E_{Dk}	E_{Sk}	E_{Bk}
1	> 0	= 0	= 0
2	= 0	> 0	= 0
3	= 0	= 0	> 0
4	= 0	> 0	< 0
5	> 0	> 0	< 0
6	> 0	> 0	= 0
7	> 0	= 0	> 0

8	= 0	> 0	> 0
9	> 0	> 0	> 0
10	= 0	= 0	= 0
11	= 0	= 0	< 0
12	> 0	= 0	< 0

Each scenario consists of various sub conditions, leading to possible energy savings. The diesel generation energy savings, E_{Dsavek} , and battery storage energy gain, E_{Ggaink} , for the scenarios listed in Table 7.14 can be determined using Equation 7.10 as follows:

$$1. E_{Dk} = -E_{Lk}, \text{ with } E_{Sk} = E_{Bk} = 0$$

This scenario represents the case where by the load generation consists of diesel generation only, while zero energy is transferred from to the storage system. The diesel generation energy savings and battery storage energy gain are given by:

$$E_{Dsavek} = E_{Gsavek} \text{ if } E_{Dk} > E_{Gsavek}, \quad (7.17)$$

$$E_{Dsavek} = E_{Dk} \text{ if } E_{Dk} \leq E_{Gsavek} \quad (7.18)$$

and

$$E_{Bgaink} = 0. \quad (7.19)$$

$$2. E_{Sk} = -E_{Lk}, \text{ with } E_{Dk} = E_{Bk} = 0$$

This scenario represents the case where generation consists of PV generation only, while zero energy is transferred to the storage system. The diesel generation energy savings and battery storage energy gain are given by:

$$E_{Dsavek} = 0 \quad (7.20)$$

and

$$E_{Bgaink} = 0. \quad (7.20)$$

$$3. E_{Bk} = -E_{Lk}, \text{ with } E_{Dk} = E_{Sk} = 0$$

This scenario represents the case where generation consists of storage generation only. The load reduction lowers the battery discharge rate and reduces the amount of energy imported from the battery storage system. The diesel generation energy savings and battery storage energy gain are given by:

$$E_{D_{savek}} = 0, \quad (7.21)$$

$$E_{B_{gaink}} = E_{G_{savek}} \text{ if } E_{Bk} > E_{G_{savek}} \quad (7.22)$$

and

$$E_{B_{gaink}} = E_{Bk} \text{ if } E_{Bk} \leq E_{G_{savek}}. \quad (7.23)$$

$$4. E_{Sk} = -(E_{Bk} + E_{Lk}), \text{ with } E_{Dk} = 0$$

This scenario represents the case where generation consists of PV generation only, while energy is delivered to the load as well as the storage system. The diesel savings are determined by whether the demand reduction results in an increase in the charging rate of the battery system. The diesel generation energy savings and battery storage energy gain are given by:

$$E_{D_{savek}} = 0, \quad (7.24)$$

$$E_{B_{gaink}} = -E_{G_{savek}} \text{ if } (E_{Bk} - E_{G_{savek}}) \geq E_{B_{c,max}} \quad (7.25)$$

and

$$E_{B_{gaink}} = E_{B_{c,max}} - E_{Bk} \text{ if } (E_{Bk} - E_{G_{savek}}) < E_{B_{c,max}}. \quad (7.26)$$

where $E_{B_{c,max}}$ denotes the maximum half-hourly battery storage charging rate.

$$5. E_{Dk} + E_{Sk} = -(E_{Bk} + E_{Lk})$$

This scenario represents the case where generation consists of PV generation and diesel generation, while energy is delivered to the load as well as the storage system. Depending on the magnitude of the demand reduction, diesel generation can fully or partially be reduced. The diesel generation energy savings and battery storage energy gain are given by:

$$E_{D_{savek}} = E_{G_{savek}} \text{ if } E_{Dk} > E_{G_{savek}}, \quad (7.27)$$

$$E_{D_{savek}} = E_{Dk} \text{ if } E_{Dk} \leq E_{G_{savek}}, \quad (7.28)$$

$$E_{B_{gaink}} = E_{B_{c,max}} - E_{Bk} \text{ if } E_{Bk} - (E_{G_{savek}} - E_{Dk}) < E_{B_{c,max}} \quad (7.29)$$

and

$$E_{B_{gaink}} = -(E_{G_{savek}} - E_{Dk}) \text{ if } E_{Bk} - (E_{G_{savek}} - E_{Dk}) \geq E_{B_{c,max}}. \quad (7.30)$$

$$6. E_{Dk} + E_{Sk} = -E_{Lk}, \text{ with } E_{Bk} = 0$$

This scenario represents the case where generation consists of diesel generation and storage generation. The diesel generation energy savings and battery storage energy gain are given by:

$$E_{D_{save}k} = E_{G_{save}k} \text{ if } E_{Dk} > E_{G_{save}k}, \quad (7.31)$$

$$E_{D_{save}k} = E_{Dk} \text{ if } E_{Dk} \leq E_{G_{save}k} \quad (7.32)$$

and

$$E_{B_{gain}k} = 0. \quad (7.33)$$

$$7. \quad E_{Dk} + E_{Bk} = -E_{Lk}, \text{ with } E_{Sk} = 0$$

This scenario represents the case where generation consists of diesel generation and storage system generation. The diesel generation energy savings and battery storage energy gain are given by:

$$E_{D_{save}k} = E_{G_{save}k} \text{ if } E_{Dk} > E_{G_{save}k}, \quad (7.34)$$

$$E_{D_{save}k} = E_{Dk} \text{ if } E_{Dk} \leq E_{G_{save}k}, \quad (7.35)$$

$$E_{B_{gain}k} = 0 \text{ if } E_{Dk} > E_{G_{save}k} \quad (7.36)$$

and

$$E_{B_{gain}k} = E_{G_{save}k} - E_{Dk} \text{ if } E_{Dk} \leq E_{G_{save}k}. \quad (7.37)$$

$$8. \quad E_{Sk} + E_{Bk} = -E_{Lk}, \text{ with } E_{Dk} = 0$$

This scenario represents the case where generation consists of PV generation and storage system generation. The diesel generation energy savings and battery storage energy gain are given by:

$$E_{D_{save}k} = 0, \quad (7.38)$$

$$E_{B_{gain}k} = E_{G_{save}k} \text{ if } E_{Bk} > E_{G_{save}k} \quad (7.39)$$

and

$$E_{B_{gain}k} = E_{Bk} \text{ if } E_{Bk} \leq E_{G_{save}k}. \quad (7.40)$$

$$9. \quad E_{Dk} + E_{Sk} + E_{Bk} = -E_{Lk}$$

This scenario represents the case where generation consists of PV generation, diesel generation and storage system generation. The diesel generation energy savings and battery storage energy gain are given by:

$$E_{D_{save}k} = E_{G_{save}k} \text{ if } E_{Dk} > E_{G_{save}k}, \quad (7.41)$$

$$E_{D_{save}k} = E_{Dk} \text{ if } E_{Dk} \leq E_{G_{save}k}, \quad (7.42)$$

$$E_{B_{gain}k} = 0 \text{ if } E_{Dk} > E_{G_{save}k} \quad (7.43)$$

and

$$E_{B_{gain}k} = E_{G_{save}k} - E_{Dk} \text{ if } E_{Dk} \leq E_{G_{save}k}. \quad (7.44)$$

Scenarios 10 to 12 will never occur or will not be able to save any energy. Condition 10 represents a total blackout at the site with no generation. Conditions 11 and 12 are invalid as the battery storage cannot charge without any energy supply from the PV system.

The geyser load demand reduction can affect the battery storage in two behaviours. As determined by the saving scenarios set out above, the storage system energy savings are either defined as a positive or negative half-hourly value. Negative energy values represent energy gained during charging phases, while the positive values represent energy reduction during discharge phases. The battery storage energy gains, together with the historical storage system energy profiles, are used to derive a battery state of charge profile, subject to the condition that the storage system has a fixed maximum energy storage capacity. The energy saved during battery storage supplying periods are subtracted from the forecasting battery energy profile. The extra battery capacity gained during the charging phase is then added to the forecasting battery profile, possibly reducing the energy imported from the diesel generators.

7.7.3 Payback Period of Heat Pump Systems

7.7.3.1 Overview

A single day were chosen to illustrate the energy savings in terms of 48 half-hour averaging intervals. Averaged energy profiles obtained from the historical data are also used to conclude on the effect of averaging using the same set of energy saving scenarios. The heat pump installations and landed diesel costs at the site are finally used to calculate the payback period.

7.7.3.2 Energy Savings

The payback period of the heat pump systems is calculated using the historical data, energy saving scenarios 1 to 9 (Equations 7.17 to 7.44) and CoP ratio of the heat pump systems. As given in [34], and by using Equation 7.16, the geyser energy savings profile is calculated based on the heat pump system CoP ratio. As highlighted by [34] [35], the CoP ratio is highly depended on the ambient temperature and roughly varies between 3 and 4 during the four seasons of the year. The study at Robben Island were executed during the winter months of the year, leading to an estimated fixed CoP ratio of 3. Using the lower COP ratio, forecasts the lowest possible energy savings and the longest payback period.

The total geyser energy profile for the 6st of September is given in Figure 7.33, for a sunny day with no cloud cover. The geyser energy savings are calculated using Equation 7.16 for every half-hour averaging interval and is illustrated by the green bar plot in Figure 7.33.

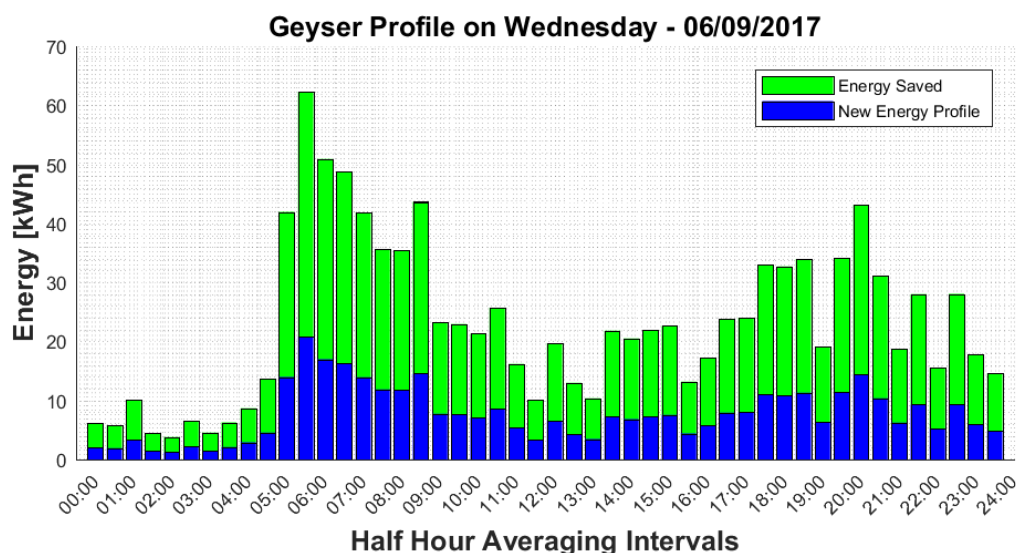


Figure 7.33 Total forecasted daily energy savings profile for the 6th of September 2017

The total energy savings for this day is 1 477.3 kWh. The diesel generator energy savings profile is given in Figure 7.34 for the 6th of September 2017. The energy savings calculated does not always affect the diesel generation profile as energy is sometimes supplied by other energy sources, i.e. PV plant or battery storage system, instead of the diesel generators.

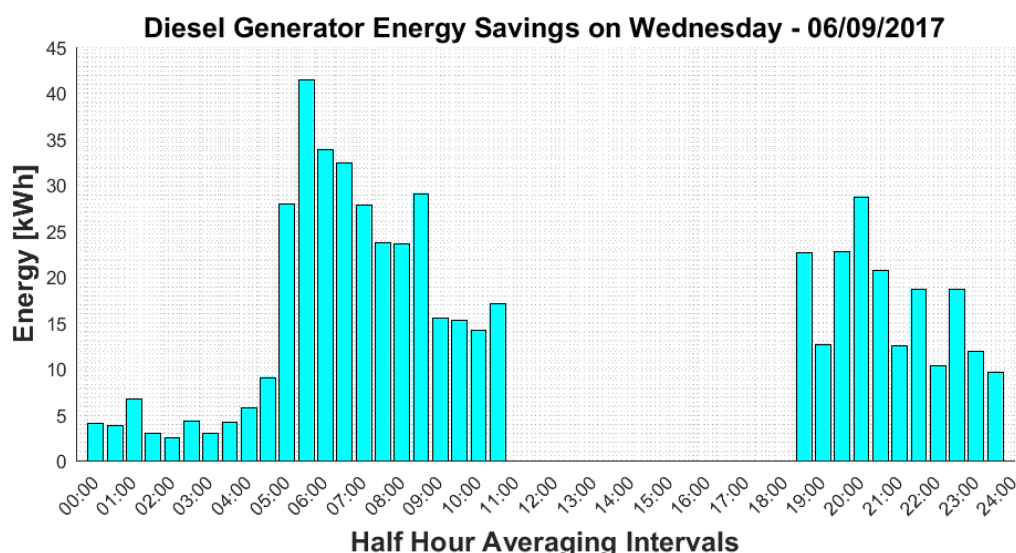


Figure 7.34 Diesel generator energy savings profile for the 6th of September 2017

The energy savings included in the forecasted daily energy savings profile, shown in Figure 7.33, represents energy saved during times where the diesel generators were operating. The additional energy savings occur during the period where the diesel generators are not operating and where the PV system and battery storage system are active. The additional battery energy gained during battery storage charging periods and the battery energy reduction during supplying periods are given in Figure 7.35 for the 6th of September 2017.

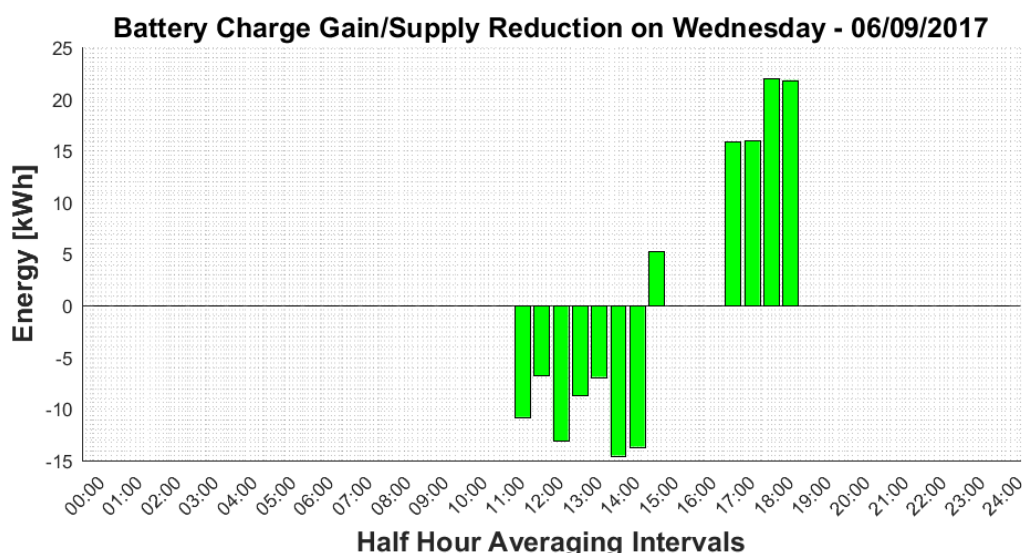


Figure 7.35 Additional battery energy gained and energy reduction profile for the 6th of September 2017

Each averaged half-hour energy value shown in Figure 7.35 is formulated using the set of energy saving scenarios 3-5 and 7-9, where $E_{B_{gain}k}$ receives a value greater than zero for every

k^{th} averaging interval. The additional battery charge energy gain is 148.8 kWh for this day. The additional battery charge gain for the day is given by the total of all half-hours with an energy value less than zero. The energy can only be stored if the battery system hasn't reached the maximum charging capacity at the specific half-hour. The energy is cumulatively added while the battery charge status is updated. Figure 7.36 shows the battery charge status for the 6th of September 2017. The battery charge energy is more noticeable for a day where the PV plant is not producing enough energy. Such a day is demonstrated in Appendix B.

The energy saved during the battery supplying period, illustrated by the energy values greater than zero in Figure 7.35, extends the battery storage's capacity as less energy is exported during these half-hours. The additional battery storage system supply capability is added to the battery profile at half-hours where the diesel generators serviced the demand. Figure 7.37 illustrate the impact of the charge energy gain and supply energy reduction on the battery system, leading to extra battery supply capability.

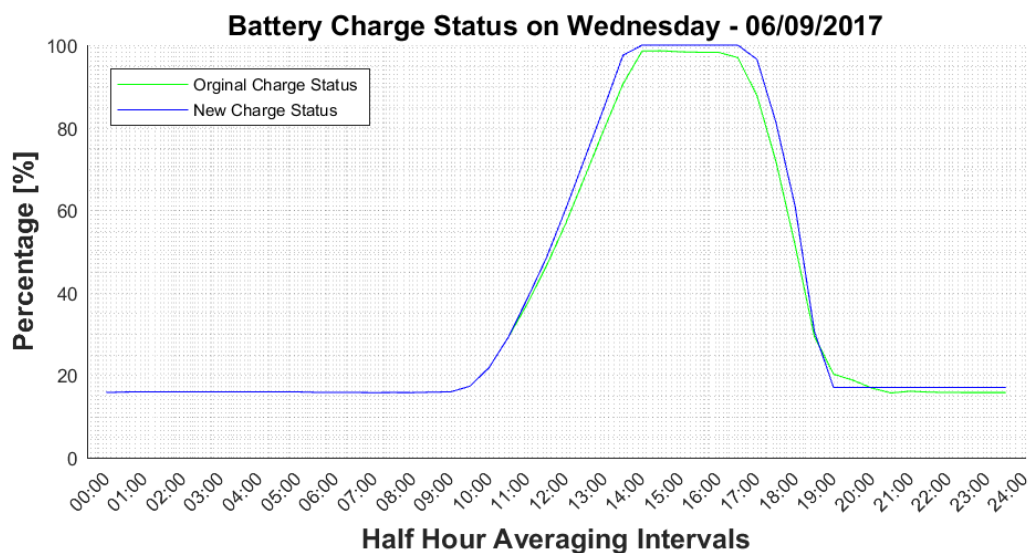


Figure 7.36 Battery storage charge status for the 6th of September 2017

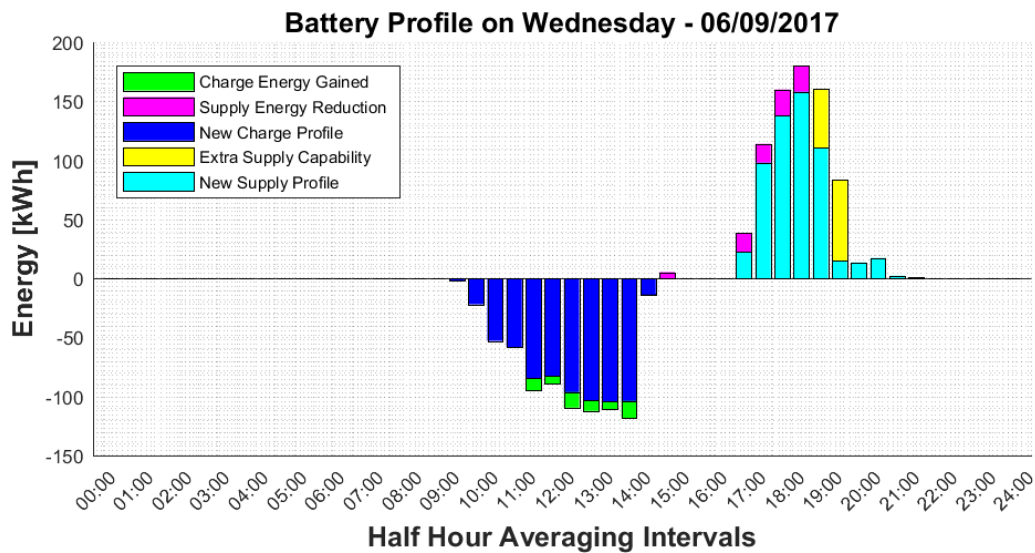


Figure 7.37 Illustration of the impact on the battery storage system for the 6th of September 2017

The extra supply capability of the battery system, affecting the diesel generation profile, is added to the diesel generator energy savings profile for the day. The daily diesel generator energy savings profile is given in Figure 7.38 for the 6th of September 2017. The new diesel generation profile is shown in Figure 7.39.

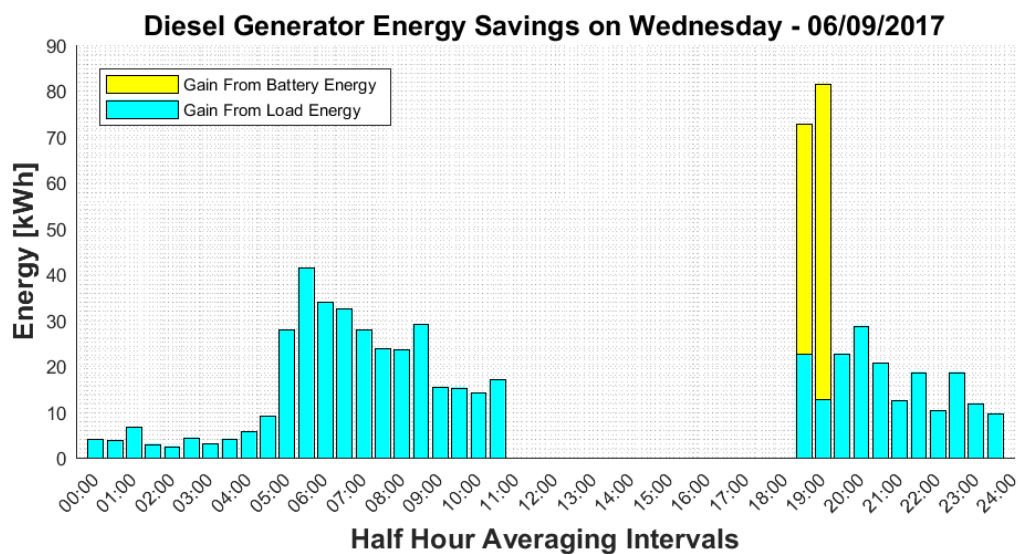


Figure 7.38 Total daily diesel generator energy savings for the 6th of September 2017

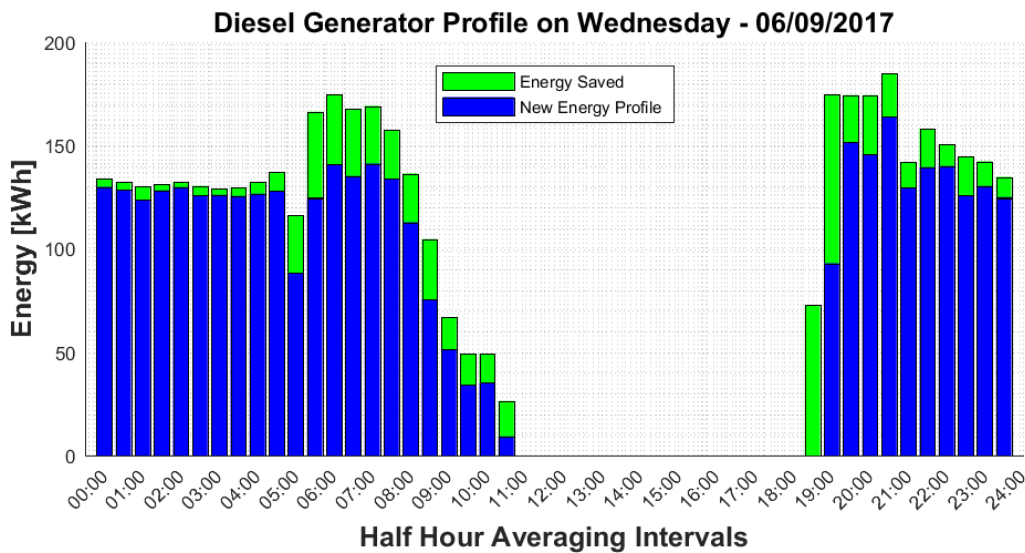


Figure 7.39 Daily diesel generation profile with energy savings for the 6th of September 2017

The total energy of all 48 half-hours represents the total diesel generator energy savings, which is used to calculate the diesel cost savings. The total diesel generator energy savings, E_{TDSi} , for the i^{th} day of the year is given by

$$E_{TDSi} = 2 \times \sum_{k=1}^{48} E_{D_{savek}} \quad k = 1, 2, 3 \dots 48; \quad i = 1, 2, 3 \dots 365 \quad (7.45)$$

where $E_{D_{savek}}$ denotes the energy at the k^{th} half-hour averaging interval. The total diesel generator energy savings depends on factors such as solar irradiance, battery charging status and geyser loads. Table 7.15 summarises the total diesel generator energy savings for the first week of September 2017.

Table 7.15 Predicted diesel generator energy savings over a period of ten days

Date	Total Diesel Generator Energy Savings [kWh]
Friday, 01/09/2017	942.9
Saturday, 02/09/2017	883.1
Sunday, 03/09/2017	834.5
Monday, 04/09/2017	1 075.0
Tuesday, 05/09/2017	1 149.0
Wednesday, 06/09/2017	1 315.3
Thursday, 07/09/2017	1 186.4
Friday, 08/09/2017	1 278.8
Saturday, 09/09/2017	827.9

Sunday, 10/09/2017	466.7
--------------------	-------

A few methods arise to calculate the diesel cost savings and payback period using the energy savings given in Figure 7.38. The first method is by calculating the total diesel generator energy savings for each day and to find the average energy savings over the period of the study. The average energy savings is given by the relationship

$$\widetilde{E}_{TDS} = \frac{1}{M} \sum_{i=S}^M E_{TDSi} \quad i = S, S + 1, S + 2, \dots, M \quad (7.46)$$

where \widetilde{E}_{TDS} denotes the average diesel generator energy savings, while S and M denotes the start and end day of the study respectively.

The second method is to determine the average diesel generation energy savings by using the averaged historical profiles. Profile averaging typically converge to one point and removes detail of each individual half-hour within each energy profile. This influences the set of energy saving scenarios, as the averaged energy profiles typically do not consist of finer details, such as when the diesel generators were switched off. However, the averaged profiles were used to demonstrate the difference between the two methods as given in Appendix B.

The daily average diesel generator energy savings for the period of the study is summarised in Table 7.16.

Table 7.16 Daily average diesel generator energy savings for the period of the study

Averaging Method	\widetilde{E}_{TDS} Per Day [kWh]
Averaged per day savings	996.0
Averaged per historical profile savings	1 150.2

The daily average diesel generator energy savings are different for the two averaging methods due to the stage where the averaging were executed, before and after the set of energy saving scenarios.

7.7.3.3 System Installation Costs

The project at hand requires the heat pump system installation costs to determine the payback period of the heat pump systems. The installation costs include all costs such as water cylinders, heat pump units, insulation materials, piping, valves, brackets and labour. The pricing should also take transportation costs to and from the site into consideration, as well as a set of water filters for each residence for the desalinated water used at the site.

A general price for heat pump systems is found by inquiring quotes from local providers and installers. Different providers have different standards, services and system warranties meaning that they cannot be directly compared. Quotes from *ITS Heat Pumps (PTY) LTD* and *Deacon's Solar and Plumbing CC* are used to set up a price curve for a total of 60 heat pump installations. As most residences at the site consist of older geysers, the quotes include new water cylinders, mounting brackets and new piping. The quotes, however, do not include water filtration devices or ferry transport to and from the site and is more aimed at the heat pump installations.

Figure 7.40 compares the cost of heat pump installations from the two providers. The numerical cost breakdown is given in Appendix C, Table C.1 and Appendix C, Table C.2. The total installation cost for both quotes are summarised in Table 7.17.

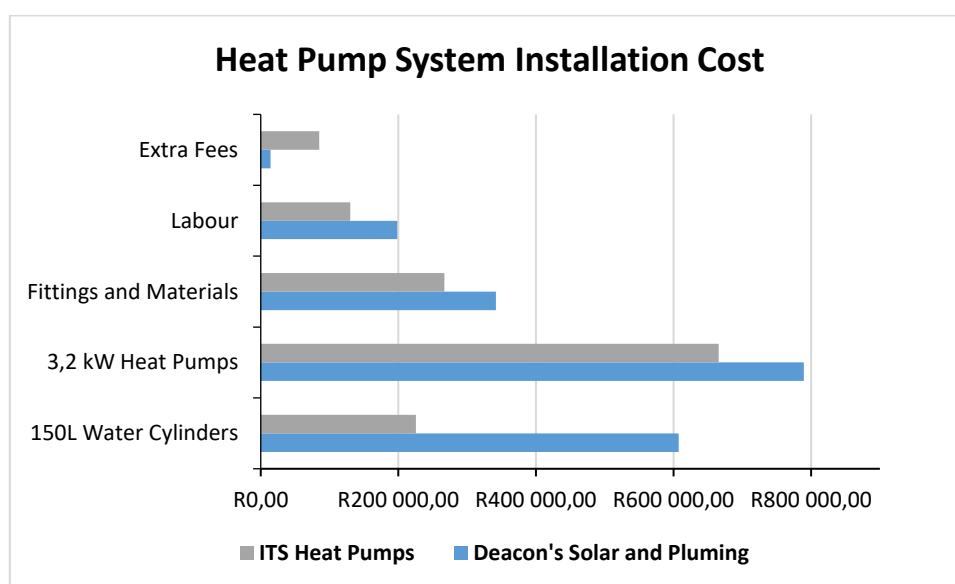


Figure 7.40 Heat pump system installation cost comparison

Table 7.17 Total heat pump installation costs of two different suppliers

	Total cost (60 Heat Pumps) [R]
ITS Heat Pumps	1 373 244,00
Deacon's Solar and Plumbing	1 951 615,70

The quote from *ITS Heat Pumps* is provided as a special deal with the condition that a mass order of 60 heat pump systems is submitted. The noticeable difference between the two providers is due to the cost of water cylinders. *ITS Heat Pumps* quoted for trendline water cylinders, while *Deacon's Solar and Plumbing* quoted on *X-Stream* solar geysers, which include solar panels. This makes the two quotes incomparable. The quotes were used to predict the payback period of the heat pump installations, however, the study does not incorporate the extra

energy savings gained from the solar warm water cylinders. The solar panel addition will affect the energy consumption of the heat pump systems and reduce the diesel consumption even more.

7.7.3.4 Diesel electricity generation costs

The payback period calculations of heat pump installations also require the cost of generating electricity using the diesel generators. The cost of electricity generation is calculated using three factors that contribute to the cost:

- Generator fuel consumption rate.
- Generator output power.
- Price of diesel, including transportation costs.

With a set of generators manufactured by different companies, operating at various sequences, the figure can vary and have deviations in efficiency rates. This also eliminates the use of fuel consumption information provided in the datasheets of these generators. In terms of specific fuel consumption of all diesel generators at the site, standard numbers were used from research [54]. These standards typically depend on the size and the load of each generator. The following assumptions were made for simplification reasons:

- Generator Power Factor (PF) of 0.8.
- Same generator efficiency whether the unit is operating at half load or full load.

All four diesel generators currently in operation at site has an apparent power, S (VA), rating of 500 kVA. The real power, P (W), for a single generator is given by:

$$P(W) = |S(VA)| \times PF \quad (7.47)$$

with

$$PF = \cos \emptyset \quad (7.48)$$

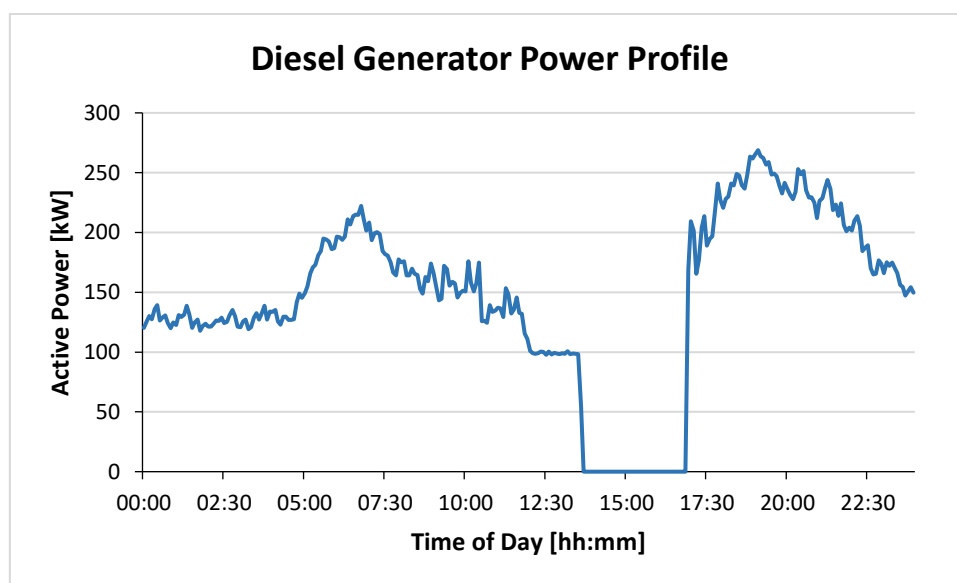
where \emptyset denotes the apparent power phase angle.

Using the assumption of $PF = 0.8$ and the apparent power rating of $|S| = 500 \text{ kVA}$, the real power is calculated as a constant 400 kW. The approximate diesel fuel consumption standards for a 400 kW generator are listed in Table 7.18 [54].

Table 7.18 Approximate diesel fuel consumption standards for a 400 kW generator [54]

Generator Size	¼ Load [L/h]	½ Load [L/h]	¾ Load [L/h]	Full Load [L/h]
400 kW / 500 kVA	33.3	55.6	79.6	107.0

Using a diesel generator power profile from the historical data for a typical operational day, an average power output can be derived. Figure 7.41 shows the diesel generator power profile with an operating-average power output of 168 kW.

**Figure 7.41 Typical diesel generator power profile as retrieved from [78]**

Based on the average standard power output of 168 kW, the fuel consumption can be calculated in terms of power. With the average standard power output less than half the rated power of the diesel generator, the half-load fuel consumption standard is used from Table 7.20. The fuel consumption rate can be expressed in terms of power as:

$$b_P = \frac{55.6 \frac{L}{h}}{168 \text{ kW}} = 0.331 \text{ L/kWh} \quad (7.49)$$

Using the fuel consumption rate, b_P , given by Equation 7.49, and the price of landed diesel at the site, C_{LD} , the price per kWh for diesel electricity generation is expressed by:

$$C_{GD} = C_{LD} \left(\frac{R}{L} \right) \times b_P \left(\frac{L}{kWh} \right) \quad (7.50)$$

By the time of writing this thesis, the landed cost of diesel is confirmed at $C_{LD} = R11.70/L$, which include transportation costs. With $C_{LD} = R11.70/L$, the price per kWh for diesel electricity generation results in:

$$C_{GD} = R3.872 \text{ per kWh} \quad (7.51)$$

The result in (7.51) is used in the payback period calculations, however, it remains a varying estimation. By using the result, the assumption can be made that the generators are operating at the same efficiency throughout its operation, above and below half the rated power.

7.7.3.5 Payback Period

The payback period is finally calculated based on the cost of electricity generation obtained in (7.51). The total diesel cost savings is shown in Figure 7.42 for the installation of 60 heat pump systems. The total diesel cost savings is forecasted as R2 815 250 for a period of two years.

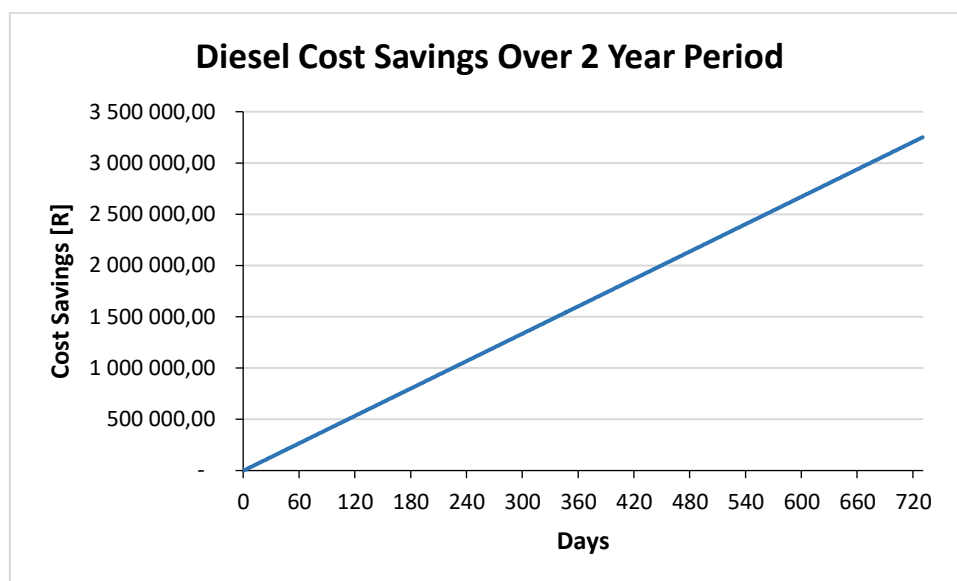


Figure 7.42 Forecasted diesel cost savings over a period of two years

The quoted heat pump installation cost is about R22 887.4 per residence when installing traditional water cylinders and R32 526.9 per residence for full solar heat pump installations. These costs do not include transportation and water filtration costs, which will slightly extend the payback period. The payback period is not calculated for the solar heat pump installations as the possible energy savings on such a system is unknown and require data regarding the solar addition. With the total quoted cost of R1 951 615.70 for solar heat pump installations, the payback period will certainly be within two years after installation.

Using Figure 7.42, it is clear that the traditional water cylinder and heat pump systems will be paid off within one year after installation. The payback period in terms of the number of days, P_b , is given by:

$$P_b = \frac{\widetilde{ETDS} \times C_{GD}}{C_{HPS} \times N} \quad (7.52)$$

where C_{HPS} denotes the installation cost of a single heat pump system while N denotes the amount of heat pump systems installed at the site.

Using the per day average diesel energy savings as summarized in Table 7.16, the payback period is calculated in terms of the two averaging methods introduced in Section 7.7.3.2. The payback period results are listed in Table 7.19.

Table 7.19 Predicted payback period for two types of energy saving results

Averaging Method	Payback Period, P_b [Days]
Averaged per day savings	357
Averaged per historical profile savings	309

Figure 7.43 compares the two averaging methods in terms of remaining cost over the payback period of a year. On a day scale, the averaging method used shows a noticeable difference in the payback period. The longer payback period can be seen as more reliable due to the inclusion of detail in the data used to determine this figure. The forecasted payback period remains very short compared to similar projects depended on national power supplies.

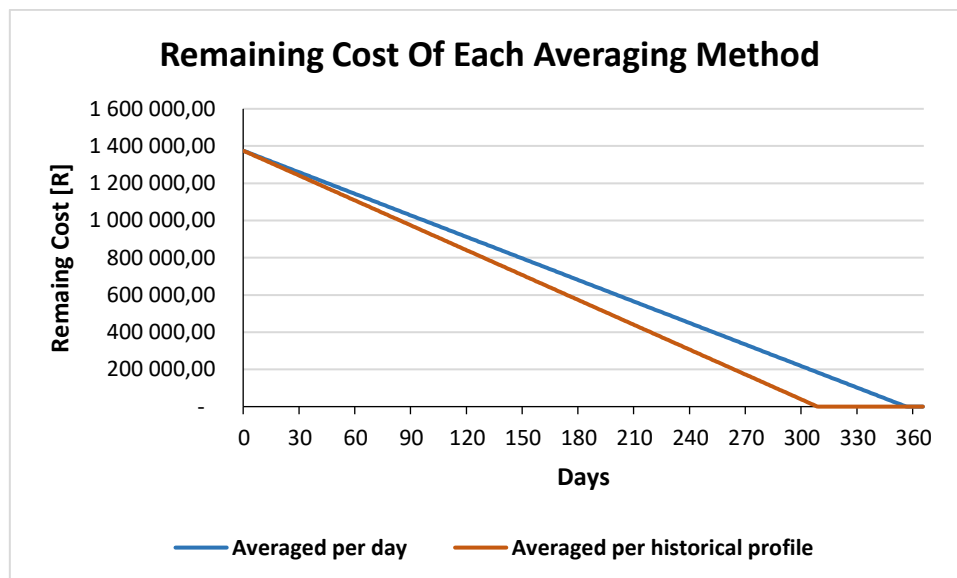


Figure 7.43 Remaining cost after a number of days for two profile averaging methods

8 Conclusions and Recommendations

8.1 Overview

The chapter presents conclusions and recommendations for future development and research. The conclusions are presented with reference to the research objectives set out in section 1.3.1. These include the following:

- How can de-aggregated load data be acquired by a low-cost data logger?
- How well does the proposed system perform with reference to power consumption and cost?
- Is the concept of histogram event recording plausible and does it reduce the manufacturing cost, memory requirements and the physical footprint?
- How can the proposed system be used to highlight EE and EM interventions in an islanded micro-grid energy system?
- What other residential appliances in a micro-grid system can be targeted to achieve energy savings?
- Will the energy savings and payback period be satisfactory when replacing resistant type geysers with heat pump systems?
- What future work can be done to enhance the proposed system in terms of power consumption, practicality and costs?

The literature study discusses important topics relevant to the design and development of the proposed system as well as background information on micro-grid energy systems.

8.2 Conclusions

8.2.1 Design and Development

To acquire de-aggregated load data for load modelling analysis and studies, a system is proposed based on various load modelling techniques reviewed. A literature review of de-aggregated load modelling delivered the following:

- *Appliance load monitoring*: Various techniques exist to acquire de-aggregated load data for individual appliance in the residential and commercial sector. These include attempts to

classify these appliances based on their operational state as researched by Hart [10]. Further research built upon the work of Hart, gave rise to various load monitoring techniques [14]. However, none of the methods are completely accurate and still requires an expensive data logger.

- *Non-intrusive load monitoring*: Modern load monitoring technologies all use non-intrusive metering approaches [13] [17] [18]. These metering approaches produce various advantages such as full isolation from the utility boundary and a reduction in manufacturing cost.
- *Load profile forecasting*: Various load profile forecasting strategies exist, which is categorised into top-down and bottom-up modelling approaches [20] [21]. An explanation of each modelling approach is given by Jacobsen [20], emphasising the focus of each. The lack of de-aggregated load data is emphasised by various researchers when developing or using load profile forecasting techniques [4] [6] [24] [25] [26]. The lack of Time-of-Use profiles and usage profiles remains challenges for accurate load profile forecasting techniques.

The proposed load logging system is developed based on the requirements for modern load monitoring technologies as stipulated by literature. Focus was placed on a low-cost and small physical footprint hardware design. The design is kept simple to speed up installation procedures for de-aggregated load monitoring projects.

Various data acquisition modes were developed and implemented. These data acquisition modes can be classified into two main categories, namely raw data recording mode and histogram recording mode. Event and analog recording features were included for each recording mode. The concept of histogram data logging [7] [8] [9] reduces the memory storage requirements of the system, which in turn reduces the cost, size and power consumption of the unit.

A computer software application was developed for device configuration, data retrieval and data exchange. The application provides a user-friendly interface to interact with the device. Device configuration includes the setup of important system parameters such as the real-time clock, memory counters, data acquisition mode, device ID and installation location. The USB communication interface between the device and application performed satisfactorily, although it was one of the most challenging features to implement.

The system performed satisfactorily in terms of functionality, cost and feasibility. A power consumption audit of the system was performed for operational acquisition modes as well as during sleeping modes. The battery lifetime was calculated based on the average number of events and data acquisition mode selected and was found suitable for load modelling applications.

8.2.2 Case Study and Analysis

The performance of the proposed system was tested by installing several units in a micro-grid energy system. A literature review of the islanded micro-grid energy system delivered the following insights:

- *Micro-grids*: Micro-grids are typically proposed as a solution to integrate small scale renewable projects [36] and usually contain a combination of energy sources depending on the location [40] [41]. Micro-grids can be classified into various types of energy systems based on factors such as national grid or “off-grid” connections. Islanded micro-grids do not connect to a centralized electrical grid, making it completely independent.
- *Smart Grids*: The different energy sources in a micro-grid system requires control mechanisms to ensure a stable and synchronized energy system [42] [43] [44] [45] [46]. These control schemes are classified into three levels, namely primary control, secondary control and tertiary control [47] [48] [49]. The control schemes give rise to smart-grid energy systems, which is a modern micro-grid with feedback information. The aim with smart-grids are to improve energy delivery networks and deliver power more efficiently.
- *Diesel Generators and Fuel Consumption*: Diesel generators are the most common energy source found in islanded micro-grid energy systems. They are also responsible for high costs associated with constructing and operating micro-grid energy systems. The ideal usage for diesel generators in a micro-grid is to compensate for PV and wind power fluctuations [51] [52]. However, in some micro-grid systems, the diesel generators are operating relatively often or even continuously [53].
- *Battery Storage Systems*: Energy from renewable energy sources are typically stored in battery storage systems, which are considered as the most viable storage solution at present. Over the past few years, batteries have developed and improved significantly, especially for applications in the transport and renewable energy industries [55] [56] [57] necessary to understand and design battery storage systems for micro-grid energy systems.

De-aggregated load data was acquired by deploying a number of the histogram data loggers developed as part of the project on residential geysers and stoves in the Robben Island micro-grid. The loggers were predominantly operating in raw event recording to gather as much data as possible during the period of installation.

Additional energy profile data were acquired from the *Meteo Control* intelligent energy system control website (Meteo Control) for the PV plant, battery storage system and diesel generators.

All profiles, namely the demand profile, diesel generation profile, solar generation profile and battery system profile, were formulated in a standard load profile format with 48 half-hourly averaging intervals. The energy profiles were derived for individual days, the Megaflex TOU days as well as total average profiles for the test period.

Algorithms were derived and implemented to determine the energy savings when replacing the current resistive heating elements with modern heat pumps. It was found that averaging the energy profiles at different stages during the simulation, results in a small difference in the calculated energy savings. Thus, simulations were executed for two types of averaging. It was noticed that the difference between the two methods are mostly due to off-periods of data being omitted during averaging, resulting in less accurate energy saving simulations. Although the two methods generate a slight different energy saving over a certain period, the result were satisfactory to calculate the payback period of the heat pump systems.

Additional energy savings were gained from the battery storage system as a reduction in load energy will provide additional charging energy as well as a reduction in battery storage usage. The results show that there are room for additional battery capacity, as the energy delivered by the PV plant are partly unused during late afternoons. If more energy can be stored during the day, a greater reduction in diesel generation can be achieved.

The diesel consumption standards given in [54], together with the total predicted energy savings, were used to estimate the possible diesel savings. The investigation showed that a substantial amount of diesel can be saved by replacing the geysers heating elements at the site with heat pumps. The total cost of installing 60 heat pumps was compared to the cost of the diesel saved to calculate a payback period for the heat pump installations. Similar projects connected to a national energy network will typically have a payback period of between 10 and 20 years. Due to the high cost of the diesel fuel used for electricity generation in the Robben Island micro-grid, however, the payback period for the heat pump retrofits is less than a year.

Additional energy can be saved by installing compound hot water systems, which do not only replace the resistive heating element with a heat pump, but adds an additional solar water heating system.

In conclusion, the case study results confirm that the histogram event logger developed in this investigation performs well for bottom-up load modelling.

8.3 Recommendations

8.3.1 Future Work

The investigation focussed on the development and performance evaluation of a histogram data recorder for load modelling applications. The design objectives focussed on aspects such as battery power consumption and memory usage. The system implemented feature various data acquisition modes. Further work is required to optimise the design for the case when only histogram recording is required. In terms of the hardware design, components such as the external EEPROM, can be omitted to reduce the physical footprint and cost of the design.

Further work can be done with the focus to make use of a smaller and low-cost microprocessor suitable for single mode recording applications. Different software sets can also be developed for different applications.

A practical difficulty in terms of data retrieving was experienced during the deployment of the loggers at Robben Island. Retrieving data from every logger required regular visits to each residence at the site, which required expensive transportation and special permissions for access. Future work can investigate on more practical methods to retrieve data from the units using wireless technology and some connection to a communication network to retrieve data remotely.

Wireless additions will require the current battery system to be redesigned to cater for the increased power consumption. Depending on the data acquisition mode of the logger, the high frequency power consumption of the device should be recalculated to establish a new battery lifetime estimate.

The case study conducted in this thesis highlights various opportunities for EM and EE interventions appropriate to the islanded micro-grid system targeted in the case study. The focus was placed on the geysers present at the site. However, additional energy saving opportunities lies within the remaining two main energy consuming loads at the site, the desalination water

plant and stoves. Usage data and energy profiles of the two loads are included in the case study to understand the total load profile. It emphasizes the requirement of more energy efficient machinery in the desalination water plant and alternatives to electric stoves, such as gas stoves.

The work done in the case study can be extended to simulate the possible energy savings from the desalination water plant and electric stoves. Such EM and EE interventions will further reduce the dependency on diesel fuel. Additional opportunities also exist to extend the energy storage capacity of the battery storage system and even the size of the PV plant.

References

- [1] U.S Department of Energy Federal Energy Management Program, "M&V Guidelines: Measurement and Verification for Performance-Based Contracts," vol. 4, pp. 2-15, November 2015.
- [2] Z. J. Kolter and M. J. Johnson, "REDD: A Public Data Set for Energy Disaggregation Research," vol. 25, pp. 59-62, 2011.
- [3] S. Barker, S. Karla, D. Irwin and P. Shenoy, "Empirical Characterization and Modeling of Electrical Loads in Smart Homes," in *Green Computing Conference (IGCC)*, Arlington, VA, 2013.
- [4] A. Capasso, W. Grattieri, R. Lamedica and A. Prudenzi, "A bottom-up approach to residential load modeling," *IEEE Transactions on Power Systems*, vol. 9, no. 2, pp. 957-964, May 1994.
- [5] Z. Kang, M. Jin and C. Spanos, "Modeling of End-Use Energy Profile: An ApplianceData-Driven Stochastic Approach," in *40th Annual Conference of the IEEE Industrial Electronics Society*, Dallas, TX, USA, 2014.
- [6] K. d. Preez and H. Vermeulen, "Development of a Bottom-Up Methodology for Modelling Electrical Residential Load from Event Data," Stellenbosch, 2016.
- [7] K. H. Knuth, "Optimal Data-Based Binning for Histograms," in *Departments of Physics and Informatics*, University at Albany, 2013.
- [8] D. W. Scott, "On Optimal and Data-Based Histograms," *Biometrika*, vol. 66, no. 3, pp. 605-910, December 1979.
- [9] D. Freedman and P. Diaconis, "On the Histogram as a Density Estimator: L 2 Theory," *Z. Wahrscheinlichkeitstheorie verw. Gebiete*, vol. 57, pp. 453-476, 1981.
- [10] G. W. Hart, "Nonintrusive appliance load monitoring," *Proceedings of the IEEE*, vol. 80, no. 12, pp. 1870-1891, December 1992.
- [11] J. K. Gruber and M. Prodanovic, "Residential Energy Load Profile Generation Using a Probabilistic Approach," in *2012 Sixth UKSim/AMSS European Symposium on Computer Modeling and Simulation*, Valetta, Malta, 2012.
- [12] M. Baranski and J. Voss, "Nonintrusive appliance load monitoring based on an optical sensor," in *Power Tech Conference*, Bologna, Italy, 2003.
- [13] M. Zeifman and K. Roth, "Nonintrusive appliance load monitoring: Review and outlook," *IEEE Transactions on Consumer Electronics*, vol. 57, no. 1, pp. 76-84, March 2011.
- [14] H. Najmeddine, K. E. K. Drissi, C. Pasquier, C. Faure, K. Kerroum, A. Diop, T. Jouannet and M. Michou, "State of art on load monitoring methods," in *Power and Energy Conference, 2008 PECon 2008. IEEE 2nd International*, Johor Bahru, Malaysia, 2008.
- [15] O. Ardakanian, N. Koochakzadeh, R. P. Singh, L. Golab and S. Keshav, "Computing Electricity Consumption Profiles," in *Workshop Proceedings of the EDBT/ICDT 2014 Joint Conference*, Athens, Greece, 2014.

- [16] S. Rastogi, M. Sharma and P. Vershney, "Internet of Things based Smart Electricity Meters," *International Journal of Computer Applications (0975 – 8887)*, vol. 133, no. 8, pp. 13-16, 2016.
- [17] B. Naghibi and S. Deilami, "Non-intrusive load monitoring and supplementary techniques for home energy management," in *Power Engineering Conference (AUPEC)*, Perth, WA, Australia, 2014.
- [18] L. K. Norford and S. B. Leeb, "Non-intrusive electrical load monitoring in commercial buildings based on steady-state and transient load-detection algorithms," *Energy and Buildings*, vol. 24, no. 1, pp. 51-64, 1999.
- [19] S. R. Vetrivel, L. Visveswaran, S. Vignesh and C. Amutha, "A Low-Cost Non-Intrusive Load Monitoring System for Rural Applications," *International Journal of Advanced Research in Basic Engineering Sciences and Technology (IJARBEST)*, vol. 3, no. 29, pp. 99-103, March 2017.
- [20] H. K. Jacobsen, "Integrating the bottom-up and top-down approach to energy-economy modelling: the case of Denmark," *Energy Economics*, vol. 20, no. 1, pp. 443-461, 1998.
- [21] C. Bohringer and T. F. Rutherford, "Combining bottom-up and top-down," *Energy Economics*, vol. 30, no. 1, pp. 574-596, 2008.
- [22] M. Kavgić, A. Mavrogianni, D. Mumovic, A. Summerfield, Z. Stevanovic and M. Djurovic-Petrovic, "A review of bottom-up building stock models for energy consumption in the residential sector," *Building and Environment*, vol. 45, no. 1, pp. 1683-1697, 2010.
- [23] L. G. Swan and V. I. Ugursal, "Modeling of end-use energy consumption in the residential sector: A review of modeling techniques," *Renewable and Sustainable Energy Reviews*, vol. 13, no. 1, pp. 1819-1835, 2009.
- [24] B. M. Larsen and R. Nesbakken, "Household electricity end-use consumption: results from econometric and engineering models," *Energy Economics*, vol. 26, no. 1, pp. 179-200, 2004.
- [25] M. C. Sanchez, J. G. Koomey, M. M. Moezzi, A. Meier and W. Huber, "Miscellaneous electricity in US homes: Historical decomposition and future trends," *Energy Policy*, vol. 26, no. 8, pp. 585-593, July 1998.
- [26] J. V. Paatero and P. D. Lund, "A model for generating household electricity load profiles," *International Journal of Energy Research*, vol. 30, no. 5, pp. 273-290, 2005.
- [27] Population Division, "World Population Prospects: The 2017 Revision, Key Findings and Advance Tables," Department of Economic and Social Affairs, New York, 2017.
- [28] A. Ahmad, M. Hassan, M. Abdullah, H. Rahman, F. Hussin, H. Abdullah and R. Saidur, "A review on applications of ANN and SVM for building electrical energy consumption forecasting," *Renewable and Sustainable Energy Reviews*, vol. 33, no. 1, pp. 102-109, 2014.
- [29] J. E. Cohen, "Population Growth and Earth's Human Carrying Capacity," *Science, New Series*, vol. 269, no. 5222, pp. 341-346, 21 July 1995.
- [30] Q. Catherine, J. Wheeler, R. Wilkinson and G. d. Jager, "Hot water usage profiling to improve geyser efficiency," *Journal of Energy in Southern Africa*, vol. 23, no. 1, pp. 39-45, February 2012.

- [31] L. Gelazanskas and K. A. A. Gamage, "Forecasting Hot Water Consumption in Residential Houses," *Energies*, vol. 8, no. 1, pp. 12702-12717, 2015.
- [32] Eskom, "Switching off your geyser helps everybody," 14 May 2013. [Online]. Available: http://www.eskom.co.za/sites/IDM/Documents/127581ESKD_Geyser_Fact_Sheet.pdf. [Accessed 7 August 2017].
- [33] R. Gouws and E. I. Roux, "Efficiency and cost analysis of a designed in-line water heating system compared to a conventional water heating system in South Africa," *Journal of Energy in Southern Africa*, vol. 23, no. 3, pp. 9-15, August 2012.
- [34] M. Zhang, "Performance of heat pumps in South Africa," in *Energize*, 2013, pp. 66-67.
- [35] R. Rankin and M. van Eldik, "An Investigation Into The Energy Savings and Economic Viability Of Heat Pump Water Heaters Applied in the Residential and Commercial Sectors," M-Tech Industrial (Pty) Ltd / North-West University, Potchefstroom, 2008.
- [36] R. Lasseter, "MicroGrids," in *Power Engineering Society Winter Meeting*, New York, USA, 2002.
- [37] N. Hatziargyriou, H. Asano, R. Iravani and C. Marnay, "Microgrids," *IEEE Power and Energy Magazine*, vol. 5, no. 4, pp. 78-94, 2007.
- [38] S. Morozumi, N. Inoue, Y. Aeashiro, Y. Chiba and T. Iwasaki, "Strategies and Status of Grid-connection Technology Development in NEDO," in *IEEE*, Japan, 2008.
- [39] "European Research Project, 'Microgrids'," 2008. [Online]. Available: <http://www.microgrids.eu/>.
- [40] M. Ahmed, U. Amin, S. Aftab and Z. Ahmed, "Integration of Renewable Energy Resource in Microgrid," in *Energy and Power Engineering*, Lahore, South Asia, 2015.
- [41] L. Mihet-Popa, V. Groza and F. Isleifsson, "Experimental testing for stability analysis of distributed energy resources components with storage devices and loads," in *Instrumentation and Measurement Technology Conference (I2MTC), 2012 IEEE International*, Graz, Austria, 2012.
- [42] J. Lopes, C. Moreira and A. Madureira, "Defining control strategies for MicroGrids islanded operation," *IEEE Transactions on Power Systems*, vol. 21, no. 2, pp. 916-924, May 2006.
- [43] E. Planas, A. Gil-de-Muro, J. Andreu, I. Kortabarria, I. Martinez and M. de Alegria, "General aspects, hierarchical controls and droop methods in microgrids: A review," *Renewable and Sustainable Energy Reviews*, vol. 17, no. 1, pp. 147-159, October 2013.
- [44] I. Balaguer, Q. Lei, S. Yang, U. Supatti and F. Peng, "Control for Grid-Connected and Intentional Islanding Operations of Distributed Power Generation," *IEEE Transactions on Industrial Electronics*, vol. 58, no. 1, pp. 147-157, January 2011.
- [45] T. Vandoorn, B. Renders, L. Degroote, B. Meersman and L. Vandeveldel, "Active Load Control in Islanded Microgrids Based on the Grid Voltage," *IEEE Transactions on Smart Grid*, vol. 2, no. 1, pp. 139-151, March 2011.

- [46] J. Vasquez, J. Guerrero, J. Miret, M. Castilla and L. de Vicuna, "Hierarchical Control of Intelligent Microgrids," *IEEE Industrial Electronics Magazine*, vol. 4, no. 4, pp. 23-29, December 2010.
- [47] A. Bidram and A. Davoudi, "Hierarchical Structure of Microgrids Control System," *IEEE Transactions On Smart Grid*, vol. 3, no. 4, pp. 1963-1976, December 2012.
- [48] J. Guerrero, J. Vasquez and T. Remus, "Hierarchical Control of Droop-Controlled DC and AC Microgrids - A General Approach Towards Standardization," in *Proceedings of the 35th Annual Conference of the IEEE Industrial Electronics Society*, Catalonia, Spain, 2009.
- [49] M. Saleh, A. Althaibani, Y. Esa, Y. Mhandi and A. Mohamed, "Impact of clustering microgrids on their stability and resilience during blackouts," in *Smart Grid and Clean Energy Technologies (ICSGCE), 2015 International Conference*, Offenburg, Germany, 2015.
- [50] X. Fang, S. Misra, G. Xue and D. Yang, "Smart Grid – The New and Improved Power Grid: A Survey," *IEEE Communications Surveys & Tutorials*, vol. 14, no. 4, pp. 944-980, December 2012.
- [51] H. Hilal, M. Oktaufik, A. Prastawa and B. Prasetyo, "Smart Diesel Generator to Compensate On-Grid PV Fluctuation: A Case Study in Sumba Island Indonesia," in *The 3rd IEEE Conference on Power Engineering and Renewable Energy*, Jakarta, Indonesia, 2016.
- [52] Q. Tang, N. Liu and J. Zhang, "Optimal Operation Method for Microgrid with Wind/PV/Diesel Generator/Battery and Desalination," *Journal of Applied Mathematics*, vol. 2014, no. 1, pp. 2-11, 2014.
- [53] C. Hernandez-Aramburo, T. Green and N. Mugniot, "Fuel Consumption Minimization of a Microgrid," *IEEE Transactions on Industry Applications*, vol. 41, no. 3, pp. 673-681, June 2005.
- [54] ABLE Sales, "Diesel Generator Fuel Consumption Chart in Litres," 2016. [Online]. Available: www.ablesales.com.au. [Accessed 24 October 2017].
- [55] H. Chen, T. Cong, W. Yang, C. Tan, Y. Li and Y. Ding, "Progress in electrical energy storage system: A critical review," *Progress in Natural Science*, vol. 19, no. 3, pp. 291-312, 2009.
- [56] P. Hall and E. Bain, "Energy-storage technologies and electricity generation," *Energy Policy*, vol. 36, no. 12, pp. 4352-4355, 2008.
- [57] E. Hittinger, T. Wiley, J. Kluza and J. Whitacre, "Evaluating the value of batteries in microgrid electricity systems using an improved Energy Systems Model," *Energy Conversion and Management*, vol. 89, no. 1, pp. 458-472, 2015.
- [58] J. Besenhard, *Handbook of Battery Materials*, Austria: John Wiley & Sons, 2008, 2008.
- [59] J. Li, L. Wang, C. Lyu, W. Luo, K. Ma and L. Zhang, "A Method of Remaining Capacity Estimation for Lithium-Ion Battery," *Advances in Mechanical Engineering*, vol. 2013, no. 1, pp. 1-7, 2013.
- [60] B. Scrosati and J. Garche, "Lithium batteries: Status, prospects and future," *Journal of Power Sources*, vol. 195, no. 9, pp. 2419-2430, May 2010.
- [61] Bloomberg New Energy Finance, "Lithium-ion Battery Costs: Squeezed Margins and New Business Models," Bloomberg New Energy Finance, 10 July 2017. [Online]. Available:

<https://about.bnef.com/blog/lithium-ion-battery-costs-squeezed-margins-new-business-models/>. [Accessed 12 October 2017].

- [62] W. Chang, M. Brunig and E. Nardo, "The State of Charge Estimating Methods for Battery: A Review," *ISRN Applied Mathematics*, vol. 2013, no. 1, pp. 1-7, 2013.
- [63] H. He, R. Xiong and H. Guo, "Online estimation of model parameters and state-of-charge of LiFePO₄ batteries in electric vehicles," *Applied Energy*, vol. 89, no. 1, pp. 413-420, 2012.
- [64] V. Prajapati, H. Hess, E. William, V. Gupta, M. Huff, M. Manic, F. Rufus, A. Thakker and J. Govar, "A literature review of state of-charge estimation techniques applicable to lithium poly-carbon monoflouride (Li/CFx) battery," in *Power Electronics (IICPE), 2010 India International Conference*, New Delhi, India, 2010.
- [65] B. Vairamohan and J. Chiasson, "Estimating the state of charge of a battery," *IEEE Transactions on Control Systems Technology*, vol. 13, no. 3, pp. 465-470, May 2005.
- [66] K. Ng, C. Moo, Y. Chen and Y. Hsieh, "State-of-charge estimation for lead-acid batteries based on dynamic open-circuit voltage," in *Power and Energy Conference, 2008. PCon 2008. IEEE 2nd International*, Johor Bahru, Malaysia, 2008.
- [67] I. Buchmann, "Battery University," 2017. [Online]. Available: http://batteryuniversity.com/learn/article/what_is_the_c_rate. [Accessed 24 October 2017].
- [68] D. Doerffel and S. Sharkh, "A critical review of using the Peukert equation for determining the remaining capacity of lead-acid and lithium-ion batteries," *Journal of Power Sources* 155, vol. 155, no. 1, p. 395-400, 2006.
- [69] M. a. Atmel, "Atmel Studio 7," [Online]. Available: <http://www.atmel.com/microsite/atmel-studio/>. [Accessed 10 October 2017].
- [70] Eclipse, "Eclipse IDE," 11 October 2017. [Online]. Available: <https://www.eclipse.org/home/>.
- [71] The Qt Company, "Qt Creator," [Online]. Available: <https://www1.qt.io/download/>. [Accessed 25 October 2017].
- [72] Altium, "Altium Designer," [Online]. Available: <http://www.altium.com/>. [Accessed 25 October 2017].
- [73] Matlab, "Matlab," [Online]. Available: <https://ch.mathworks.com/products/matlab.html>. [Accessed 25 October 2017].
- [74] Python Software Foundation, "Python," 11 October 2017. [Online]. Available: <https://www.python.org/>.
- [75] Linear Technology, "LTC1966 - Precision Micropower $\Delta\Sigma$ RMS-to-DC Converter," 18 January 2017. [Online]. Available: <http://cds.linear.com/docs/en/datasheet/1966fb.pdf>.
- [76] W. Terblanche and H. Vermeulen, "Development of as lowe-cost, low-power histogram data logger for load modelling applications," in *25th Southern African Universities Power Engineering Conference*, Stellenbosch, 2017.

- [77] NXP Semiconductors, "PCF8563 Real-time Clock Product Data Sheet," 26 October 2015. [Online]. Available: <https://www.nxp.com/docs/en/data-sheet/PCF8563.pdf>. [Accessed 12 February 2017].
- [78] Atmel Microchip, "ATxmega128A4U Product Datasheet," 05 May 2017. [Online]. Available: http://ww1.microchip.com/downloads/en/DeviceDoc/Atmel-8387-8-and16-bit-AVR-Microcontroller-XMEGA-A4U_Datasheet.pdf.
- [79] H. Vermeulen and J. Bekker, "Pre-implementation Energy Consumption Scoping and Baseline Report for Robben Island World Heritage Site," Stellenbosch, 2015.
- [80] Meteo Control, "Meteo Control, Energy & Weather Services," [Online]. Available: <https://www.meteocontrol.com/en/>. [Accessed July 2017].

Appendix A: Case study energy profile data

Appendix Table A.1 Energy supplied by the diesel generators on the 1st of September 2017 (Sunny day)

Time [hh:mm]	Energy [kWh]
0:00	261,6
0:30	264,2
1:00	253,1
1:30	255,7
2:00	255,9
2:30	258,6
3:00	259,2
3:30	253,4
4:00	262,1
4:30	267,0
5:00	305,1
5:30	330,3
6:00	335,4
6:30	322,4
7:00	321,5
7:30	312,0

Time [hh:mm]	Energy [kWh]
8:00	304,3
8:30	251,1
9:00	147,5
9:30	98,6
10:00	98,7
10:30	57,3
11:00	0,0
11:30	0,0
12:00	0,0
12:30	0,0
13:00	0,0
13:30	0,0
14:00	0,0
14:30	0,0
15:00	0,0
15:30	0,0

Time [hh:mm]	Energy [kWh]
16:00	0,0
16:30	0,0
17:00	0,0
17:30	0,0
18:00	0,0
18:30	0,0
19:00	2,6
19:30	336,9
20:00	335,6
20:30	344,5
21:00	240,8
21:30	320,5
22:00	296,7
22:30	288,6
23:00	237,3
23:30	298,7

**Appendix Table A.2 Energy supplied by the diesel generators on the 5th of September 2017
(Cloudy day)**

Time [hh:mm]	Energy [kWh]
0:00	274,6
0:30	259,8
1:00	265,0
1:30	263,1
2:00	270,5
2:30	259,4
3:00	258,6
3:30	260,4
4:00	266,5
4:30	272,9
5:00	296,3
5:30	324,3
6:00	327,7
6:30	324,3
7:00	332,8
7:30	326,7

Time [hh:mm]	Energy [kWh]
8:00	289,0
8:30	284,8
9:00	273,1
9:30	285,7
10:00	281,1
10:30	270,7
11:00	190,5
11:30	125,3
12:00	100,4
12:30	98,8
13:00	99,2
13:30	15,2
14:00	0,0
14:30	0,0
15:00	0,0
15:30	0,0

Time [hh:mm]	Energy [kWh]
16:00	0,0
16:30	156,4
17:00	197,3
17:30	249,6
18:00	319,8
18:30	342,0
19:00	378,5
19:30	388,0
20:00	387,1
20:30	399,4
21:00	374,9
21:30	294,5
22:00	339,6
22:30	308,4
23:00	300,4
23:30	289,8

Appendix Table A.3 Averaged energy supplied by the diesel generators for the period of the study

Time [hh:mm]	Energy [kWh]
0:00	201,1
0:30	193,2
1:00	189,2
1:30	185,8
2:00	184,1
2:30	182,3
3:00	177,5
3:30	178,0
4:00	180,0
4:30	185,2
5:00	201,8
5:30	215,8
6:00	222,8
6:30	221,5
7:00	213,2
7:30	203,3

Time [hh:mm]	Energy [kWh]
8:00	184,9
8:30	155,7
9:00	130,1
9:30	108,6
10:00	80,5
10:30	58,5
11:00	42,0
11:30	33,1
12:00	25,1
12:30	23,8
13:00	20,1
13:30	13,0
14:00	8,7
14:30	8,3
15:00	11,9
15:30	21,7

Time [hh:mm]	Energy [kWh]
16:00	28,9
16:30	46,1
17:00	64,8
17:30	80,0
18:00	97,4
18:30	127,7
19:00	172,7
19:30	221,6
20:00	253,7
20:30	267,9
21:00	268,9
21:30	261,6
22:00	246,0
22:30	228,6
23:00	213,6
23:30	205,4

Appendix Table A.4 Energy delivered by the PV plant on the 1st of September 2017 (Sunny day)

Time [hh:mm]	Energy [kWh]
0:00	0,0
0:30	0,0
1:00	0,0
1:30	0,0
2:00	0,0
2:30	0,0
3:00	0,0
3:30	0,0
4:00	0,0
4:30	0,0
5:00	0,0
5:30	0,0
6:00	0,0
6:30	0,0
7:00	0,3
7:30	4,5

Time [hh:mm]	Energy [kWh]
8:00	26,2
8:30	57,8
9:00	142,3
9:30	228,9
10:00	298,3
10:30	359,3
11:00	403,9
11:30	437,3
12:00	464,3
12:30	486,7
13:00	500,6
13:30	512,4
14:00	366,8
14:30	218,6
15:00	285,7
15:30	275,9

Time [hh:mm]	Energy [kWh]
16:00	273,9
16:30	209,6
17:00	143,5
17:30	68,6
18:00	7,5
18:30	0,0
19:00	0,0
19:30	0,0
20:00	0,0
20:30	0,0
21:00	0,0
21:30	0,0
22:00	0,0
22:30	0,0
23:00	0,0
23:30	0,0

Appendix Table A.5 Energy delivered by the PV plant on the 5th of September 2017 (Cloudy day)

Time [hh:mm]	Energy [kWh]
0:00	0,0
0:30	0,0
1:00	0,0
1:30	0,0
2:00	0,0
2:30	0,0
3:00	0,0
3:30	0,0
4:00	0,0
4:30	0,0
5:00	0,0
5:30	0,0
6:00	0,0
6:30	0,0
7:00	0,7
7:30	7,8

Time [hh:mm]	Energy [kWh]
8:00	27,2
8:30	32,3
9:00	40,7
9:30	43,1
10:00	44,4
10:30	73,9
11:00	142,8
11:30	203,7
12:00	252,1
12:30	280,6
13:00	298,9
13:30	319,8
14:00	411,0
14:30	356,4
15:00	172,7
15:30	234,5

Time [hh:mm]	Energy [kWh]
16:00	177,6
16:30	138,3
17:00	126,8
17:30	75,3
18:00	13,2
18:30	0,0
19:00	0,0
19:30	0,0
20:00	0,0
20:30	0,0
21:00	0,0
21:30	0,0
22:00	0,0
22:30	0,0
23:00	0,0
23:30	0,0

Appendix Table A.6 Averaged energy delivered by the PV plant for the period of the study

Time [hh:mm]	Energy [kWh]
0:00	0,0
0:30	0,0
1:00	0,0
1:30	0,0
2:00	0,0
2:30	0,0
3:00	0,0
3:30	0,0
4:00	0,0
4:30	0,0
5:00	0,3
5:30	1,2
6:00	3,5
6:30	8,2
7:00	15,5
7:30	27,2

Time [hh:mm]	Energy [kWh]
8:00	45,8
8:30	79,3
9:00	129,2
9:30	179,9
10:00	218,6
10:30	238,7
11:00	278,2
11:30	307,0
12:00	320,5
12:30	285,0
13:00	273,2
13:30	277,6
14:00	251,4
14:30	235,9
15:00	199,5
15:30	191,6

Time [hh:mm]	Energy [kWh]
16:00	164,6
16:30	133,3
17:00	94,2
17:30	42,4
18:00	7,7
18:30	0,1
19:00	0,0
19:30	0,0
20:00	0,0
20:30	0,0
21:00	0,0
21:30	0,0
22:00	0,0
22:30	0,0
23:00	0,0
23:30	0,0

Appendix Table A.7 Energy supplied/used by the battery storage system on the 1st of September 2017 (Sunny day)

Time [hh:mm]	Energy [kWh]
0:00	0,0
0:30	0,0
1:00	0,0
1:30	0,0
2:00	0,0
2:30	0,0
3:00	0,0
3:30	0,0
4:00	0,0
4:30	0,0
5:00	0,0
5:30	0,0
6:00	0,0
6:30	0,0
7:00	0,0
7:30	0,0

Time [hh:mm]	Energy [kWh]
8:00	0,0
8:30	0,0
9:00	-4,3
9:30	-42,7
10:00	-95,1
10:30	-126,6
11:00	-105,1
11:30	-148,4
12:00	-187,1
12:30	-201,2
13:00	-211,0
13:30	-218,6
14:00	-109,8
14:30	17,1
15:00	0,0
15:30	0,0

Time [hh:mm]	Energy [kWh]
16:00	0,0
16:30	26,2
17:00	128,6
17:30	211,8
18:00	285,4
18:30	306,9
19:00	270,7
19:30	0,0
20:00	0,0
20:30	3,9
21:00	0,0
21:30	0,0
22:00	0,0
22:30	0,0
23:00	0,0
23:30	0,0

Appendix Table A.8 Energy supplied/used by the battery storage system on the 5th of September 2017 (Cloudy day)

Time [hh:mm]	Energy [kWh]
0:00	0,0
0:30	0,0
1:00	0,0
1:30	0,0
2:00	0,0
2:30	0,0
3:00	0,0
3:30	0,0
4:00	0,0
4:30	0,0
5:00	0,0
5:30	0,0
6:00	0,0
6:30	0,0
7:00	0,0
7:30	0,0

Time [hh:mm]	Energy [kWh]
8:00	0,0
8:30	0,0
9:00	-4,3
9:30	0,0
10:00	0,0
10:30	0,0
11:00	0,0
11:30	-7,9
12:00	-38,1
12:30	-62,4
13:00	-83,2
13:30	-5,2
14:00	-85,2
14:30	-50,5
15:00	113,8
15:30	56,0

Time [hh:mm]	Energy [kWh]
16:00	123,6
16:30	18,4
17:00	-8,5
17:30	0,0
18:00	0,0
18:30	0,0
19:00	0,0
19:30	0,0
20:00	0,0
20:30	0,0
21:00	0,0
21:30	0,0
22:00	0,0
22:30	0,0
23:00	0,0
23:30	0,0

Appendix Table A.9 Average energy supplied/used by the battery storage system for the period of the study

Time [hh:mm]	Energy [kWh]
0:00	0,0
0:30	0,0
1:00	0,0
1:30	0,0
2:00	0,0
2:30	0,0
3:00	0,0
3:30	0,0
4:00	0,0
4:30	0,0
5:00	0,0
5:30	0,0
6:00	0,0
6:30	0,0
7:00	-4,4
7:30	-8,1

Time [hh:mm]	Energy [kWh]
8:00	-8,9
8:30	-16,6
9:00	-41,5
9:30	-67,9
10:00	-88,3
10:30	-83,9
11:00	-103,9
11:30	-122,6
12:00	-130,5
12:30	-98,5
13:00	-80,9
13:30	-71,5
14:00	-48,4
14:30	-26,6
15:00	3,7
15:30	7,1

Time [hh:mm]	Energy [kWh]
16:00	26,6
16:30	57,3
17:00	84,3
17:30	131,0
18:00	158,0
18:30	155,4
19:00	135,1
19:30	86,0
20:00	46,4
20:30	22,2
21:00	4,2
21:30	1,4
22:00	0,1
22:30	0,0
23:00	0,0
23:30	0,0

Appendix Table A.10 Energy demand on the 5th of September 2017

Time [hh:mm]	Energy [kWh]
0:00	271,1
0:30	258,4
1:00	262,7
1:30	260,9
2:00	268,4
2:30	255,5
3:00	256,2
3:30	258,3
4:00	264,6
4:30	270,5
5:00	294,0
5:30	323,7
6:00	326,4
6:30	321,5
7:00	331,8
7:30	332,6

Time [hh:mm]	Energy [kWh]
8:00	314,1
8:30	314,9
9:00	309,5
9:30	326,9
10:00	323,6
10:30	342,5
11:00	331,2
11:30	321,1
12:00	314,5
12:30	317,0
13:00	314,9
13:30	329,7
14:00	325,7
14:30	305,9
15:00	286,5
15:30	290,5

Time [hh:mm]	Energy [kWh]
16:00	301,2
16:30	313,1
17:00	315,6
17:30	325,7
18:00	332,5
18:30	341,2
19:00	376,1
19:30	386,1
20:00	384,6
20:30	397,0
21:00	373,4
21:30	290,5
22:00	339,3
22:30	306,4
23:00	297,7
23:30	287,5

Appendix Table A.11 Energy demand on the 10th of September 2017

Time [hh:mm]	Energy [kWh]
0:00	248,1
0:30	251,4
1:00	239,0
1:30	243,8
2:00	244,3
2:30	263,1
3:00	263,4
3:30	253,6
4:00	267,4
4:30	273,3
5:00	249,3
5:30	260,4
6:00	281,6
6:30	284,7
7:00	269,1
7:30	279,1

Time [hh:mm]	Energy [kWh]
8:00	278,9
8:30	282,8
9:00	271,1
9:30	273,5
10:00	275,6
10:30	280,0
11:00	280,7
11:30	250,8
12:00	148,0
12:30	152,7
13:00	138,9
13:30	132,3
14:00	137,8
14:30	132,5
15:00	139,7
15:30	135,7

Time [hh:mm]	Energy [kWh]
16:00	146,0
16:30	157,2
17:00	193,1
17:30	194,0
18:00	212,6
18:30	202,8
19:00	206,1
19:30	179,7
20:00	171,2
20:30	153,9
21:00	143,3
21:30	136,7
22:00	144,8
22:30	129,3
23:00	126,1
23:30	115,6

Appendix Table A.12 Average energy demand for the period of the study

Time [hh:mm]	Energy [kWh]
0:00	198,0
0:30	191,6
1:00	188,3
1:30	184,8
2:00	182,4
2:30	181,2
3:00	175,8
3:30	176,9
4:00	179,0
4:30	184,2
5:00	200,9
5:30	215,8
6:00	225,2
6:30	226,8
7:00	223,2
7:30	221,4

Time [hh:mm]	Energy [kWh]
8:00	220,6
8:30	217,4
9:00	217,1
9:30	220,3
10:00	210,5
10:30	213,2
11:00	216,3
11:30	217,4
12:00	215,1
12:30	211,3
13:00	213,1
13:30	218,5
14:00	211,0
14:30	217,0
15:00	214,4
15:30	219,4

Time [hh:mm]	Energy [kWh]
16:00	219,4
16:30	236,5
17:00	243,3
17:30	253,2
18:00	262,9
18:30	282,5
19:00	307,3
19:30	306,9
20:00	299,8
20:30	289,8
21:00	272,7
21:30	260,5
22:00	245,5
22:30	228,0
23:00	213,0
23:30	204,5

Appendix Table A.13 Total daily energy consumed by the desalination water plant

Date	Energy [kWh]
17/08/2017	1.0
18/08/2017	0.9
19/08/2017	0.9
20/08/2017	0.8
21/08/2017	1.1
22/08/2017	0.8
23/08/2017	355.6
24/08/2017	808.5
25/08/2017	1 109.9
26/08/2017	686.2
27/08/2017	607.1
28/08/2017	1 830.3
29/08/2017	1 899.1
30/08/2017	1 896.8
31/08/2017	1 833.1
01/09/2017	1 777.2
02/09/2017	1 679.9
03/09/2017	1 870.6
04/09/2017	1 870.8
05/09/2017	1 865.7
06/09/2017	1 801.1
07/09/2017	40.6
08/09/2017	682.6
09/09/2017	942.3
10/09/2017	1 125.3
11/09/2017	621.8

12/09/2017	1 866.8
13/09/2017	1 351.2
14/09/2017	1.6
15/09/2017	0.4

Appendix Table A.14 Average geyser energy consumption for the period of the study

Time [hh:mm]	Energy [kWh]
0:00	18,6
0:30	13,0
1:00	11,9
1:30	12,3
2:00	15,7
2:30	12,1
3:00	10,8
3:30	10,5
4:00	14,2
4:30	19,7
5:00	60,9
5:30	81,6
6:00	82,6
6:30	73,2
7:00	59,8
7:30	60,2

Time [hh:mm]	Energy [kWh]
8:00	57,3
8:30	57,8
9:00	54,5
9:30	49,0
10:00	41,5
10:30	39,2
11:00	36,5
11:30	34,5
12:00	34,2
12:30	25,9
13:00	30,8
13:30	31,1
14:00	35,1
14:30	27,4
15:00	30,5
15:30	31,7

Time [hh:mm]	Energy [kWh]
16:00	26,0
16:30	33,4
17:00	33,7
17:30	35,9
18:00	38,4
18:30	46,1
19:00	54,1
19:30	53,6
20:00	55,9
20:30	49,3
21:00	46,3
21:30	46,1
22:00	37,1
22:30	34,2
23:00	28,9
23:30	21,0

Appendix Table A.15 Memory map of the average geyser usage data over a period of two weeks

Event On-time [hh:mm]	Event Duration [minutes]							
	12	24	36	48	60	72	84	96
00:30	1,26	1,61	0,00	0,00	0,00	0,00	0,00	0,00
01:00	2,94	0,81	1,30	0,00	0,00	0,00	0,00	0,00
01:30	3,78	0,00	0,00	0,00	0,00	0,00	0,00	0,00
02:00	2,94	0,00	0,00	0,00	0,00	0,00	0,00	0,00
02:30	2,52	0,00	0,00	0,00	0,00	0,00	0,00	0,00
03:00	0,42	0,00	0,00	0,00	0,00	0,00	0,00	0,00
03:30	0,84	0,00	0,00	0,00	0,00	0,00	0,00	0,00
04:00	1,68	2,42	2,60	5,97	0,00	0,00	5,66	2,94
04:30	2,52	4,03	0,00	1,49	2,33	3,33	0,00	8,82
05:00	1,68	2,42	0,00	7,46	0,00	5,00	3,77	0,00
05:30	0,84	0,81	2,60	0,00	2,33	0,00	0,00	8,82
06:00	0,42	1,61	2,60	1,49	0,00	0,00	3,77	0,00
06:30	0,42	0,81	0,00	0,00	0,00	0,00	0,00	0,00
07:00	0,42	3,23	2,60	2,99	11,63	8,33	16,98	14,71
07:30	0,42	0,81	5,19	2,99	2,33	0,00	0,00	0,00
08:00	7,98	4,03	2,60	5,97	11,63	1,67	1,89	0,00
08:30	2,94	0,00	3,90	5,97	0,00	13,33	1,89	0,00
09:00	5,46	0,00	1,30	1,49	0,00	6,67	0,00	0,00
09:30	2,94	4,84	0,00	0,00	11,63	0,00	11,32	0,00
10:00	5,88	9,68	6,49	16,42	18,60	20,00	16,98	14,71
10:30	5,04	15,32	6,49	7,46	11,63	3,33	7,55	11,76
11:00	4,62	13,71	14,29	8,96	0,00	3,33	5,66	2,94
11:30	2,52	1,61	0,00	0,00	0,00	1,67	1,89	14,71
12:00	0,00	1,61	6,49	0,00	0,00	0,00	1,89	0,00
12:30	0,00	0,00	0,00	0,00	0,00	0,00	0,00	0,00

13:00	0,42	0,00	0,00	0,00	0,00	0,00	0,00	0,00
13:30	0,00	0,81	1,30	1,49	0,00	0,00	0,00	0,00
14:00	3,36	1,61	5,19	5,97	4,65	0,00	1,89	0,00
14:30	2,52	1,61	0,00	0,00	0,00	1,67	1,89	0,00
15:00	2,52	2,42	2,60	0,00	0,00	0,00	0,00	0,00
15:30	1,68	1,61	0,00	0,00	0,00	1,67	0,00	0,00
16:00	0,42	0,00	0,00	0,00	0,00	0,00	0,00	0,00
16:30	0,00	0,00	0,00	1,49	0,00	0,00	0,00	0,00
17:00	0,42	0,00	0,00	1,49	0,00	0,00	0,00	0,00
17:30	0,84	0,00	0,00	0,00	0,00	0,00	0,00	0,00
18:00	6,30	1,61	5,19	4,48	6,98	3,33	0,00	0,00
18:30	4,20	0,81	2,60	2,99	0,00	1,67	0,00	2,94
19:00	2,94	3,23	0,00	5,97	2,33	10,00	7,55	14,71
19:30	1,68	0,81	5,19	1,49	0,00	3,33	0,00	0,00
20:00	4,20	4,03	7,79	1,49	9,30	8,33	1,89	2,94
20:30	4,20	6,45	3,90	0,00	4,65	3,33	5,66	0,00
21:00	0,84	4,84	7,79	4,48	0,00	0,00	1,89	0,00
21:30	0,42	0,00	0,00	0,00	0,00	0,00	0,00	0,00
22:00	0,00	0,81	0,00	0,00	0,00	0,00	0,00	0,00
22:30	0,00	0,00	0,00	0,00	0,00	0,00	0,00	0,00
23:00	1,68	0,00	0,00	0,00	0,00	0,00	0,00	0,00
23:30	0,84	0,00	0,00	0,00	0,00	0,00	0,00	0,00
00:00	1,68	0,00	0,00	0,00	0,00	0,00	0,00	0,00

Event On-time [hh:mm]	Event Duration [minutes]							
	108	120	132	144	156	168	180	192
00:30	0,00	0,00	0,00	0,00	0,00	0,00	0,00	0,00
01:00	0,00	0,00	0,00	0,00	0,00	0,00	0,00	0,00
01:30	0,00	0,00	2,27	0,00	3,85	0,00	0,00	0,00
02:00	0,00	0,00	0,00	0,00	0,00	0,00	0,00	0,00

02:30	0,00	0,00	0,00	0,00	0,00	0,00	0,00	0,00
03:00	0,00	0,00	0,00	0,00	0,00	0,00	0,00	0,00
03:30	0,00	0,00	0,00	0,00	0,00	0,00	0,00	0,00
04:00	3,45	0,00	0,00	2,27	7,69	0,00	0,00	0,00
04:30	0,00	0,00	0,00	0,00	0,00	0,00	0,00	0,00
05:00	3,45	3,51	0,00	0,00	0,00	0,00	0,00	0,00
05:30	0,00	0,00	0,00	0,00	0,00	0,00	0,00	0,00
06:00	6,90	0,00	0,00	0,00	0,00	0,00	0,00	0,00
06:30	0,00	0,00	0,00	0,00	0,00	0,00	0,00	0,00
07:00	0,00	3,51	0,00	0,00	0,00	0,00	0,00	0,00
07:30	0,00	1,75	0,00	0,00	0,00	0,00	5,26	0,00
08:00	3,45	1,75	0,00	0,00	3,85	0,00	5,26	0,00
08:30	0,00	0,00	4,55	0,00	0,00	0,00	0,00	0,00
09:00	3,45	1,75	2,27	2,27	0,00	3,85	0,00	0,00
09:30	0,00	0,00	9,09	18,18	0,00	15,38	0,00	33,33
10:00	20,69	12,28	11,36	25,00	23,08	30,77	5,26	12,50
10:30	10,34	15,79	15,91	18,18	0,00	0,00	0,00	16,67
11:00	0,00	7,02	11,36	4,55	30,77	3,85	42,11	20,83
11:30	0,00	0,00	2,27	0,00	19,23	11,54	5,26	8,33
12:00	0,00	1,75	2,27	0,00	0,00	0,00	0,00	0,00
12:30	0,00	0,00	0,00	0,00	0,00	0,00	0,00	0,00
13:00	0,00	0,00	0,00	0,00	0,00	0,00	0,00	0,00
13:30	0,00	0,00	0,00	0,00	3,85	0,00	0,00	0,00
14:00	0,00	0,00	0,00	0,00	0,00	0,00	0,00	4,17
14:30	0,00	0,00	0,00	0,00	0,00	0,00	0,00	4,17
15:00	0,00	0,00	0,00	0,00	0,00	0,00	0,00	0,00
15:30	0,00	0,00	0,00	0,00	0,00	0,00	0,00	0,00
16:00	0,00	1,75	0,00	0,00	0,00	0,00	0,00	0,00
16:30	0,00	0,00	0,00	0,00	0,00	3,85	0,00	0,00
17:00	0,00	0,00	0,00	0,00	0,00	0,00	0,00	0,00

17:30	0,00	0,00	0,00	0,00	0,00	0,00	0,00	0,00
18:00	10,34	0,00	0,00	6,82	0,00	3,85	5,26	0,00
18:30	0,00	21,05	4,55	6,82	0,00	3,85	5,26	0,00
19:00	17,24	10,53	2,27	15,91	0,00	7,69	0,00	0,00
19:30	10,34	7,02	15,91	0,00	0,00	11,54	0,00	0,00
20:00	6,90	1,75	0,00	0,00	7,69	3,85	5,26	0,00
20:30	0,00	3,51	0,00	0,00	0,00	0,00	10,53	0,00
21:00	3,45	5,26	15,91	0,00	0,00	0,00	10,53	0,00
21:30	0,00	0,00	0,00	0,00	0,00	0,00	0,00	0,00
22:00	0,00	0,00	0,00	0,00	0,00	0,00	0,00	0,00
22:30	0,00	0,00	0,00	0,00	0,00	0,00	0,00	0,00
23:00	0,00	0,00	0,00	0,00	0,00	0,00	0,00	0,00
23:30	0,00	0,00	0,00	0,00	0,00	0,00	0,00	0,00
00:00	0,00	0,00	0,00	0,00	0,00	0,00	0,00	0,00

Event On-time [hh:mm]	Event Duration [minutes]			
	204	216	228	240
00:30	0,00	0,00	0,00	0,00
01:00	0,00	0,00	0,00	0,00
01:30	0,00	0,00	0,00	0,00
02:00	0,00	0,00	0,00	0,00
02:30	0,00	0,00	0,00	0,00
03:00	0,00	0,00	0,00	0,00
03:30	0,00	0,00	0,00	0,00
04:00	0,00	0,00	1,18	1,37
04:30	0,00	0,00	2,35	0,00
05:00	0,00	0,00	2,35	0,00
05:30	0,00	0,00	0,00	0,00
06:00	0,00	0,00	0,00	0,00
06:30	0,00	0,00	0,00	0,00

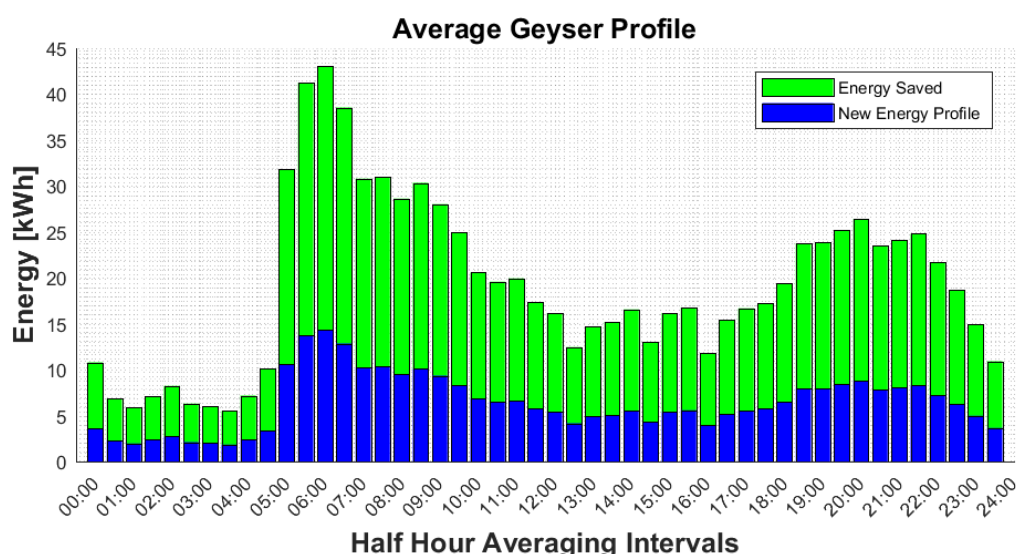
07:00				0,00
	0,00	0,00	0,00	
07:30				0,00
	0,00	0,00	0,00	
08:00				1,37
	0,00	0,00	0,00	
08:30				2,74
	0,00	3,23	3,53	
09:00				2,74
	0,00	16,13	1,18	
09:30				2,74
	0,00	0,00	4,71	
10:00				10,96
	15,15	3,23	7,06	
10:30				5,48
	0,00	3,23	8,24	
11:00				13,70
	42,42	22,58	8,24	
11:30				8,22
	18,18	0,00	4,71	
12:00				0,00
	0,00	0,00	0,00	
12:30				0,00
	0,00	0,00	0,00	
13:00				0,00
	0,00	0,00	0,00	
13:30				0,00
	0,00	0,00	0,00	
14:00				1,37
	0,00	0,00	2,35	
14:30				0,00
	6,06	6,45	3,53	
15:00				0,00
	0,00	0,00	0,00	
15:30				0,00
	0,00	0,00	0,00	
16:00				0,00
	0,00	0,00	0,00	
16:30				0,00
	0,00	0,00	0,00	
17:00				0,00
	0,00	0,00	0,00	
17:30				0,00
	0,00	0,00	1,18	
18:00				1,37
	0,00	0,00	0,00	
18:30				2,74
	3,03	0,00	1,18	
19:00				5,48
	12,12	0,00	15,29	
19:30				10,96
	0,00	22,58	15,29	
20:00				12,33
	0,00	9,68	10,59	
20:30				2,74
	0,00	12,90	4,71	
21:00				10,96
	3,03	0,00	2,35	
21:30				2,74
	0,00	0,00	0,00	

22:00	0,00	0,00	0,00	0,00
22:30	0,00	0,00	0,00	0,00
23:00	0,00	0,00	0,00	0,00
23:30	0,00	0,00	0,00	0,00
00:00	0,00	0,00	0,00	0,00

Appendix B: Energy saving calculations for a non-ideal solar day

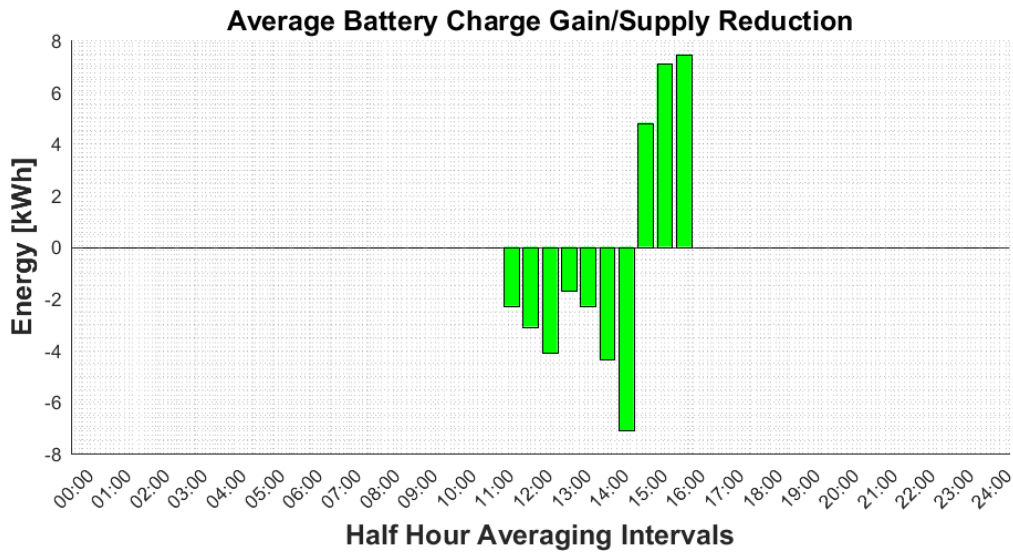
The total diesel generator energy savings is calculated using the average historical profiles given in Figure 7.4, Figure 7.8, Figure 7.13 and Figure 7.16 with the half-hour data given in Appendix A. The same set of energy saving scenarios are used to forecast the direct diesel generator energy savings and the battery system's charge gain and supply reduction energy as given by Equations 7.17 to Equation 7.44.

The average geyser profile is given in Appendix Figure B.1, representing the new average geyser profile and the possible energy savings when replacing the current geysers with heat pump systems.

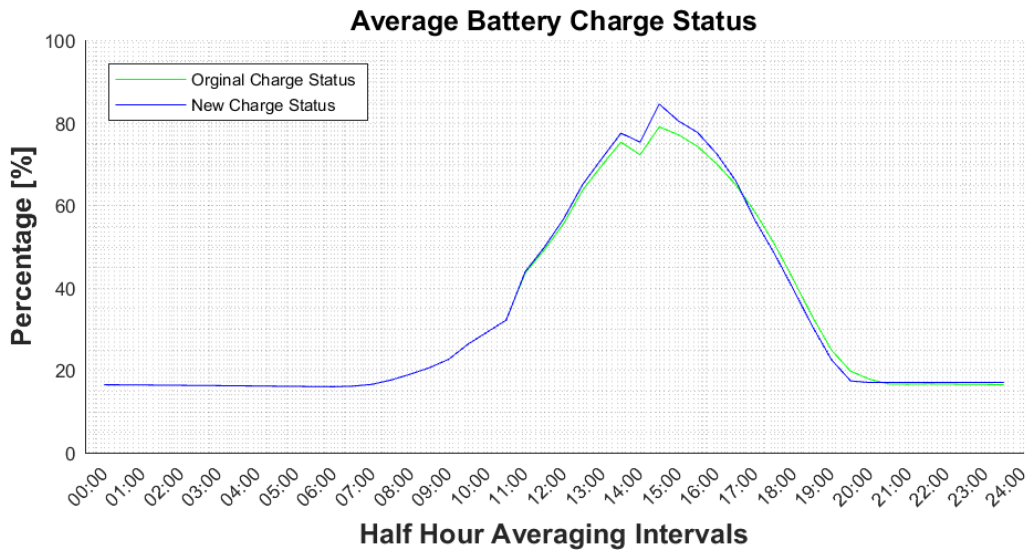


Appendix Figure B.1 Total forecasted energy saving profile for a cloudy and rainy day

The energy savings affects the diesel generator profile as well as the battery storage profile. The additional average battery charge energy is presented in Appendix Figure B.2 as negative energy values. The average battery reduction energy is given as positive values in this figure. With the extra energy available from the battery system, the battery charging status is adjusted accordingly. Appendix Figure B.3 shows the average battery charging status for each half-hour of the day.

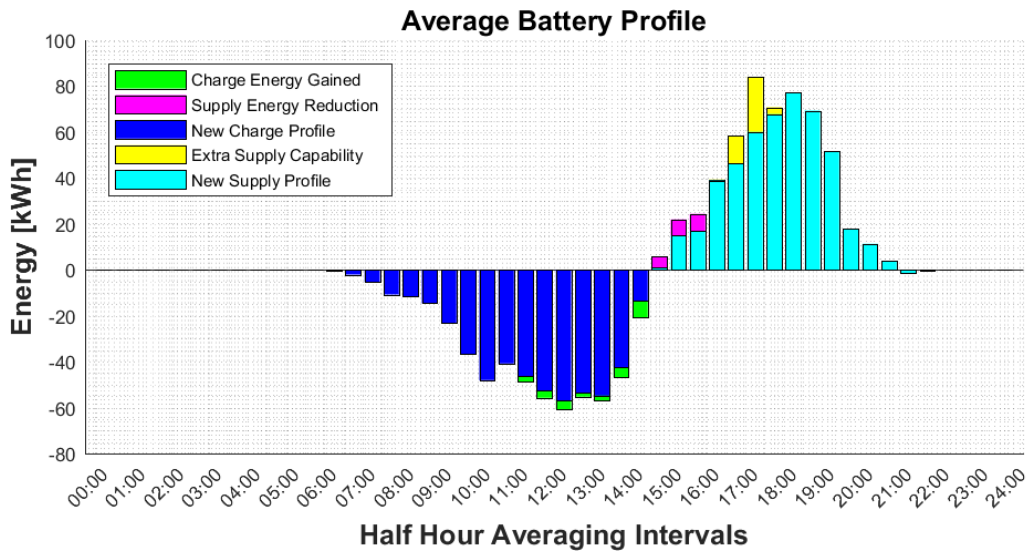


Appendix Figure B.2 Additional battery energy gained and energy reduction profile for a cloudy and rainy day



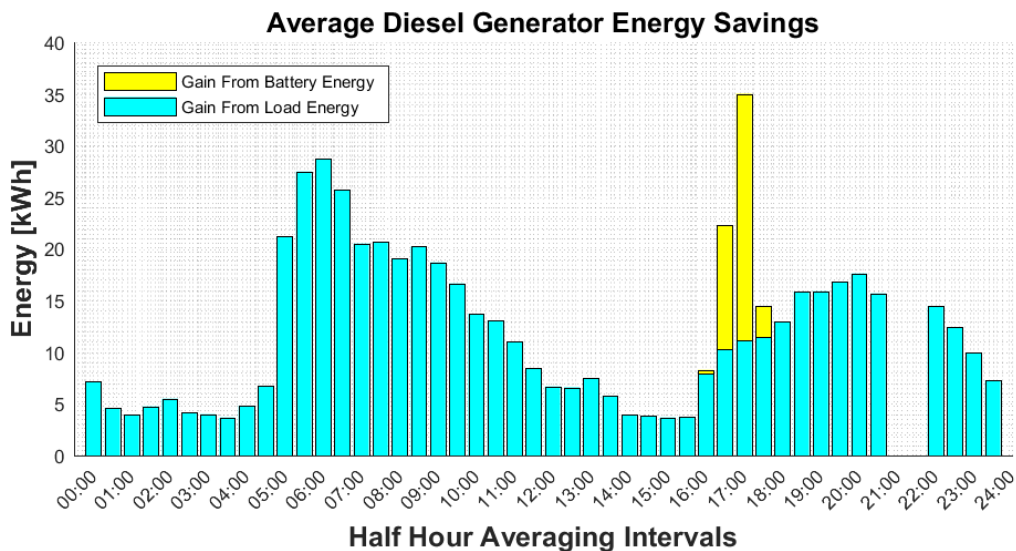
Appendix Figure B.3 Battery system charge status for a cloudy and rainy day

The average battery charge status never reaches full charging capacity as the average historical profiles include low solar irradiance days. A cloudy day reduces the average battery savings as less battery energy is available, however with more energy imported from the diesel generators, more energy savings are acquired from the diesel generators. The average battery profile is impacted by the energy charge gain and energy reduction as shown in Appendix Figure B.4.

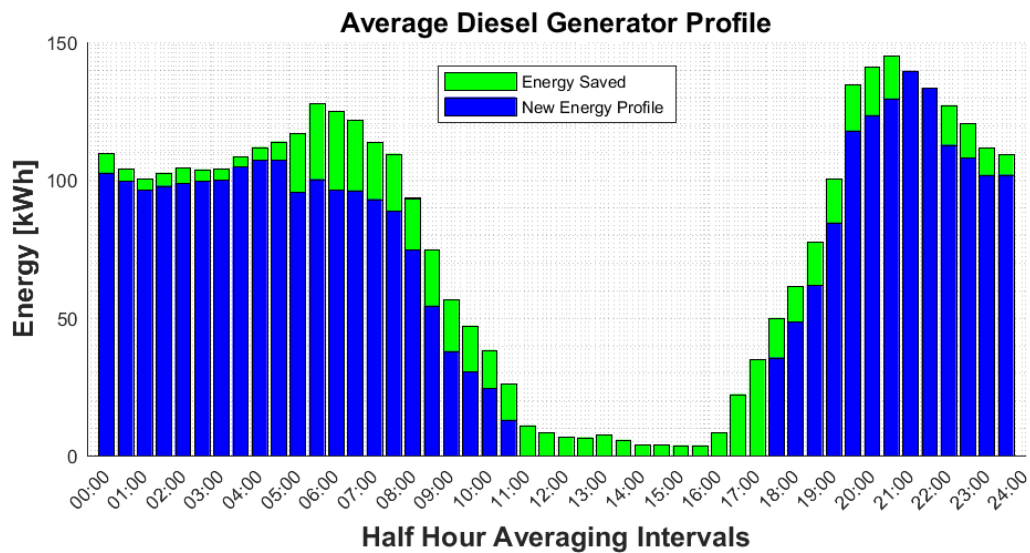


Appendix Figure B.4 Illustration of the impact on the battery storage system for a cloudy and rainy day

The additional supply capability of the battery system is cumulatively added to the average diesel generator energy savings profile. The average diesel generator energy savings were determined by the set of energy saving scenarios directly. The average diesel generator energy savings profile is given in Appendix Figure B.5 with the additional battery supply capability added. The average diesel generator energy savings are subtracted from the original average diesel profile. Appendix Figure B.6 shows the forecasted average diesel profile.



Appendix Figure B.5 Total diesel generator energy savings for a cloudy and rainy day



Appendix Figure B.6 Diesel generator profile with energy savings for a cloudy and rainy day

The per day average diesel generator energy savings are calculated using Equation 7.46 and results to a total per day average energy saving of 1150.2 kWh.

Appendix C: Heat pump systems cost breakdown

Appendix Table C.1 Heat pump system installation cost breakdown quoted by ITS Heat Pumps

Component	Cost for 60 Heat Pump Systems [R]
150L Water Cylinders	607 697,06
3,2 kW Heat Pumps	789 308,64
Fittings and Materials	342 000,00
Labour	198 360,00
Extra Fees	14 250,00
Total	1 951 615,70

Appendix Table C.2 Heat pump system installation cost breakdown quoted by Deacon's Solar and Plumbing

Component	Cost for 60 Heat Pump Systems [R]
150L Water Cylinders	225 651,60
3,2 kW Heat Pumps	665 463,60
Fittings and Materials	267 102,00
Labour	129 960,00
Extra Fees	85 066,80
Total	1 373 244,00

Appendix D: Data logger manufacturing costs

Appendix Table D.1 Cost of components required for one logic core unit

Component	Component Name	Quantity	Price (Excl VAT)	Total
Microprocessor	ATXMEGA128A4U-AU	1	R111,92	R111,92
LDO Voltage Regulator	LP2985AIM5-3,6V	1	R7,87	R7,87
EEPROM	AT24CM01	1	R18,95	R18,95
Real Time Clock	PCF8563T	1	R7,48	R7,48
Schottky Barrier Diode	BAT54C	1	R0,51	R0,51
Silicon Schottky Diode	BAT64	1	R0,64	R0,64
Capacitor	Tantalum 4,7 μ F 16 V dc	2	R2,11	R4,22
Capacitor	Tantalum 2,2 μ F 16 V dc	1	R1,83	R1,83
Capacitor	SMD 0603 0,1 μ F	6	R0,25	R1,50
Capacitor	SMD 0603 10pF	1	R0,05	R0,05
USB Connector	Mini Type B	1	R10,44	R10,44
ESD Protection	PRTR5V0U2X	1	R3,60	R3,60
MOSFET Transistor	FDN342P	1	R3,15	R3,15
PDI Header	6 Way 2 Row Male	1	R0,77	R0,77
Breakout Header	12 Way Male	3	R1,11	R3,33
Crystal	32,768kHz	1	R7,52	R7,52
Inductor	Ferrite Bead	1	R0,24	R0,24
Resistor	SMD 0603 10K0	3	R0,17	R0,51
Resistor	SMD 0603 75E	2	R0,15	R0,30
Resistor	SMD 0603 4K7	4	R0,05	R0,20
LED	SMD 0603 GREEN	1	R1,65	R1,65
LED	SMD 0603 RED	1	R1,89	R1,89
PCB Manufacturing	Mother Board	1	R14,65	R14,65
PCB Transport	DHL International Shipping	1	R17,80	R17,80
Manufacturing	Labour (Per Hour)			R0,00
Subtotal				R221,02
VAT		14%		R30,94
Total Cost Per Logic Core				R251,96

Appendix Table D.2 Cost of components required for one current sensor unit

Component	Component Name	Quantity	Price (Excl VAT)	Total
Silicon Schottky Diode	BAT64	1	R0,64	R0,64
Capacitor	Tantalum 2,2 μ F 16 V dc	2	R1,83	R3,66
Capacitor	Tantalum 1 μ F 16 V dc	2	R1,11	R2,22
Capacitor	SMD 0603 0,1 μ F	2	R0,25	R0,50
Resistor	SMD 0603 75E	2	R0,15	R0,30
Resistor	SMD 0603 4K7	1	R0,05	R0,05
Resistor	SMD 0603 270K	2	R0,22	R0,44
Resistor	SMD 0603 100K	4	R0,07	R0,28
Resistor	SMD 0603 750K	1	R0,25	R0,25
Resistor	SMD 0603 43E	1	R0,19	R0,19
LED	SMD 0603 Green	1	R1,65	R1,65
Comparator	TS881ILT	1	R8,01	R8,01
2-Input NAND Logic Gate	NC7WZ00K8X	1	R2,00	R2,00
True RMS-DC Converter	LTC1967CMS8	1	R103,44	R103,44
Quick Release Connector	Female Straight Crimp	1	R0,46	R0,46
Connector Contacts	Crimp Contact	2	R0,29	R0,58
System Battery	1,2Ah 3,6V Lithium Battery	1	R74,34	R74,34
Sensor Connection	Wire (Per Meter)	1	R2,40	R2,40
Wire Isolation	Heatshrink	2	R0,60	R1,20
Current Transformer	Talema 1:2500 (50A)	1	R52,35	R52,35
Breakout Header	12 W Female	2	R3,42	R6,84
Breakout Header	3 W Female	2	R2,28	R4,56
Onboard Push Button	SMD Tactile Push	2	R1,65	R3,30
Enclosure	72mmx50mmx25mm	1	R9,20	R9,20
External Push Button	Red-Top/Black-Top	1	R11,73	R11,73
External LED Indicator	3mm Green LED	1	R0,55	R0,55
LED Holder	3mm Plastic Clip	1	R1,11	R1,11
PCB Manufacturing	Current Sensor Board	1	R10,00	R10,00
PCB Transport	DHL International Shipping	1	R18,50	R18,50
Manufacturing	Labour (Per Hour)			R0,00
Subtotal				R320,75
VAT		14%		R44,91
Total Cost Per Sensor Board				R365,66